UNIVERSITY OF CALIFORNIA, SAN DIEGO

Investigating Antarctic ice sheet subglacial processes beneath the Whillans Ice Plain, West Antarctica, using satellite altimetry and GPS

A dissertation submitted in partial satisfaction of the
requirements for the degree
Doctor of Philosophy

in

Earth Sciences

by

Matthew Ross Siegfried

Committee in charge:

Helen Amanda Fricker, Chair
Adrian Borsa
Eugene Pawlak
David Sandwell
Slawek Tulaczyk

2015

The dissertation of Matthew Ross Siegfried is approved, and it is acceptable in quality and form for publication on microfilm and electronically:

_____

_____

_____

_____

_____

Chair

University of California, San Diego

2015

DEDICATION

To all my teachers since 1986,

whose integrated effect somehow led me here...

EPIGRAPH

The numerous people who imagine that a long stay in the Polar regions makes a man less susceptible of cold than other mortals are completely mistaken. The direct opposite is more likely to be the case.

— *Roald Amundsen*, The South Pole

TABLE OF CONTENTS

LIST OF FIGURES

LIST OF TABLES

ACKNOWLEDGEMENTS

One hundred and forty-three times over the past five years, I woke up in a tent pitched (at most) a few 10s of miles from the path Roald Amundsen skied on his way to becoming the first person at the South Pole, peered at a mountain range a human first laid eyes on only a century earlier, and was, each one of those mornings, amazed that this was part of my PhD research. To this day, I am still unsure exactly how I ended up as a student of glaciology, studying one of the least explored, least accessible environments on the planet. I am, however, quite sure that I have many people to thank for nudging me in this incredible direction.

Before thanking those that helped in the creation of this dissertation, I have to acknowledge that, while I was refusing to consider advancing my education past my Master's degree, Bob Hawley, my Master's advisor, and Jill Mikucki, then a postdoctoral scholar at Dartmouth College, continually disregarded my obstinance and pushed me to pursue a PhD at an oceanographic institution 3,000 miles away with a Brit I had never met. They knew (and still know) better than I; I would not be here without their guidance (and their persistence).

A dissertation is, to me, a strange document in that it has one name on the cover, and one person may receive a degree because of it, but it ultimately reflects the input of dozens of people. First and foremost, I have to thank my supervisor Helen Fricker, who guided me through the past five years and provided me with every professional opportunity I could imagine—from letting me help on proposals the day I arrived, to nominating me while I was out of communication in Antarctica to observe a Pontifical Academy of Sciences meeting on climate change at the Vatican, to sending me to give her invited talk at a workshop hosted by the Royal Society of London. Perhaps most importantly though, she was the ideal role model, proving to me that it is possible to be a top-level scientist with a personal life

outside of academics. I also would like to thank my dissertation committee—Adrian Borsa, Geno Pawlek, David Sandwell, and Slawek Tulaczyk—for their questions, their guidance, and for righting the ship whenever I needed it.

I benefited greatly from my scientific peers at Scripps and elsewhere. The members of Scripps Glaciology Group, past and present, provided a fortnightly-ish sounding board for all of my scientific ideas. Each of my co-authors (of manuscripts included in this dissertation or otherwise) shared with me a little of their magic for communicating science that I will always carry with me. The burgeoning Polar group at SIO provided me with a wider context for my research. The larger Scripps community was a source of continual support, especially my fellow graduate students who started with me in Fall 2010. My officemates and pseudo-officemates down the hall in Revelle 4200 at times provided much needed distractions, and my family, friends, and teammates on the UCSD Triathlon team offered outlets outside of academia.

There is much behinds-the-scene work that allows us graduate students at Scripps to focus almost exclusively on science. Thank you to the business office of IGPP for keeping the lights on (and keeping me paid), NetOps for helping with the multitude of computer problems that arise from repeated freeze-thaw cycles, and the SIO Department Office for taking care of so much that I often forgot I was still a student. I particularly want to thank former SIO Student Affairs Coordinator Adam Petersen, whose drive to improve the graduate student experience at Scripps inspired me to be a little less cynical about much more than school.

Fieldwork in Antarctica is a logistical nightmare and there are countless people to thank for my successful forays to Antarctica: the WISSARD field teams 2011–2015, especially Knut Christianson and Lucas Beem for showing me the ropes my first year "on the ice"; Raytheon Polar Services, Antarctic Support Contract

(ASC), and specifically the WISSARD logistics wizard, Julie Raine; Joe Petit, Seth White, Thomas Nylen, and the rest of UNAVCO for endless GPS support; the Polar Geospatial Center; the New York Air National Guard; and Kenn Borek Air. Finally, my dissertation was graciously funded by NASA through an Earth and Space Science Fellowship (grant NNX11AQ78H), the National Science Foundation (grant ANT-0838885), and Scripps Institution of Oceanography, through the C. Hugh Friedman Fellowship.

Chapter 2, in full, is a reprint of material as it appears in Geophysical Research Letters: Siegfried, M. R., Fricker, H. A., Roberts, M., Scambos, T. A., Tulaczyk, S., "A decade of West Antarctic subglacial lake interactions from combined ICESat and CryoSat-2 altimetry", *Geophysical Research Letters*, 41(3), 891–898, doi:10.1002/2013GL058616, 2014. The dissertation author was the primary investigator and author of the paper.

Chapter 3, in full, is currently being prepared for submission for publication of the material. The dissertation author was the primary investigator and author of this material.

Chapter 4, in full, has been submitted for publication of the material as it may appear in Geophysical Research Letters: Siegfried, M. R., Fricker, H. A., Carter, S. P., Tulaczyk, S., "Rapid basal water system evolution triggered by subglacial floods in West Antarctica", *Geophysical Research Letters*, 2015. The dissertation author was the primary investigator and author of the paper.

Chapter 5, in full, is currently being prepared for submission for publication of the material. The dissertation author was the primary investigator and author of this material.

VITA

2008	A. B. in Earth Sciences *magna cum laude*, Dartmouth College
2010	M. Sc. in Earth Sciences, Dartmouth College
2015	Ph. D. in Earth Sciences, University of California, San Diego

PUBLICATIONS

Fricker, H.A., **Siegfried, M.R.**, and Carter, S.P., "A decade of progress in observing and modeling Antarctic subglacial water systems", *Philos. Trans. Roy. Soc. A*, 2015, *Accepted*.

Mikucki, J.A., Lee, P., Ghosh, D., Purcell, A., Mitchell, A., Mankoff, K., Fisher, A.T., Tulaczyk, S., Carter, S.P., **Siegfried, M.R.**, Fricker, H.A., Hodson, T., Coenen, J., Powell, R., Scherer, R.P., Vick-Majors, T., Achberger, A.M., Christner, B.C., and Tranter, M., "Subglacial Lake Whillans Biogeochemistry: A synthesis of current knowledge", *Philos. Trans. Roy. Soc. A*, 2015, *Accepted*.

Siegfried, M.R., Fricker, H.A., Roberts, M., Scambos, T.A., and Tulaczyk, S., "A decade of West Antarctic subglacial lake interactions from combined ICESat and CryoSat-2 altimetry", *Geophys. Res. Lett.*, 41(3), 2014.

Holt, T.O., Glasser, N.F., Fricker, H.A., Padman, L., Luckman, A., King, O., Quincey, D.J., and **Siegfried, M.R.**, "The structural and dynamic responses of Stange Ice Shelf to recent environmental change", *Antarct. Sci.*, 26(06), 2014.

Tulaczyk, S., Mikucki, J.A., **Siegfried, M.R.**, Priscu, J.C., Barcheck, C.G., Beem, L.H., Behar, A., Burnett, J., Christner, B.C., Fisher, A.T., Fricker, H.A., Mankoff, K.D., Powell, R.D., Rack, F., Sampson, D., Scherer, R.P., Schwartz, S.Y., and the WISSARD Science Team, "WISSARD at Subglacial Lake Whillans, West Antarctica: scientific operations and initial observations", *Ann. Glaciol.*, 55(65), 2014.

Carter, S.P., Fricker, H.A., and **Siegfried, M.R.**, "Evidence of rapid subglacial water piracy under Whillans Ice Stream, West Antarctica", *J. Glaciol.*, 59(218), 2013.

Holt, T.O., Glasser, N.F., Quincey, D.J., and **Siegfried, M.R.**, "Speedup and fracturing of George VI Ice Shelf, Antarctic Peninsula", *Cryosphere*, 7(3), 2013.

Horgan, H.J., Alley, R.B., Christianson, K., Jacobel, R.W., Anandakrishnan, S., Muto, A., Beem, L.H., and **Siegfried, M.R.**, "Estuaries beneath ice sheets", *Geology*, 41(11), 2013.

Priscu, J.C., Achberger, A.M., Cahoon, J.E., Christner, B.C., Edwards, R.L., Jones, W.L., Michaud, A.B., **Siegfried, M.R.**, Skidmore, M.L., Spigel, R.H., Switzer, G.W., Tulaczyk, S., and Vick-Majors, T.J., "A microbiologically clean strategy for access to the Whillans Ice Stream subglacial environment", *Antarct. Sci.*, 25(05), 2013.

Taylor, V.F., Jackson, B.P., **Siegfried, M.R.**, Navratilova, J., Francesconi, K.A., Kirshtein, J., and Voytek, M., "Arsenic speciation in food chains from mid-Atlantic hydrothermal vents", *Environ. Chem.*, 9(2), 2012.

Siegfried, M.R., Hawley, R.L., Burkhart, J.F., "High-Resolution Ground-Based GPS Measurements Show Intercampaign Bias in ICESat Elevation Data Near Summit, Greenland", *IEEE T. Geosci. Remote*, 49(10), 2011.

ABSTRACT OF THE DISSERTATION

Investigating Antarctic ice sheet subglacial processes beneath the Whillans Ice Plain, West Antarctica, using satellite altimetry and GPS

by

Matthew Ross Siegfried

Doctor of Philosophy in Earth Sciences

University of California, San Diego, 2015

Professor Helen Amanda Fricker, Chair

The Antarctic ice sheet has an extensive basal water system that lubricates the ice-bed interface and enables the fast flow of ice streams and outlet glaciers, which account for a majority of Antarctic ice discharge to the ocean. In the past decade, observational evidence has suggested that the subglacial hydrology of Antarctica can be non-steady, changing on sub-decadal timescales, but the effect of dynamic hydrology on ice flow remains uncertain. The Whillans Ice Plain (WIP), at the confluence of the Whillans and Mercer ice streams, West Antarctica, has been studied for over 50 years and has been identified as a region with extensive active

subglacial hydrology. In this dissertation, we develop and implement methods using a combination of ground-based Global Positioning System (GPS) data and satellite-based radar and laser altimetry to observe the surface expression of water movement beneath WIP, quantify the dynamic ice-flow response to an evolving basal water system, and investigate processes driven by the interaction of WIP with ocean tides that may impact subglacial water flow near the grounding line. We find that the coupled subglacial-ice stream system can respond rapidly to basal perturbations on sub-annual timescales and in ways that are not captured by simple models. We demonstrate that the location where subglacial water enters the ocean is a complex interface that requires significant improvement to our measurement precision to better understand important time-varying processes. We also apply our method for observing dynamic ice-surface height changes to the inventory of known subglacial lakes in Antarctica to extend our observational record and assess variability of the subglacial hydrologic system in different physical settings. Through this continent-wide analysis of subglacial lakes, we suggest that our current knowledge of the characteristic spatial and temporal scales of hydrologic variability is still limited by our observational capacity. We conclude by proposing future studies that would address knowledge gaps currently preventing the inclusion of an evolving basal water system into large-scale predictive models of ice-sheet flow.

Chapter 1

Introduction

1.1 Background

1.1.1 Antarctica and sea-level rise

Global ocean volume can change by altering the density of seawater or by moving water from the continents to the ocean. Both of these processes have contributed to modern eustatic sea-level rise, with 1.1 ± 0.3 mm yr^{-1} of sea-level change between 1993 and 2010 due to thermal expansion of seawater and 1.84 ± 0.41 mm yr^{-1} due to additional water mass (*Church et al.*, 2013). Ice melted from the grounded portion of the Antarctic ice sheet only accounted for 15% of the additional water mass (0.27 ± 0.11 mm yr^{-1}), but Antarctica contains 26,500,000 km^3 of ice (*Fretwell et al.*, 2013), representing the largest land-based storage of water on Earth. If this volume melted entirely, it would raise global sea level by over 58 meters.

While a complete, catastrophic collapse is unlikely, some sectors of Antarctica are hypothesized to be unstable and could potentially cause a rapid increase of

over 1 m in sea level in the coming centuries (e.g., *Joughin et al.*, 2014; *Mengel and Levermann*, 2014; *Rignot et al.*, 2014), directly impacting over 100 million people who live within 1 m of their local sea level (*Li et al.*, 2009), over half of whom live in developing countries (*Dasgupta et al.*, 2008). Mitigating these potentially serious consequences of rapid sea-level rise requires understanding how ice flow of the Antarctic ice sheet will evolve over decades and centuries to a changing climate. As a result, a recent National Academies report on Antarctic and Southern Ocean research highlighted quantification of the rate and magnitude of Antarctica's contribution to sea level as the top strategic priority for future research (*National Academies of Sciences, Engineering, and Medicine*, 2015).

1.1.2 Ice flow in Antarctica

The Antarctic ice sheet has a complex flow pattern, in which slow-moving interior ice feeds fast-moving ice streams and outlet glaciers (Figure 1.1). Although the termini of ice streams and outlet glaciers occupy only 13% of the Antarctic coastline, their velocities can exceed 1 km yr^{-1} and they account for as much as 90% of the total ice discharge (*Morgan et al.*, 1982; *Bamber et al.*, 2000; *Cuffey and Paterson*, 2010). Therefore, the dynamics of these ice streams and glaciers fundamentally control the future mass loss of the Antarctic ice sheet.

Early work investigating ice-stream dynamics suggested that most, if not all, of the motion of ice streams is likely accommodated by the ice sliding over the underlying bed, rather than the ice column deforming under its own weight (e.g., *Rose*, 1979; *Budd et al.*, 1984; *Lingle*, 1984). The classical models of basal sliding related sliding velocity to basal shear stress through mechanisms of enhanced ice creep and regelation (i.e., pressure-related melting and freezing) around obstacles in the underlying substrate (e.g., *Kamb and LaChapelle*, 1964; *Weertman*, 1964).

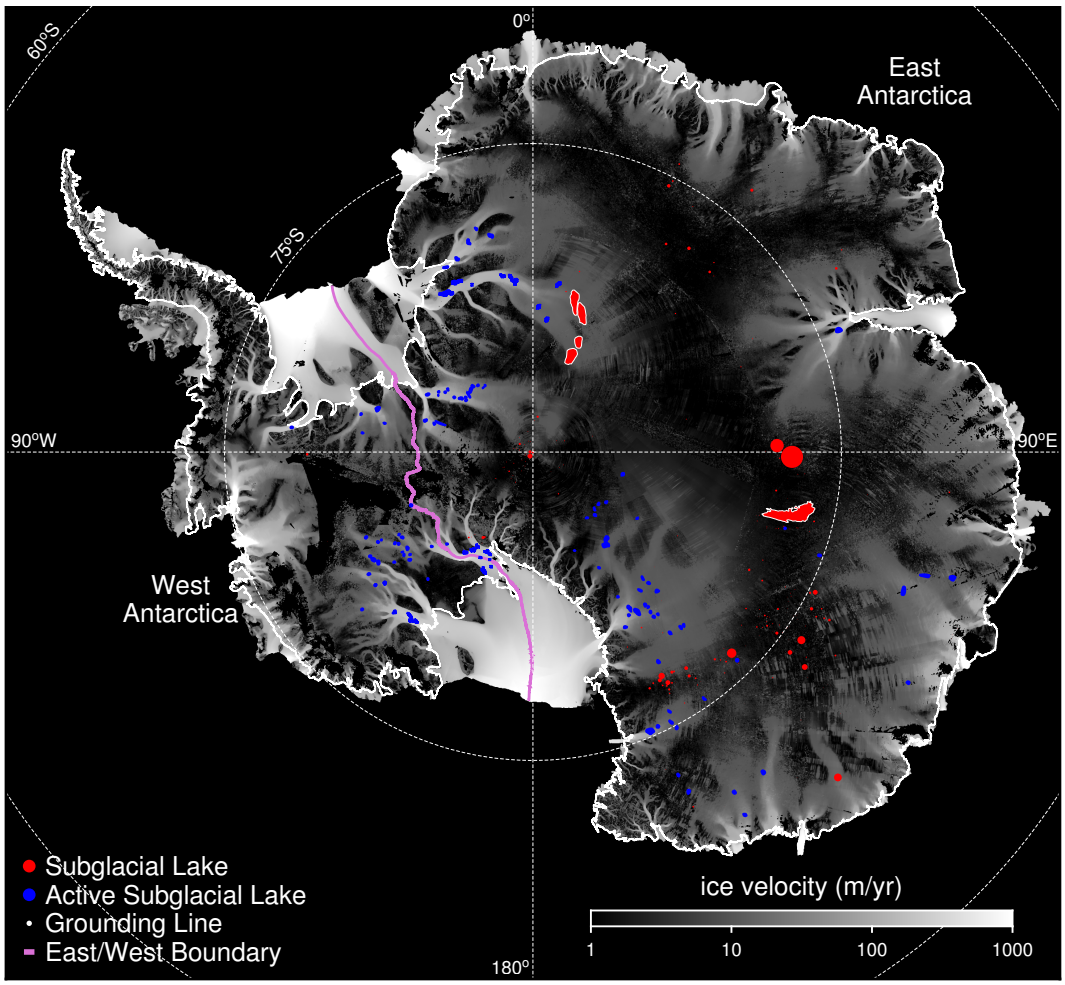

Figure 1.1: Antarctic ice-surface velocity structure and distribution of subglacial lakes. Ice velocity was derived from InSAR (*Rignot et al.*, 2011b), with the boundary of East and West Antarctica from *Zwally et al.* (2012). Active subglacial lakes, with outlines from *Smith et al.* (2009); *Fricker and Scambos* (2009); *Fricker et al.* (2010, 2014), shown in blue; stable subglacial lakes shown as red circles with their size proportional to their inferred volume (*Wright and Siegert*, 2012), except upper Recovery Ice Stream lakes and Subglacial Lake Vostok, whose actual outlines are drawn (*Bell et al.*, 2007; *Studinger et al.*, 2003, respectively). Grounding line from *Scambos et al.* (2007).

These models for basal motion, however, did not seem to fit observations of fast flow since observed velocities increased with constant, or even decreasing, driving stress (*Morgan et al.*, 1982). Evidence from laboratory experiments (e.g., *Budd et al.*, 1979) and observations of mountain glaciers (e.g., *Iken and Bindschadler*, 1986; *Kamb*, 1987) suggested that water played a fundamental role in controlling (and rapidly altering) basal ice motion, but observations of an ice stream sole in Antarctica were sparse (*Kamb*, 2001). At the Whillans Ice Stream (formerly Ice Stream B), West Antarctica, in one of the first field programs dedicated to investigating ice stream basal mechanics, seismic observations and related modeling provided evidence that deformation of a thin (<12 m), water-saturated till underneath the ice column was likely the primary basal process contributing to rapid ice stream motion, confirming the importance of subglacial water to ice flow (*Alley et al.*, 1986; *Blankenship et al.*, 1986).

1.1.3 Antarctic subglacial hydrology

Seasonal meltwater on the surface of mountain glaciers and Greenland can access the bed through the englacial water system, where it can then modulate ice flow speeds (e.g., *Röthlisberger*, 1972; *Zwally et al.*, 2002; *Das et al.*, 2008). In Antarctica, however, there is almost no surface melt, thus the only input into the subglacial hydrologic system is water produced at the bed through basal melting, insulating the basal water system from atmospheric changes (e.g., increased surface temperatures). This subglacial water was hypothesized either to be part of a steady-state transport system required to maintain fast flow (e.g., *Engelhardt and Kamb*, 1997; *Joughin et al.*, 2004b) or to reside in isolated subglacial lakes (e.g., *Kapitsa et al.*, 1996), which were of scientific interest mainly due to the unique biological ecosystem in the lake and the potential of an undisturbed sediment column to

reconstruct ice sheet histories (*Siegert*, 2005). Over timescales of centuries or longer, evolving subglacial hydrology was identified as a possible driver of large-scale ice stream oscillations (e.g., *Alley et al.*, 1994).

More recently, a series of three independent studies identified clusters of spatially-coherent surface-height displacements (O(1–10) m), which were interpreted as the surface expression of subglacial water movement in and out of individual lakes (*Gray et al.*, 2005; *Wingham et al.*, 2006b; *Fricker et al.*, 2007). Water was inferred to move rapidly (timescales of months to years) through these lakes, with drainage that occurred as steady outflow or as an episodic release of water. These dynamic lakes with fluctuating water volumes have since been referred to as "active" subglacial lakes and provide a stark contrast to the previously identified subglacial lakes, which were inferred to be volumetrically stable for centuries to millennia (e.g., *Bell et al.*, 2002).

As a result of their clear surface expression, active lakes could be effectively mapped using remote methods and provided a window into the otherwise inaccessible basal water system. While multiple methods have been used for mapping active subglacial lakes across the ice sheet, the Ice, Cloud, and land Elevation Satellite (ICESat), a NASA laser altimetry mission from 2003 to 2009, has proven to be the most effective tool for this application due to its small footprint and precise observations (see *Fricker et al.* (2015) for additional discussion about different methods for observing active subglacial lakes). Using repeated surveys of the same ground tracks (i.e., repeat-track analysis), *Smith et al.* (2009) performed a continent-wide survey, finding 124 active subglacial lakes over the 4.5-year study period (2003–2008). These lakes tended to be located beneath fast-flowing ice streams and outlet glaciers, unlike the previously-known subglacial lakes, which were located primarily under slow, interior ice (Figure 1.1). Furthermore, linkages

between the filling and draining of nearby lakes indicated that a widespread, complex, dynamic hydrologic system likely exists beneath the most of the Antarctic ice sheet (*Wingham et al.*, 2006b; *Fricker and Scambos*, 2009).

1.1.4 Effect of subglacial lakes on ice dynamics

Active subglacial lakes have the ability to affect ice dynamics well beyond their shorelines as they can temporarily increase or decrease the amount of water available for lubrication of the ice-bed interface downstream. Observations connecting active hydrology in Antarctica to dynamic changes in ice flow, however, are sparse: only two studies have made a connection between the drainage of a subglacial lake and modified ice velocity. At Byrd Glacier, East Antarctica, the release of 1.7 km^3 of water from a subglacial lake correlated to a 14-month period of increased velocity along the 75 km trunk of the glacier (*Stearns et al.*, 2008). On the Antarctic Peninsula, Crane Lake, a previously-undocumented lake beneath Crane Glacier, discharged 0.2 km^3 of water due to a dynamic surface-slope change. While velocities were observed to increase, the specific impact of the change in subglacial hydrology could not be disentangled from the regional changes stemming from the disintegration of the Larsen B Ice Shelf (*Scambos et al.*, 2011).

Episodic subglacial hydrology could also impact ice dynamics by modifying the transport of cold, fresh water and sediment downstream to the ice-ocean boundary, where it then flows into the sub-ice-shelf cavity. Modeling studies have proposed that active subglacial lakes increase the variability in the supply of freshwater to the ocean cavity (*Carter and Fricker*, 2012). Mixing between subglacial meltwater and warm ocean water (e.g., *Jenkins*, 1991, 2011; *Holland*, 2008) as well as deposition of entrained sediment (e.g., *Alley et al.*, 2007; *Anandakrishnan et al.*, 2007; *Dowdeswell et al.*, 2008) likely has significant implications for overall ice sheet

stability. With only a few observations of the interaction between active subglacial hydrology and ice dynamics, the role of non-steady transport of basal water in Antarctica remains unclear.

1.2 Field location

The Whillans Ice Plain is a $\sim 200 \times 100$ km area ($\sim$800 m thick) of fast flowing ice at the confluence of Mercer Ice Stream (formerly Ice Stream A) and Whillans Ice Stream (formerly Ice Stream B) and has eight inter-connected subglacial lakes (*Fricker and Scambos*, 2009). Although the complex subglacial hydrology was only discovered recently (*Fricker et al.*, 2007), this region has been studied extensively since 1963 (*Thomas et al.*, 1984; *Bindschadler et al.*, 1987; *Whillans et al.*, 1987; *Joughin et al.*, 1999, 2002, 2005; *Beem et al.*, 2014). Due to the ongoing research in the area, when the inter-connected subglacial system was discovered, the region was quickly instrumented with Global Positioning System (GPS) stations to monitor for dynamic changes related to subglacial hydrology.

An array of up to 23 continuous GPS stations were deployed between 2008 and 2010 to monitor both horizontal and vertical change at multiple locations across the ice plain (Figure 1.2); this experiment was the first of its kind specifically designed to detect dynamic changes related to subglacial hydrology. Whillans Ice Plain was also the field location for the National Science Foundation's Whillans Ice Stream Subglacial Access Research Drilling (WISSARD) project (2010–2015). This project culminated with the successful sampling of a subglacial lake in January 2013 (*Tulaczyk et al.*, 2014), marking the first conclusive evidence demonstrating a hydrological feature beneath a surface-height anomaly mapped from space. The long history of investigation on Whillans Ice Plain, as well as direct sampling of a subglacial lake, provide context to modern observations unlike any other location

in Antarctica.

1.3 Scientific questions of this dissertation

Due to in part to the scarcity of data (*Flowers*, 2015), subglacial hydrology and its relationship to basal sliding has, in one form another, been an open question since the 18th century (*Clarke*, 1987). Active subglacial hydrology in Antarctica is a recently-discovered process, with only two coarse connections to ice dynamics (*Stearns et al.*, 2008; *Scambos et al.*, 2011). Our existing record of basal water movement is short, but since subglacial hydrology and ice dynamics coevolve with each other, unraveling the underlying driver of any change in ice stream behavior will require detailed, long-term context to any observations. The overarching goal of the dissertation is then to decrease the observational scarcity and use our new, longer datasets to provide insight into the physical processes that allow for rapid ice stream motion.

With this in mind, this dissertation revolves around three main objectives:

1. Extend the observational record of active subglacial lakes,

2. Assess the impact of subglacial lake drainage events on regional ice dynamics, and

3. Investigate processes that affect subglacial water transport as it nears the grounding line.

An important aspect embedded in each of these questions is the role of spatiotemporal variability. Extending the record of active lakes is a requirement to answer even basic questions about the variability inherent in the system: Are these permanent or ephemeral features? Does a lake exhibit the same behavior

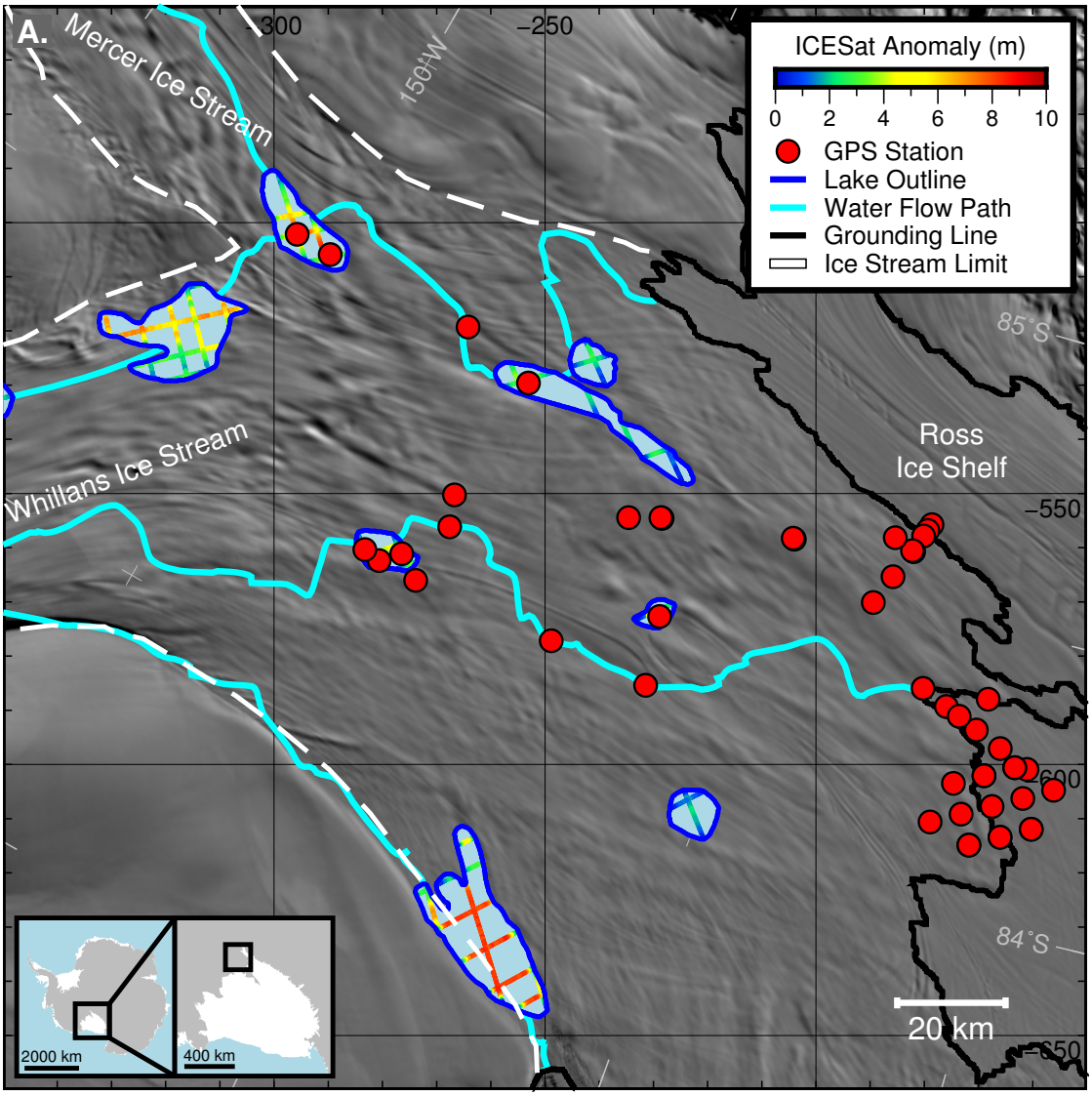

Figure 1.2: Map of GPS stations deployed on Whillans Ice Plain for at least one year between 2007 and 2015. ICESat height-change anomaly amplitudes and lake outlines are from *Fricker and Scambos* (2009); subglacial water flow paths are from *Carter et al.* (2013). Background imagery and grounding line (black) are from the MODIS Mosaic of Antarctica (MOA) (*Scambos et al.*, 2007); limit of fast ice flow is based on *Rignot et al.* (2011b). Projection is south polar stereographic (in km) with standard latitude at 71°S.

every time it drains? Are hydrologic connections between lakes maintained between fill/drain cycles? Spatial variability is especially important to think about when considering the impact on dynamics. The substrate underlying the Antarctic ice sheet varies immensely, from crystalline bedrock to loosely-consolidated, fully-saturated sediments. These geologic differences, along with geometric differences (e.g., surface and basal slopes), will influence any dynamic ice response to increased water flux. While I will address these questions in this dissertation, a true "answer" will require a community-wide effort over many decades to capture the full continuum of active subglacial lakes, their impact on ice dynamics, and how their discharge enters the ocean.

1.4 Outline of the Dissertation

This dissertation is divided into six chapters. The next four chapters were written to be stand-alone documents, which necessarily requires some overlap in material. **Chapter 2** focuses on the lakes of the Whillans Ice Plain to develop a new method for extending the observational record of active subglacial lakes in Antarctica using CryoSat-2 radar altimetry, the only polar-orbiting altimetry mission since the end of the ICESat mission in October 2009. This chapter was published in *Geophysical Research Letters* in January 2014. **Chapter 3** applies the method developed in **Chapter 2** to the continent-wide inventory of active subglacial lakes to understand better the spatiotemporal variability of subglacial lakes. This chapter is in preparation for publication. **Chapter 4** investigates the dynamic ice response of a subglacial lake drainage event using GPS-derived velocity estimates. This chapter, in full, has been submitted for publication to *Geophysical Research Letters*. **Chapter 5** explores the impact of two tidally-driven processes on the mixing of subglacial water with seawater near the grounding line using GPS

observations and modeling techniques. This chapter is also being prepared for publication. Finally, **Chapter 6** provides some concluding remarks and discusses avenues for future research.

Chapter 2

A decade of West Antarctic subglacial lake interactions from combined ICESat and CryoSat-2 altimetry

2.1 Abstract

We use CryoSat-2 interferometric satellite radar altimetry over the Mercer and Whillans ice streams, West Antarctica, to derive surface elevation changes due to subglacial lake activity at monthly resolution for the period 2010 to 2013. We validate CryoSat-2 elevation measurements, trends, and spatial patterns of change using satellite image differencing and *in situ* vertical movement from Global Positioning System (GPS) data. Two subglacial lake discharge events occur in the same subglacial hydrological catchment within a nine-month period. Using GPS measurements spanning the gap between the ICESat and Cryosat-2 missions, we cross-calibrate the two missions to establish the efficacy of CryoSat-2 altimetry to measure dynamic changes on the ice sheets.

2.2 Introduction

Water beneath an ice sheet provides lubrication at the ice-bed interface and may cause increased ice flow velocities (e.g., *Kamb*, 1987); this in turn would lead to increased ice mass flux and reduce the net mass balance of the ice sheet. Understanding the distribution of subglacial water and its changes over time is therefore critical to modeling ice dynamics and predicting ice sheet evolution (e.g., *Le Brocq et al.*, 2009). While the existence of subglacial lakes in Antarctica has long been known (*Robin et al.*, 1970), until recently they were thought to be isolated and in a steady state (e.g., *Kapitsa et al.*, 1996; *Christoffersen and Tulaczyk*, 2003; *Parizek et al.*, 2003; *Siegert*, 2005).

Recent work has shown that lake volume changes cause surface displacements that are detectable in satellite data, e.g., interferometric synthetic aperture radar (InSAR) images (*Gray et al.*, 2005) or satellite radar and laser altimetry (*Wingham et al.*, 2006b; *Fricker et al.*, 2007). These three pivotal studies demonstrated that water in active subglacial lakes can move through the hydrologic system rapidly (on the order of months) and fill-drain cycles can occur as quasi-steady flow or as episodic flooding events. Linkages between the filling and draining of adjacent lakes indicate that a widespread, complex hydrologic system exists beneath the lower Mercer and Whillans ice streams (formerly ice streams A and B, respectively). It is likely that many other ice streams and large glaciers have similar hydrologic systems (*Wingham et al.*, 2006b; *Fricker and Scambos*, 2009). The implications of a dynamic subglacial hydrologic regime on ice dynamics and ice-sheet mass balance are not yet fully understood (*Bell*, 2008; *Bell et al.*, 2011); however, at Byrd Glacier, East Antarctica, a subglacial discharge event caused a temporary 10% increase in ice velocity, which was sustained for 14 months and ceased at the same time as the

termination of the flood (*Stearns et al.*, 2008).

The Ice, Cloud, and land Elevation Satellite (ICESat) laser altimetry mission has proven to be the most effective method to date for mapping of subglacial water movement due to its small footprint (∼70 m), dense along-track spacing of independent elevation measurements, and high vertical accuracy (*Fricker et al.*, 2007; *Fricker and Scambos*, 2009; *Smith et al.*, 2009; *Fricker et al.*, 2010). However, ICESat operated only 2–3 times per year for six-years (2003–2009), limiting its ability to determine recurrence intervals or resolve sub-annual aspects of the fill-drain cycle. Past pulse-limited satellite radar altimeters (e.g., Envisat) cannot fill these temporal gaps due to their large footprints and uncertainties over undulating topography (*Fricker et al.*, 2010). Acquisition of InSAR data is infrequent over Antarctica (*Gray et al.*, 2005). CryoSat-2, a satellite radar altimeter with three acquisition modes (*Wingham et al.*, 2006a), shows the greatest promise of extending the six-year window of the ICESat mission with accurate, frequently acquired elevation data.

To date, only one study has used CryoSat-2 interferometric radar altimetry (SARIn mode) to extend the ICESat subglacial lake time-series (at Cook E2 in East Antarctica) (*McMillan et al.*, 2013). Here we examine CryoSat-2's efficacy for monitoring far smaller vertical displacements associated with cyclic lake fill-drain events.

2.3 Data and Methods

2.3.1 Field Area and Lake Activity from ICESat

Lower Mercer and Whillans ice streams (MIS/WIS) cover an area of ∼200 × 100 km (∼800 m thick); in this region these ice streams are fast flowing and

lightly grounded having a hydrologic system comprised of eight inter-connected subglacial lakes (Figure 2.1) (*Fricker and Scambos*, 2009). These lakes fall into three subglacial-hydrological catchments: the southern basin including Subglacial Lake Conway (SLC), Subglacial Lake Mercer (SLM), and Lake 7 (L7), the central basin including Subglacial Lake Whillans (SLW), and the northern basin including Subglacial Lake Engelhart (SLE) (*Fricker et al.*, 2007). *Fricker et al.* (2007) first mapped MIS/WIS's subglacial lakes and studied their activity using ICESat and since then the time series have been incrementally updated (*Fricker and Scambos*, 2009; *Fricker et al.*, 2011; *Carter et al.*, 2013). We use the most recent ICESat time-series from *Carter et al.* (2013).

2.3.2 GPS

Following the discovery of the MIS/WIS subglacial lakes (*Fricker et al.*, 2007), an array of long-term continuous Global Position System (cGPS) stations was deployed in 2007 to monitor lake activity. In 2009, this array evolved into the Whillans Ice Stream Subglacial Access Research Drilling (WISSARD) cGPS array, consisting of 23 GPS stations with 11 focused on and around the lakes, recording at either 15- or 30-second intervals (Figure 2.1). Telemetry issues resulted in only sporadic data from SLM after January 2012 (9.4% of 2012 data were telemetered) and constraints on field logistics prevented more recent data collection.

We processed GPS data using precise point positioning (PPP) techniques in kinematic mode implemented by Natural Resources Canada's online tool CSRS-PPP, and corrected the resulting elevation measurements for antenna elevation above the ice surface and advection of the unit downstream using the 125 m CryoSat-2 DEM described below (see Table 2.1 for correction values). We did not correct for vertical advection due to firn compaction or regional ice dynamical changes, as

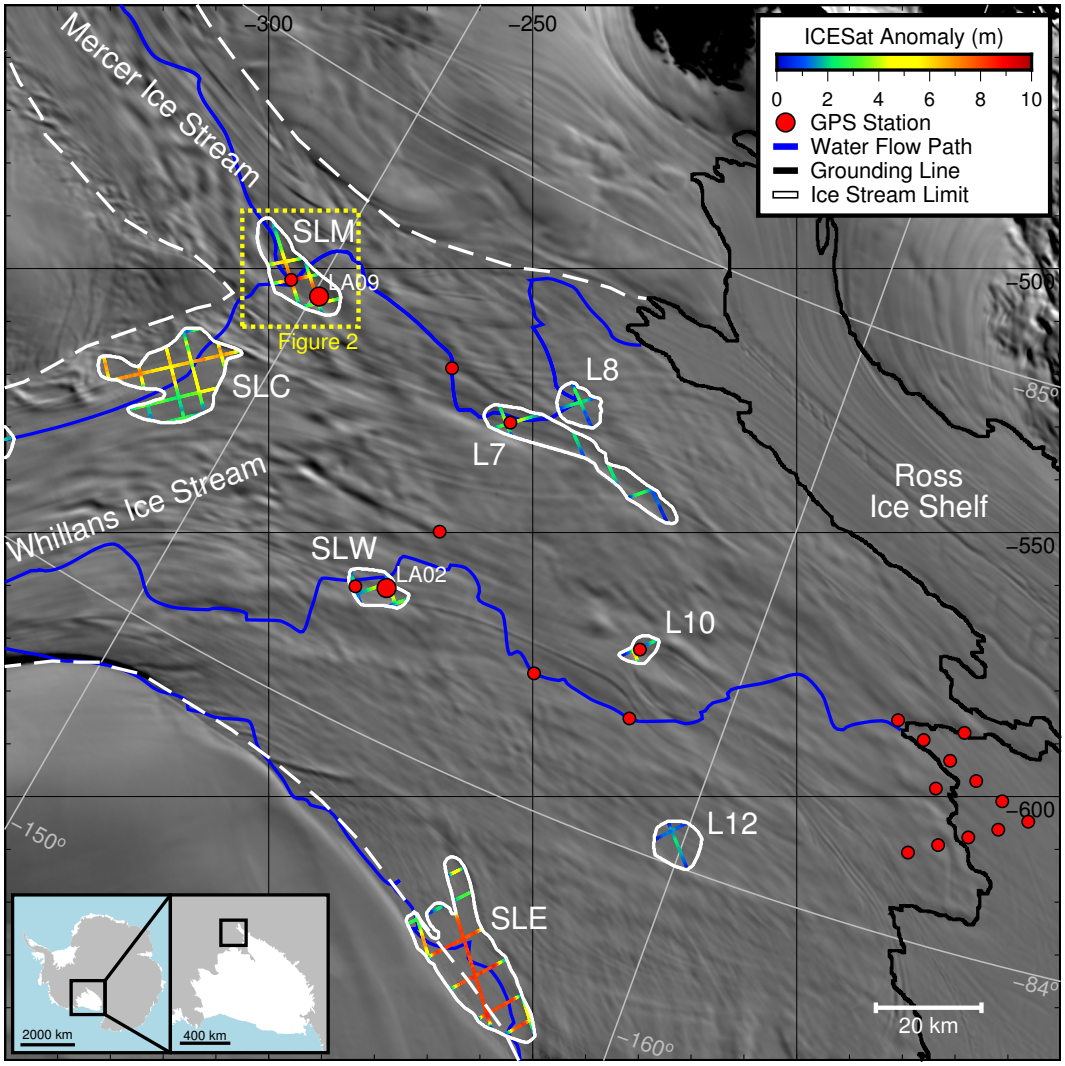

Figure 2.1: Overview of the lower Mercer/Whillans ice streams showing its inferred subglacial water system (SLC = Subglacial Lake Conway, SLM = Subglacial Lake Mercer, SLW = Subglacial Lake Whillans, SLE = Subglacial Lake Engelhardt, L7 = Lake 7, L8 = Lake 8, L10 = Lake 10, and L12 = Lake 12). ICESat elevation change anomaly amplitudes and lake outlines are from *Fricker and Scambos* (2009); subglacial water flow paths are from *Carter et al.* (2013). Background imagery and grounding line (black) are from the MODIS Mosaic of Antarctica (MOA) (*Scambos et al.*, 2007); limit of fast ice flow is based on *Rignot et al.* (2011b). Projection is south polar stereographic (in km) with standard latitude at 71°S.

these are unknown and highly spatially-variable values, though both are likely on the order of decimeters (c.f., *Pritchard et al.*, 2009).

Repeat-track analysis of ICESat data over active lakes shows that the surface elevation change signals are spatially variable across a lake (*Fricker and Scambos*, 2009); therefore, elevation changes at the point location of the GPS station do not reflect the elevation change averaged over the entire lake area derived from ICESat and CryoSat-2 data (hereafter referred to as "lake-averaged"). To account for this, we assume that the elevation changes at the GPS location are proportional to the lake-averaged changes, and we scale the GPS measurements to a lake-averaged value based on the ratio of changes in GPS elevation to lake-averaged changes during periods where we have both satellite altimeter and GPS measurements. Before scaling, we subtract the mean January–June 2012 elevation for consistency with the CryoSat-2 methods described below.

2.3.3 CryoSat-2

CryoSat-2's Synthetic aperture radar Interferometric Radar ALtimeter (SIRAL) instrument has three modes: (1) Low Rate Mode (LRM), a conventional pulse-limited radar altimeter active over the oceans and interior of the ice sheets; (2) Synthetic Aperture Radar (SAR) mode, which uses beam-forming for high along-track spatial resolution over sea-ice areas; and (3) SAR Interferometric (SARIn) mode, which uses the phase difference between two on-board antennas to precisely determine the across-track location of the return echo within the SAR footprint (*Wingham et al.*, 2006a). SARIn mode is active over areas of steep ice terrain, e.g., the ice sheet peripheries, ice caps, and mountain glaciers. We used L2 (Baseline-B release) SIRAL SARIn-mode data over lower MIS/WIS, which at the time of writing is available for the following time periods: July, August, November,

and December 2010; March, April, May, June, and July 2011; and November 2011 until August 2013.

SARIn mode is an innovative measurement scheme with no analogue from previous satellite altimeters. The interferometric technique measures the point on the undulating ice sheet terrain closest to the satellite's position, resulting in a "wandering" ground track (Figure 2.2a) with small footprints (380–410 m along track, ∼1.3 km across-track at nadir, see *McMillan et al.* (2013)). With non-repeating ground-tracks, methods such as crossover analysis (e.g., *Fricker and Padman*, 2002; *Shepherd et al.*, 2003; *Zwally et al.*, 2005) and repeat-track analysis (e.g., *Fricker et al.*, 2007; *Smith et al.*, 2009) previously used for data quality assessment and/or ice surface elevation changes (dz/dt) are ineffective. We used an overlapping footprint method over a 100 × 100 km region on MIS/WIS for estimating the precision of SARIn-mode data and determined it was ±0.50 m (Table 2.1). New methods need to be developed for estimating dz/dt from SARIn track data.

To avoid spatial biases that result from subsampling the full repeat-orbit, the SARIn-mode measurements must be corrected for local topography before calculating dz/dt. To determine this correction, we first created a high-resolution DEM of each lake and the adjacent surrounding area using six months of SARIn-mode data (January to June 2012). We applied a 3σ filter on elevation measurements and removed returns with anomalously high backscatter ($\sigma_0 > 30$ dB), then interpolated using a cubic spline in tension (*Sandwell*, 1987) and gridded the resulting data at 125 m spacing. For all SARIn-mode data, we subtracted the interpolated DEM elevation at the measurement location in order to obtain a topography-independent elevation estimate.

We used a time step, dt, of one month for SLW and SLC and two months

for SLM to obtain better spatial coverage over the oblong lake. We filtered the topography-independent SARIn-mode elevation measurements in each time interval using a 3σ filter and evaluated dz/dt in three ways: (i) spatially across the lake, (ii) at the exact GPS location, and (iii) lake-averaged to compare to the ICESat time-series.

(i) To observe spatial variation of elevation changes, we created a lake-surface DEM from CryoSat-2 data posted at 500 m for each time epoch (e.g., Figure 2.2a). (ii) For each of the DEMs from (i), we interpolated the elevation value at the GPS location for direct comparison to the GPS data (e.g., Figure 2.2c). (iii) To calculate lake-averaged elevation changes from CryoSat-2 data, we separated the measurements on the lake from those off the lake at each time step and calculated individually the mean of each set. We subtracted the mean of the off-lake points from the mean of the on-lake points to obtain a lake-averaged surface elevation that is independent of surface-topography and regional-scale ice-surface changes. We propagated errors formally, but also calculated the standard deviation of the on-lake points as this represents the spatial variability of elevation change across the lake (Tables 2.2, 2.3, 2.4).

2.3.4 Merging of ICESat, GPS, and CryoSat-2 datasets

The continuous, ground-based GPS data overlapping both the CryoSat-2 and ICESat missions are critical to merging the ICESat-derived lake-activity time series with the new CryoSat-2 time-series. While the elevations in all three datasets are lake-averaged values, they each calculate changes relative to a different location and epoch: ICESat is referenced to the campaign Laser 2a lake-averaged elevation; scaled GPS to the elevation at the GPS location during January–June 2012; and CryoSat-2 to the January–June 2012 CryoSat-2 DEM lake-averaged elevation. In

order to maintain consistency with the existing record (*Carter et al.*, 2013), we want to reference all elevations to the lake-averaged ICESat elevation during campaign Laser 2a.

We first corrected the scaled GPS time series to the CryoSat-2 reference epoch using an offset calculated from the difference between the lake-averaged elevation of the CryoSat-2 DEM and the interpolated DEM elevation at the GPS location. This combined GPS/CryoSat-2 time series is now referenced to the lake-averaged elevation at the epoch of the CryoSat-2 DEM. To merge this dataset with the ICESat time series, we subtracted the difference in scaled GPS elevation between the DEM epoch and an epoch of overlapping GPS and ICESat data. Finally we correct for the difference between ICESat elevation during the overlapping GPS/ICESat campaign and campaign Laser 2a. The resulting time series is lake-averaged elevation history where 0 is the lake-averaged elevation during ICESat campaign Laser 2a.

When GPS data were unavailable, we corrected the lake-averaged CryoSat-2 time-series to the ICESat elevation reference by subtracting the difference between the mean ICESat elevation during campaign Laser 2a and mean CryoSat-2 lake elevation during the first month of data (August 2010).

2.4 Results and Discussion

We found dynamic elevation change signals in four of the eight lakes in the study region: SLM, SLW, SLC, and L7. We focus on the two lakes for which we have GPS spanning the gap between the ICESat and CryoSat-2 (SLM and SLW). Results are also presented from SLC to highlight that the CryoSat-2 mission, like the ICESat mission, allows us to explore dynamic changes even in the absence of additional data. While we find $\sim$2 m of dynamic elevation variations at L7 that overlap with (and are comparable to) GPS data, these events do not provide

additional insight into the use of CryoSat-2 data for recovering dynamic changes and thus are beyond the scope of this paper.

2.4.1 Subglacial Lake Mercer (SLM)

Validation of Spatial Elevation Changes

At SLM, CryoSat-2 data suggest a slow, steady inflation of the lake surface through mid-2012, which reaches a maximum in July/August (Figure 2.2c, 2.3a). After the ice surface reaches its maximum elevation, a spatially variable deflation initiates near the center of the MODIS-derived lake outline from *Fricker and Scambos* (2009) (Figure 2.2a). The surface elevation minimum expands longitudinally across the southern portion of the lake, then widens in the final two months of the year-long flood. At the conclusion of the event, the minimum surface elevation is 17 m lower than at high-stand, which is twice the magnitude of the ICESat signal (*Fricker and Scambos*, 2009). These new insights are a direct result of the spatial resolution afforded by non-repeat, "wandering" ground tracks.

We validated the spatial pattern of elevation change by comparing it to a slope-change map that we derived from MODIS image differencing, following the methods of *Fricker et al.* (2007), *Fricker and Scambos* (2009), and *Bindschadler et al.* (2010). Image differencing is conducted by subtracting two composite images (in this case, MODIS images of a snow-covered surface) with near-identical illumination and viewing geometry. It has been used successfully in multiple regions for ice-surface change detection (see Section 2.6.1).

To simulate the MODIS-derived slope change map using CryoSat-2 data, we calculated the difference between the two CryoSat-2 DEMs coincident with the MODIS images (Nov/Dec 2011 and Jan/Feb 2013). We then computed the Lambertian radiance given the mean azimuth and solar illumination angle from

the MODIS images. The similarity between the synthetic MODIS image difference (Figure 2.2b, left panel) and the actual MODIS image difference (Figure 2.2b, right panel) demonstrates that the spatial patterns of elevation change of this magnitude over areas of 10s of km^2 can be retrieved from CryoSat-2 SARIn-mode data on timescales as short as 60 days.

Validation of Elevation Change Time-Series

We compared the CryoSat-2-derived elevation time-series to the GPS elevation time-series using the elevations derived from the two-monthly CryoSat-2 DEMs interpolated to the GPS location (Figure 2.2c). The GPS elevation was consistently higher than the CryoSat-2 elevation by 1.70 ± 0.60 m, 0.67 m of which is a result of known ESA processing errors (*McMillan et al.*, 2013). We assumed that most of the remaining elevation bias is a result of volume scattering of the radar signal within the snowpack (*Davis and Moore*, 1993). A robust estimation of this bias is needed to combine datasets from radar altimetry and laser altimetry, where surface penetration does not occur (*Fricker and Padman*, 2012). Our estimate for the average penetration bias of the CryoSat-2 altimeter in SARIn mode over SLM was 0.73 ± 0.60 m; this value likely varies spatiotemporally due to changing surface conditions (e.g., *Davis and Zwally*, 1993).

To compare GPS and CryoSat-2 elevation changes for SLM, we applied several corrections to both datasets (Table 2.1). After these corrections, the average difference between the GPS and CryoSat-2 time-series was 0.25 ± 0.16 m (1σ), which included the poorly-telemetered GPS data after January 2012. Even with the low-quality GPS data, the trends from the GPS and CryoSat-2 during filling (0.49 m yr^{-1} and 0.55 m yr^{-1}, respectively) and draining (-10.5 m yr^{-1} and -9.1 m yr^{-1}) are consistent, with most of this difference likely resulting from our

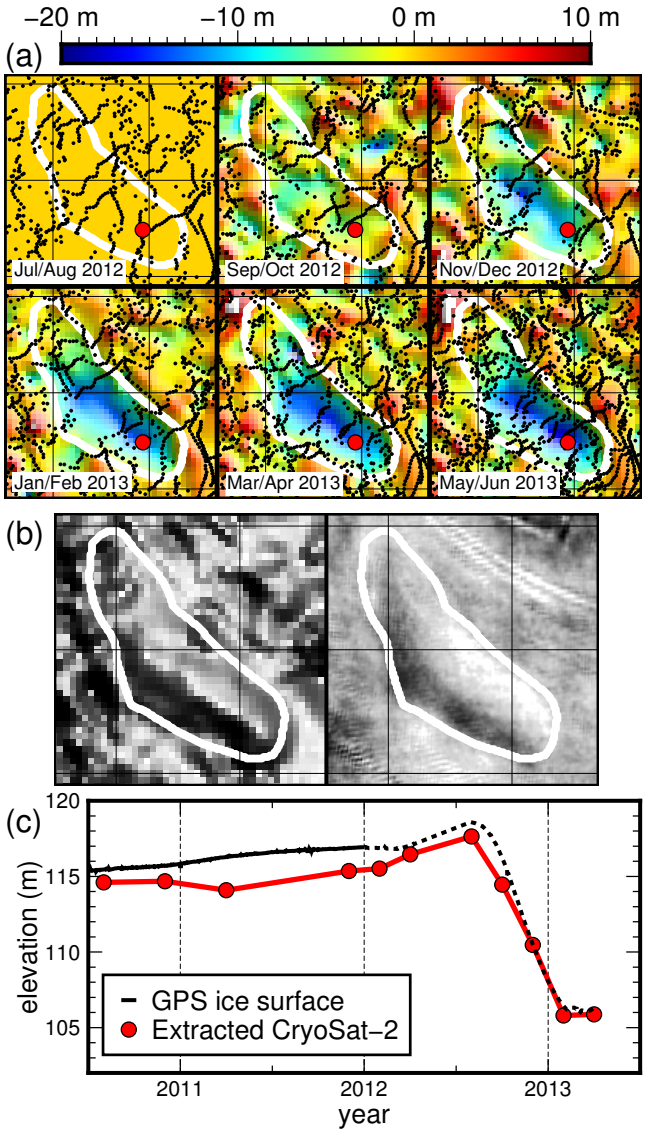

Figure 2.2: Spatial and temporal validation of CryoSat-2 SARIn-mode altimetry data at Subglacial Lake Mercer: (a) spatial evolution of a subglacial lake discharge event at SLM, with individual CryoSat-2 footprints (black dots) and location of GPS station (red circle). Gridlines are at 10 km spacing. Elevations are relative to the first CryoSat-2 DEM (July/August 2012); (b) comparison between synthetic MODIS image difference (left panel) and actual MODIS image difference (right panel) between November 2011 and January 2013; (c) comparison of GPS data (black) and CryoSat-2 data (red circles) interpolated from DEMs at the GPS location. Dashed black line indicates lower quality GPS data since January 2012.

assumption of linearity for scaling a point measurement to a lake average.

Extended SLM Time-Series

The combined ICESat/GPS/CryoSat-2 SLM time series (Figure 2.3a) provides an activity record that spans over a decade, from February 2003 to August 2013. The temporal resolution of the CryoSat-2 data at SLM is a factor of 2–3 higher than that of the ICESat mission, while the GPS data is a factor of $\sim 10^6$ higher. Instead of two points defining a subglacial discharge event as we had for the 2005–2006 event from ICESat (*Fricker et al.*, 2007), the two-month sampling of CryoSat-2 provides five points and the *in situ* GPS yields over a million (at 15-second resolution). With the increased resolution, the new time series reveals previously unseen details of subglacial floods. For example, both the CryoSat-2 and GPS time-series show a sharp elevation increase directly before the onset of flooding (Figure 2.3a). These new details provide information about how subglacial drainage events initiate, which will help better constrain models of subglacial evolution and, ultimately, how they affect larger-scale ice dynamics.

2.4.2 Subglacial Lake Whillans (SLW)

Following the same methods used for SLM we combined elevation changes derived from ICESat, GPS and CryoSat-2, using corrections as shown in Table 2.1, and an averaging interval of one month for the CryoSat-2 data. The resulting lake-averaged activity time-series spans almost a decade (October 2003–August 2013). The 2008/2009 drainage event reported by *Fricker and Scambos* (2009) was captured by both the ICESat and GPS (Figure 2.3b). The effects of the lower temporal and spatial resolution of the ICESat can be seen by comparing the two time series: ICESat both missed the peak lake stand and underestimated the

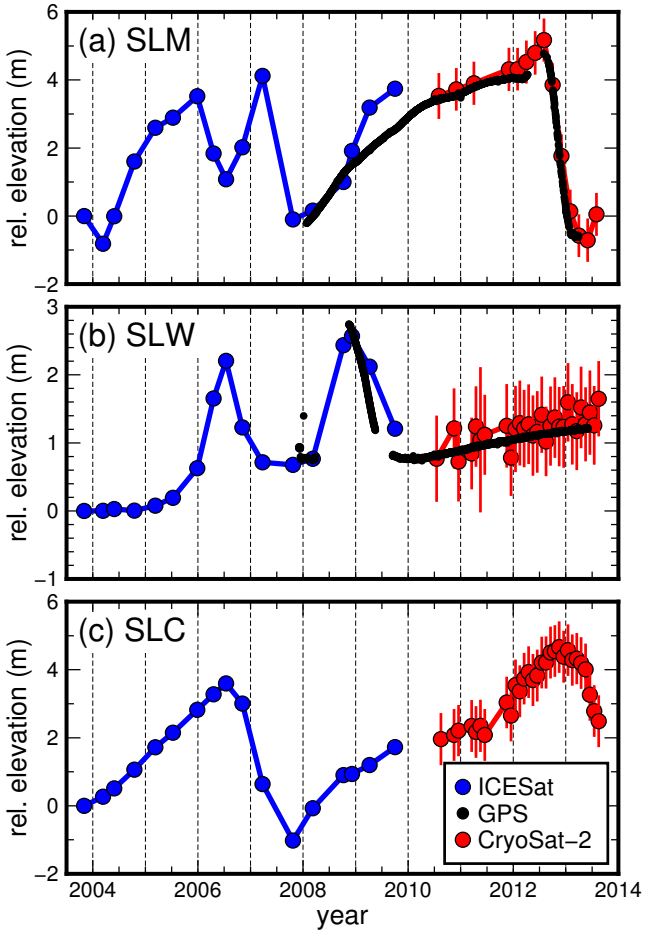

Figure 2.3: Ten-year time series of subglacial lake activity at (a) Subglacial Lake Mercer, (b) Subglacial Lake Whillans, and (c) Subglacial Lake Conway, from ICESat laser altimetry, scaled GPS data, and lake-averaged CryoSat-2 SARIn-mode radar altimetry. Error bars on CryoSat-2 data are formal error estimates.

discharge rate.

Since the 2008–2009 drainage event, the surface elevation of SLW has been steadily increasing; we infer that this is due to either the lake filling from a constant supply of local water after a flow-switching event (*Carter et al.*, 2013) or dynamic thickening resulting from variable velocities on and off the lake (*Beem et al.*, 2014). Regardless of the cause, this constant surface elevation increase allows for an assessment of how accurately CryoSat-2 SARIn mode estimates surface elevation trends. We compare dz/dt estimates for the overlapping time period during which CryoSat-2 is uninterrupted (January 2012 to May 2013), and find CryoSat-2 data (0.121 ± 0.173 m yr^{-1}) and GPS data (0.113 ± 0.001 m yr^{-1}) yield similar results. Although this is a relatively low dz/dt, CryoSat-2 SARIn mode estimates it to within 7% of the GPS-measured value, endorsing SARIn mode as a valuable method for estimating both large-magnitude, short-term and small-magnitude, long-term changes in dz/dt in Antarctica and Greenland.

2.4.3 Subglacial Lake Conway (SLC)

With no ground-based GPS at SLC to provide a penetration bias estimate, we cannot combine accurately the ICESat and CryoSat-2 time-series. Instead we:

- use an average penetration bias from SLM and SLW,
- apply the -0.67 m processing bias, and
- subtract the difference between the mean ICESat lake elevation during campaign Laser 2a (112.8 m) and mean CryoSat-2 lake elevation during August 2010 (115.2 m).

Qualitatively, the resulting time series (Figure 2.3c) appears to be consistent over the data gap.

Our decade-long record shows two SLC fill-drain events separated by 6.5 years. Previously only one fill-drain cycle had been observed and it was not clear if SLC repeats its hydrologic activity. The high-resolution record also reveals that the onset of the drainage event occurred rapidly after the lake had remained at high stand for 6 months. The estimated surface lowering rate of -6.1 m yr^{-1} corresponds to a discharge of 48.3 m^{3}s^{-1}, significantly higher than the mean ICESat-derived discharge estimate of 29.0 m^{3}s^{-1}. This difference in discharge rate is within the uncertainty resulting from the infrequent temporal sampling of the ICESat time-series. We also note that this is the second time that SLC, which is hydrologically connected to SLM and $\sim$30 km away at a higher hydropotential, apparently started to drain nine months after the onset of SLM drainage. Investigations into the ability of downstream events to "trigger" events upstream, which could illuminate a new mechanism for the propagation of downstream changes toward the ice sheet interior, are on-going.

2.5 Summary

We used GPS data from the Whillans and Mercer ice streams to link the new CryoSat-2 time-series (2010 to present) with the existing ICESat-derived time series (2003–2009) to create a history of subglacial lake activity on MIS/WIS that now spans nearly a decade (October 2003 to present). Our time series reveal two new large subglacial lake drainage events within MIS/WIS's northern basin in 2012 and 2013. This longer, ground-truthed time-series is essential to building our mechanistic understanding of the evolution of the subglacial hydrological system and its effect on ice dynamics. The relatively small footprint of CryoSat-2 SARIn-mode data combined with the spatial coverage due to non-repeating ground tracks results in a powerful altimetry dataset that can build upon the critical ice-sheet-wide

dynamic changes discovered through the ICESat mission.

2.6 Auxiliary Material

2.6.1 Supplemental Methods

MODIS Image Differencing

Composite MODIS images are generated by selecting multiple sets of images, each with cloud-free coverage of the study region and with viewing and illumination parameters as consistent as possible (typically UTC acquisition times within a 90 minute window, solar azimuths within a 15° range, solar elevation within a 10° range, and near-nadir). These images are then processed to remove whisk-broom sensor noise ('striping') from them, and (in this case) regridded to the MODIS Mosaic of Antarctica grid (MOA) (*Haran et al.*, 2002; *Scambos et al.*, 2007). The image histograms are normalized to the same mean value and then the images in a set are averaged. Images within a set have acquisition dates within a few weeks range; sets are separated in time by a few months on either side of solstice (e.g., a set centered on ∼1 November and a second set centered on ∼10 February, each set about 50 days on either side of solstice), or are separated by an integer number of years. Differencing is simple subtraction of the two identically-gridded composite images. Note that all transient features, and many effects from any non-uniform illumination components, will be present in the difference image. See Table 2.5 for details of the images used in this study.

2.6.2 Supplemental Tables and Figures

Table 2.1: Corrections and uncertainties

Correction	SLM	SLW	SLC
GPS Antenna Height (m)	1.38	1.68	N/A
GPS Scaling	2.32	2.08	N/A
SARIn Measurement[a] (m)	± 0.50	± 0.50	± 0.50
Topography[b] (m)	Variable ± 2.34		
CS2 Penetration (m)	0.73 ± 0.60	0.76 ± 0.41	N/A
ESA Processing (m)	-0.67	-0.67	-0.67
$\bar{z}_{lake} - \bar{z}_{GPS}$ (m)	-0.94	-1.32	N/A

[a]CryoSat-2 precision determined by extracting the data from one full orbit cycle (i.e., 369 days) over a 100 x 100 km region on WIP (89,313 footprints total). Within this box, we found all the footprints that are within 150 m of each other (i.e. overlap by at least 50% of the along-track footprint resolution) and were measured within 30 days (2,308 pairs). For each pair, we calculated the elevation difference and filtered for outliers using an iterative 3σ edit (*Shuman et al.*, 2006), which removed 308 pairs. We took the standard deviation of the differences to represent the single-shot precision of SARIn-mode over WIP.

[b]Topography correction (for both GPS and CryoSat-2) uncertainty calculated using 100 iterations of a Monte Carlo simulation, randomly selecting 90% of the data points to create the DEM and using the remaining 10% of the data to assess error. The resulting error estimate, which is likely an overestimate of the true error, is normally distributed as -0.01 ± 2.34 m.

Table 2.2: Subglacial Lake Mercer relative elevations, standard deviations, and formal errors of lake-averaged dz/dt

Month	Elevation (m)	1σ (m)	Formal Error (m)
Jul 2010 Aug 2010	3.53	3.03	0.67
Nov 2010 Dec 2010	3.72	1.82	0.63
Mar 2011 Apr 2011	3.90	3.96	0.63
May 2011 Jun 2011			
Nov 2011 Dec 2011	4.31	1.44	0.63
Jan 2012 Feb 2012	4.32	1.23	0.63
Mar 2012 Apr 2012	4.53	1.16	0.63
May 2012 Jun 2012	4.80	1.41	0.64
Jul 2012 Aug 2012	5.17	2.04	0.64
Sep 2012 Oct 2012	3.85	1.93	0.64
Nov 2012 Dec 2012	1.77	3.64	0.64
Jan 2013 Feb 2013	0.14	3.97	0.63
Mar 2013 Apr 2013	-0.58	4.57	0.63
May 2013 Jun 2013	-0.71	4.15	0.64
Jul 2013 Aug 2013	0.05	4.79	0.63

Table 2.3: Subglacial Lake Whillans relative elevations, standard deviations, and formal errors of lake-averaged dz/dt

Month	Elevation (m)	1σ (m)	Formal Error (m)
Jul 2010	0.77	1.33	0.63
Aug 2010	N/A	N/A	N/A
Nov 2010	1.21	1.05	0.59
Dec 2010	0.72	0.97	0.59
Mar 2011	0.84	1.14	0.53
Apr 2011	1.24	0.87	0.59
May 2011	1.05	0.53	1.07
Jun 2011	1.12	0.48	0.59
Nov 2011	1.25	0.44	0.61
Dec 2011	0.78	0.98	0.56
Jan 2012	1.20	0.30	0.63
Feb 2012	1.29	0.87	0.62
Mar 2012	1.21	0.37	0.57
Apr 2012	1.27	0.35	0.59
May 2012	1.11	0.31	0.59
Jun 2012	1.16	0.38	0.60
Jul 2012	1.41	0.65	0.56
Aug 2012	1.02	1.34	0.51
Sep 2012	1.25	0.57	0.58
Oct 2012	1.37	0.54	0.59
Nov 2012	1.24	0.78	0.58
Dec 2012	1.24	0.38	0.60
Jan 2013	1.60	0.71	0.59
Feb 2013	1.27	0.90	0.59
Mar 2013	1.17	0.48	0.73
Apr 2013	1.52	0.26	0.60
May 2013	1.27	0.51	0.54
Jun 2013	1.45	0.51	0.62
Jul 2013	1.26	0.78	0.58
Aug 2013	1.65	0.68	0.55

Table 2.4: Subglacial Lake Conway relative elevations, standard deviations, and formal errors of lake-averaged dz/dt

Month	Elevation (m)	1σ (m)	Formal Error (m)
Jul 2010	N/A	N/A	N/A
Aug 2010	1.96	1.34	0.77
Nov 2010	2.08	1.47	0.76
Dec 2010	2.21	1.65	0.75
Mar 2011	2.35	1.50	0.76
Apr 2011	2.17	1.31	0.76
May 2011	2.35	1.68	0.77
Jun 2011	2.08	1.63	0.76
Nov 2011	3.04	1.32	0.76
Dec 2011	2.65	1.26	0.76
Jan 2012	3.55	0.70	0.75
Feb 2012	3.37	0.68	0.76
Mar 2012	3.74	0.89	0.76
Apr 2012	3.93	0.75	0.76
May 2012	3.70	0.80	0.76
Jun 2012	3.83	1.14	0.76
Jul 2012	4.21	0.94	0.76
Aug 2012	4.21	1.56	0.77
Sep 2012	4.51	1.41	0.76
Oct 2012	4.55	0.92	0.76
Nov 2012	4.67	0.95	0.76
Dec 2012	4.384	0.92	0.76
Jan 2013	4.58	1.32	0.76
Feb 2013	4.28	1.00	0.75
Mar 2013	4.33	1.23	0.75
Apr 2013	4.20	0.96	0.76
May 2013	4.01	0.83	0.76
Jun 2013	3.26	1.02	0.76
Jul 2013	2.78	1.09	0.76
Aug 2013	2.49	1.43	0.76

Table 2.5: MODIS image details

Date	Solar Elevation	Azimuth	Position
2 Nov 2011	10.41°	212.75°	-14.66°
3 Nov 2011	11.49°	226.24 °	-14.97°
18 Nov 2011	17.88°	228.06°	-21.25°
28 Jan 2013	13.97°	214.88°	-18.13°

2.7 Acknowledgements

This work was carried out as part of the WISSARD project, supported by NASA grants NNX11AQ78H (Siegfried and Fricker) and NNX10AG21G (Scambos), and NSF grants ANT-0636970 (Tulaczyk) and ANT-0838885 (Severinghaus and Fricker). We thank UNAVCO, Raytheon Polar Services, Antarctic Support Contract (ASC), Kenn Borek Air, and the New York Air National Guard for logistical support; the European Space agency for CryoSat-2 data; S. Carter, D. Sandwell, E. Garcia, A. Borsa, and A. Shepherd for helpful discussion; and two anonymous reviewers for insightful comments.

Chapter 2, in full, is a reprint of material as it appears in Geophysical Research Letters: Siegfried, M. R., Fricker, H. A., Roberts, M., Scambos, T. A., Tulaczyk, S., "A decade of West Antarctic subglacial lake interactions from combined ICESat and CryoSat-2 altimetry", *Geophysical Research Letters*, 41(3), 891–898, doi:10.1002/2013GL058616, 2014. The dissertation author was the primary investigator and author of the paper.

Chapter 3

Extending the active subglacial lake record across Antarctica

3.1 Abstract

The ability to infer the movement of water beneath the Antarctic ice sheet using remote sensing techniques has fundamentally altered our perception of the subglacial environment. What used to be considered system in steady-state is now known to be a dynamic environment, with inferred variability on timescales ranging from sub-annual to multi-century or longer. The changing basal environment has direct implications on regional glaciological parameters (e.g., ice flow and grounding-line dynamics), as well as on boundary conditions for other disciplines (e.g., freshwater flux to the ocean and global carbon cycling). Our understanding of subglacial hydrological variability on timescales that are likely important for the near-term prediction of ice sheet fluctuations driven by global climate change (multi-year to decadal) is limited by the short temporal window of our current record of active subglacial hydrology, which comes from the Ice, Cloud, and land

Elevation Satellite (ICESat) laser altimetry mission (2003–2009). Using the only polar altimeter in operation since the retirement of ICESat in October 2009, we extend the activity record of the 37 subglacial lakes covered by the SARIn mode of the CryoSat-2 mission (launched 2010) to generate a time series until the end of 2014. We found large surface-height change events at nine of these known subglacial lakes during the post-ICESat period, including one of the highest surface-ice displacement rates ever observed, indicating that at least some of these features are stable and cyclic. We also found many locations with small (10s of cm) changes during the ICESat period that had no apparent surface height changes during the later CryoSat-2 mission, suggesting that some of the regions in the existing inventory of subglacial lakes may not be true hydrological features. We conclude that our current knowledge of the full distribution of active subglacial lakes is still limited. Continued monitoring of lakes in the existing inventory for both height and velocity changes as well as method development for identifying additional lake locations are critical to understanding the role of active subglacial hydrology in the ice sheet system.

3.2 Introduction

The majority of the ice of the Antarctic ice sheet drains from the continent to the ocean through fast-flowing ice streams and outlet glaciers (e.g., *Bamber et al.*, 2000). The high velocities sustained by these features are thought to be accommodated by the presence of meltwater at the bed, which reduces frictional resistance (e.g., *Engelhardt and Kamb*, 1997; *Tulaczyk et al.*, 2000). Thermodynamic ice stream models suggest, however, that in downstream reaches of fast flow, where driving stresses are low and ice is thin, the basal temperature regime favors freezing of subglacial water (e.g., *Hulbe and MacAyeal*, 1999). Sustaining fast ice flow in

areas where basal freezing is predicted then requires transport of large quantities of subglacial water from upstream areas of basal melt to these downstream regions (e.g., *Kamb*, 2001; *Joughin et al.*, 2004b). Thus both the location and movement of water at the ice-bed interface are likely first-order controls on the mass balance of Antarctica.

The movement of water from the upstream melt zones to downstream regions of fast flow was assumed to be a steady-state process over short timescales (e.g., *Parizek et al.*, 2002; *Christoffersen and Tulaczyk*, 2003; *Joughin et al.*, 2004b), but could play a fundamental role in large-scale ice-flow reorganizations over longer time periods (e.g., *Alley et al.*, 1994; *Anandakrishnan and Alley*, 1997; *Vaughan et al.*, 2008). Recent satellite measurements have indicated, however, that the movement of subglacial water through the basal drainage system on short timescales may be episodic rather than steady (*Gray et al.*, 2005; *Wingham et al.*, 2006b; *Fricker et al.*, 2007). These studies used observations of ice-surface height change over months to years to map spatially-coherent (over 1s to 10s of km) anomalies. These features were interpreted as the surface expression of water moving in and out of subglacial lakes.

After the initial discovery of these "active" lakes, *Smith et al.* (2009) used 4.5 years (late 2003 to early 2008) of data from the Ice, Cloud, and land Elevation Satellite (ICESat) mission (which continued collecting data until October 2009) to map 124 of these features across Antarctica. While the hypothesis of lakes beneath thick Antarctic ice was already well-established (e.g., *Robin et al.*, 1970; *Oswald and Robin*, 1973), previously mapped subglacial lakes (red in Figure 3.1) were mainly located beneath slow-moving interior of the ice sheet and thought to be in relative steady-state, with only local impacts on ice flow (e.g., *Siegert et al.*, 2005). The new category of active lakes included many that were located beneath

fast-flowing ice streams and outlet glaciers (blue and cyan lakes in Figure 3.1); therefore, they could potentially alter the overall mass balance of Antarctica on sub-decadal timescales by temporally starving major ice-drainage routes of basal lubrication.

There have been three reports of large, temporary ice accelerations resulting from the drainage of water from a subglacial lake in Antarctica. At Byrd Glacier, East Antarctica, *Stearns et al.* (2008) found a velocity increase of about 10% sustained over 14 months that correlated to the release of about 1.7 km^3 of water from two large subglacial lakes. At Crane Glacier, Antarctic Peninsula, *Scambos et al.* (2011) used optical-image feature-tracking to show a four-fold increase in ice velocity that was correlated to the release of about 0.2 km^3 of water. Because of on-going change related to the disintegration of Larsen B Ice Shelf, however, the precise effect of subglacial lake drainage on ice dynamics was difficult to assess. Finally, at Whillans and Mercer ice streams, West Antarctica, three episodic acceleration events were observed over two years related to two discharges of about 0.7 and 1.3 km^3 from subglacial lakes, with velocity peaks of nearly 4% above background (see **Chapter 4** of this dissertation).

Only a small subset of active subglacial lakes identified in the *Smith et al.* (2009) inventory have had their record of surface anomalies extended beyond the original length of 4.5 years. On lower Whillans and Mercer ice streams, West Antarctica, the original ICESat-based methods were incrementally updated and extended to the end of the ICESat mission (October 2009) by *Fricker and Scambos* (2009), *Fricker et al.* (2011), and *Carter et al.* (2013). This subset of lakes was then used by *Siegfried et al.* (2014) for developing new methods to monitor subglacial lake activity using data from the CryoSat-2 radar altimetry mission (July 2010 to present); **Chapter 4** extends the surface-height anomaly record until the end of

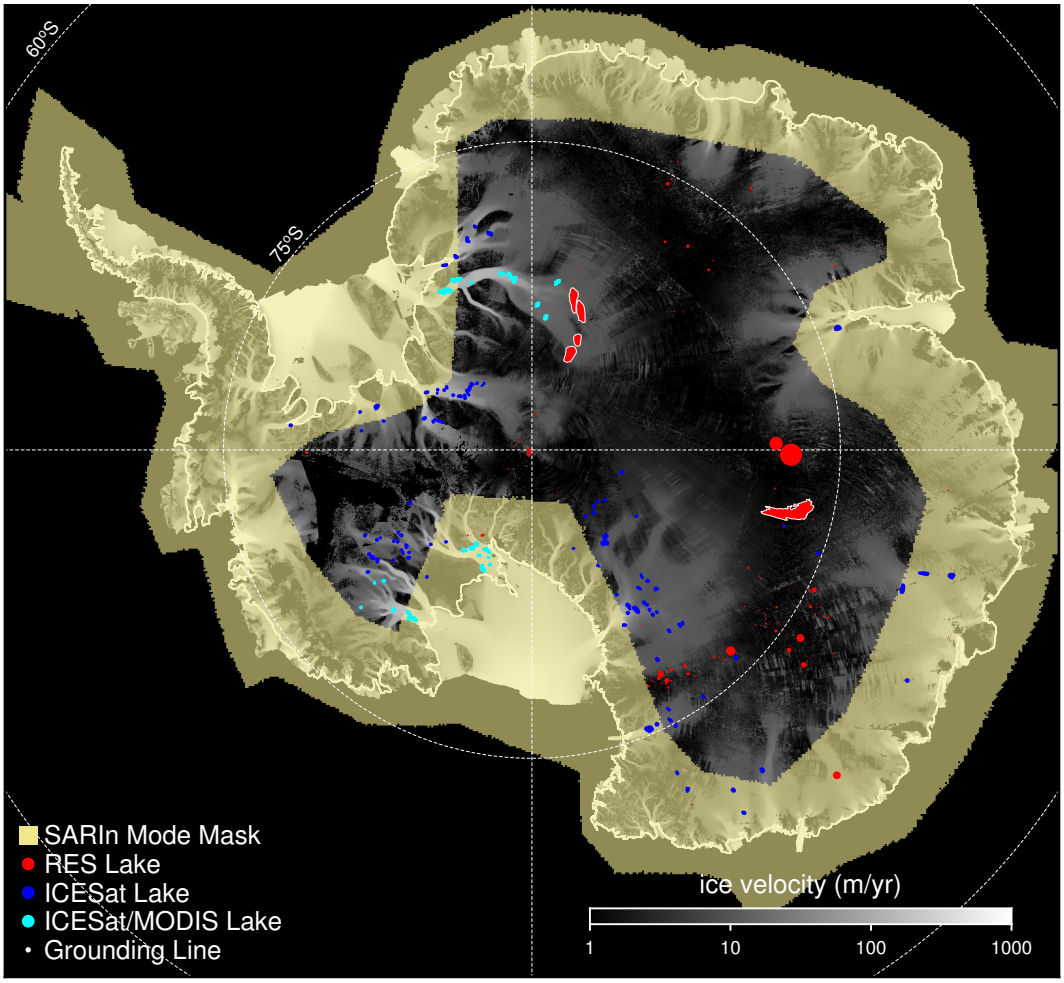

Figure 3.1: Distribution of subglacial lakes in Antarctica. Lakes studied by RES shown as red circles with their size proportional to their inferred volume (*Wright and Siegert*, 2012), except upper Recovery Ice Stream lakes and Subglacial Lake Vostok, whose actual outlines are drawn (*Bell et al.*, 2007; *Studinger et al.*, 2003, respectively). Active subglacial lakes studied by ICESat are shown in blue (*Smith et al.*, 2009), while those with refined outlines from MODIS image analysis are shown in cyan (*Fricker and Scambos*, 2009; *Fricker et al.*, 2010, 2014). The complete inventory of active subglacial lakes includes both blue and cyan lakes. Background is a map of InSAR-derived ice velocity (*Rignot et al.*, 2011b) and the extent of CryoSat-2 SARIn-mode data coverage for Jan.–Mar. 2014 is shown in yellow.

2014, yielding a time series of over 11 years. This work established that some active subglacial lakes in the Whillans/Mercer region are stationary features, experiencing cyclic fill-drain events. The hydrologic gradients in this region, however, are low and are sensitive to changes in surface topography, such that small variations can cause periods of water piracy that can isolate a subglacial lake from its upstream source (*Carter et al.*, 2013), indicating that some subglacial lakes may be ephemeral. One lake in this system, Subglacial Lake Whillans, was directly drilled into and sampled, verifying the interpretation that these surface anomalies relate to hydrologic features at the bed (*Tulaczyk et al.*, 2014). However, the actual transfer function between basal processes and their surface expression remains poorly understood as the movement of subglacial water can simultaneously cause dynamic changes in ice thickness (e.g., *Sergienko et al.*, 2007).

On Recovery Ice Stream, East Antarctica, *Fricker et al.* (2014) extended the subglacial lake activity record for some lakes in the catchment until the end of 2012 using improved ICESat data processing techniques and airborne laser altimetry campaigns flown as part of NASA's Operation IceBridge (OIB) in 2011 and 2012. Reanalysis of ICESat data combined with new OIB data led to a reinterpretation of the configuration of lakes in the system: (i) two separate lakes identified in the *Smith et al.* (2009) inventory were actually one single lake; and (ii) another lake further upstream showed no evidence of surface anomalies in the new analysis and likely was not a lake. It is unlikely that this new interpretation resulted from a change in water routing, as occurred on lower Whillans/Mercer ice stream, because the Recovery Ice Stream subglacial lakes lie in a narrow, deep (>2000 m at some locations) trough. The steep bedrock gradients of the trough, rather than ice-surface slopes, provide the first-order control on hydropotential gradients in this system, likely contributing to a more stable lake system compared to the Whillans/Mercer

subglacial lakes.

Other studies have investigated the nature of active subglacial lakes using radio-echo sounding (RES). Subglacial lakes typically appear as flat, bright reflectors at the ice-bed interface in RES images (*Carter et al.*, 2007). Recent RES surveying of active subglacial lakes with relatively low-amplitude signals in ICESat analysis under Byrd Glacier (*Wright et al.*, 2014), Institute Ice Stream (*Siegert et al.*, 2014) and Totten Glacier (*Wright et al.*, 2012), however, showed no such reflector beneath the locations of surface-height anomalies measured by ICESat, concluding that these features are likely not deep-water lakes and probably ephemeral.

After 10 years of investigation, important aspects of the physical nature of active subglacial lakes remain uncertain, yet their potential impact on ice flow is unequivocal. The existing height-change record of known active subglacial lakes is short (4.5 years) compared to typical timescales considered important to ice streams (decades to centuries), inhibiting our understanding of their spatiotemporal variability within the larger ice-sheet context. To develop a better understanding of active subglacial lakes, we need to extend and refine our current time series. In this chapter, we extend the subglacial lake activity time series for all lakes for which more recent satellite altimetry data is available. We then use the extended records to assess how variable these features are, both in terms of lake location and fill/drain characteristic.

3.3 Methods

3.3.1 ICESat Time Series

The ICESat-derived active subglacial inventory of *Smith et al.* (2009)[1] reports lake boundaries and time series of water volume changes for 124 lakes during a subset of the ICESat mission (August 2003 to March 2008). These were estimated using an early release of ICESat data (likely release 428, although it is not directly stated) and significant improvements to ICESat data quality have been made since then, including an updated precise orbit determination algorithm and the identification of a waveform processing error (*Borsa et al.*, 2014). Consequently, errors in the ICESat data used in the deposited subglacial lake time series are likely higher than the reported 0.1 m. Instead of presenting the time-series of *Smith et al.* (2009) as volume changes like they were presented in both the published manuscript and the deposited dataset, we convert to lake-averaged height change by dividing by the lake area. This step highlights the magnitude of the original observation rather than the magnitude of the interpretation (i.e., a low-magnitude signal of 0.5 m over an area of 1000 km^2 can lead to a moderate-magnitude interpreted volume—0.5 km^3).

We note that naming conventions occasionally differ between the published inventory (i.e., the manuscript *Smith et al.*, 2009) and the deposited inventory (i.e., the data housed at from the National Snow and Ice Data Center (NSIDC) that is freely available for download). For clarity, we use the names in the deposited inventory and point to any inconsistencies in the published inventory as a parenthetical statement.

In some regions, the active subglacial lake record has already been extended

[1] available at http://nsidc.org/data/NSIDC-0523

(lower MacAyeal Ice Stream, Recover Ice Stream, lower Whillans and Mercer ice streams). For these lakes, we use the updated lake boundaries and time series (*Fricker et al.*, 2010, 2014; **Chapter 4**, respectively). In these areas, the boundaries were determined using more precise optical-image differencing techniques and are shown in cyan in Figure 3.1. For all other lakes, we use the boundaries from *Smith et al.* (2009), which were determined by drawing a polygon around a spatially-coherent height anomaly greater than ∼0.1 m identified on multiple ICESat groundtracks. These lake boundaries are shown in blue in Figure 3.1.

3.3.2 CryoSat-2 Time Series

With the end of ICESat operations in October 2009, we need to use other instruments to extend the subglacial lake record. Launched in 2010 with an inclination of 92° and a 369-day orbit repeat (with a 30-day sub-orbit), the European Space Agency's (ESA) CryoSat-2 satellite aims to provide accurate ice-surface height trends for the continental ice sheets (*Wingham et al.*, 2006a). Following the methods of *Siegfried et al.* (2014), we use Synthetic Aperture Radar Interferometric (SARIn) mode data, wherein the the phase difference between two on-board antennas can be calculated to precisely determine the across-track location of the return echo within a SAR footprint (*Wingham et al.*, 2006a). The other two modes of CryoSat-2 mission data are Synthetic Aperture Radar (SAR) mode, which is only operational over regions of sea ice, and Low Resolution Mode (LRM), which is a typical pulse-limited altimeter mode using a single antenna (similar to ERS-1/2 and Envisat) and therefore has limited utility for observing small features on fast moving ice (see *Fricker et al.* (2010) for further discussion of this issue). LRM-mode data may have utility for observing larger lakes in the interior of the ice sheet (*Wingham et al.*, 2006b), which can be considered in future work. SARIn-mode data has

"wandering" ground tracks because it effectively tracks the point of closest approach (i.e., topographic highs) within the pulse-limited footprint. Figure 3.1 shows the extent of CryoSat-2 SARIn-mode between Jan. 2014 and Mar. 2014, relative to locations of subglacial lakes. CryoSat-2's mode mask was dynamic over the duration of the mission, resulting in data limited to only a subset of the 2010–2015 period for lakes near the boundary of the mask.

The method for estimating the subglacial lake activity time series from CryoSat-2 SARIn-mode data largely follows that of **Chapter 2**. For each lake in the *Smith et al.* (2009) inventory, we first subset the CryoSat-2 SARIn-mode data (release Baseline B) for box 50% larger than the lake length and width. We then remove data with anomalously high backscatter, filter the data using an iterative (95% convergence threshold) three-sigma filter for outliers, and make a digital elevation model (DEM) over the region. Due to large surface height ranges in the region near some active subglacial lakes, instead of applying the three-sigma filter over the entire region at once as performed in **Chapter 2**, we apply it over 10 km $\times$ 10 km subsections and concatenate the results. We filter the DEM using a 2 km median filter.

After DEM creation, we process the CryoSat-2 data relative to the DEM to generate a time-series of lake-averaged surface-height anomalies. To construct this time series, we use CryoSat-2 data from overlapping three-month intervals, centered every month for Jul. 2010 to Dec. 2014. For each datapoint in the three-month interval, we subtract the DEM-height interpolated at the footprint location to estimate a topography-free height anomaly. Finally, we calculate the mean height anomaly within the subglacial lake boundary, a value that contains height changes due to both subglacial water movement and regional ice dynamics. To isolate the hydrology-driven height change, we also calculate the mean height anomaly outside

the boundary to provide an estimate of regional dynamic height changes. We report the difference of the two ($h_{in} - h_{out}$) as the lake-averaged surface-height anomaly independent of regional trends.

We note that we do not cross-calibrate the CryoSat-2 time series with the ICESat time series as done in **Chapter 2** because there was no GPS to calculate penetration bias, which is a local correction determined by surface processes.

3.4 Results

There are 64 active subglacial lakes within the CryoSat-2 SARIn-mode mask (Figure 3.1). Of these lakes, 27 only had data during one month during which the SARIn observational limits were extended south (typically June 2013, except Nimrod_2, which was only observed in July 2010). One additional datapoint acquired more than 5 years after the last data point does not provide much additional insight into the physical processes governing subglacial lakes. We therefore focus on the 37 active subglacial lakes that had more than one month of new observations. These lakes lie beneath 17 different regions in both West and East Antarctica, each of which is discussed below.

3.4.1 West Antarctic Subglacial Lakes

Mercer/Whillans Lakes

The time-series for the larger lakes on lower Mercer and Whillans ice streams (subglacial lakes Engelhardt, Whillans, Conway, Mercer, and Lake 7; SLE, SLW, SLC, SLM, and L7, respectively) were the model lakes used to develop the method used in this study (**Chapter 2**) and have been updated until the end of 2014 in **Chapter 4**. The extended height-change records of these lakes show continued

subglacial lake activity at SLW, SLC, SLM, and L7 during the CryoSat-2 mission, while heights at SLE continued to increase at rates similar to those near the end of the ICESat mission. We include these time series for completeness (Figures 3.2, 3.3).

Lake10 (64 km^2), Lake12 (25 km^2), Upper Subglacial Lake Conway (USLC; 178 km^2), $Whillans_6$ (71 km^2), and $Whillans_7$ (73 km^2) were also covered by CryoSat-2 SARIn mode (Figure 3.2). Lake10 showed a steady increase in height of 1 m yr^{-1} from late 2003 to late 2006. During 2007, ice surface height increased by 1.8 m over six months and decreased by an equal amount over six months in 2008. At Lake12, surface height decreased by 1.2 m between the start of the mission in late 2003 and mid 2006, increased by 1.0 m over the next six months, decreased again by 1.2 m until late 2007, and finally increased by 1.0 m during 2008. Between 2010 and 2015, both lakes experienced height changes that were in-phase with the regional dynamics outside the lake boundary, with the only notable event being a rapid 1.2 m height increase of the on-lake height of Lake12 occurring over 4 months in mid-2014.

ICESat data over USLC were noisy, but seemed to show a broad cycle of increasing heights for 1–2 years, following by decreasing heights for two years, with an amplitude of 1–2 m averaged over the lake. CryoSat-2 data captured a period of more height-change activity at USLC, with an apparent three-year cycle: a 1.9 m height increase over the first year and decreasing by 1.5 m over the subsequent two years. From early 2013 until the end of the time series at the end of 2014, lake height steadily increased again, for a total of 1.6 m. While the periodicity differs between the ICESat-observed height-change event and the CryoSat-2-observed height-change event, the magnitude of height change is similar ($\sim$2 m).

Further upstream, height change at $Whillans_6$ was -1.6 m between early

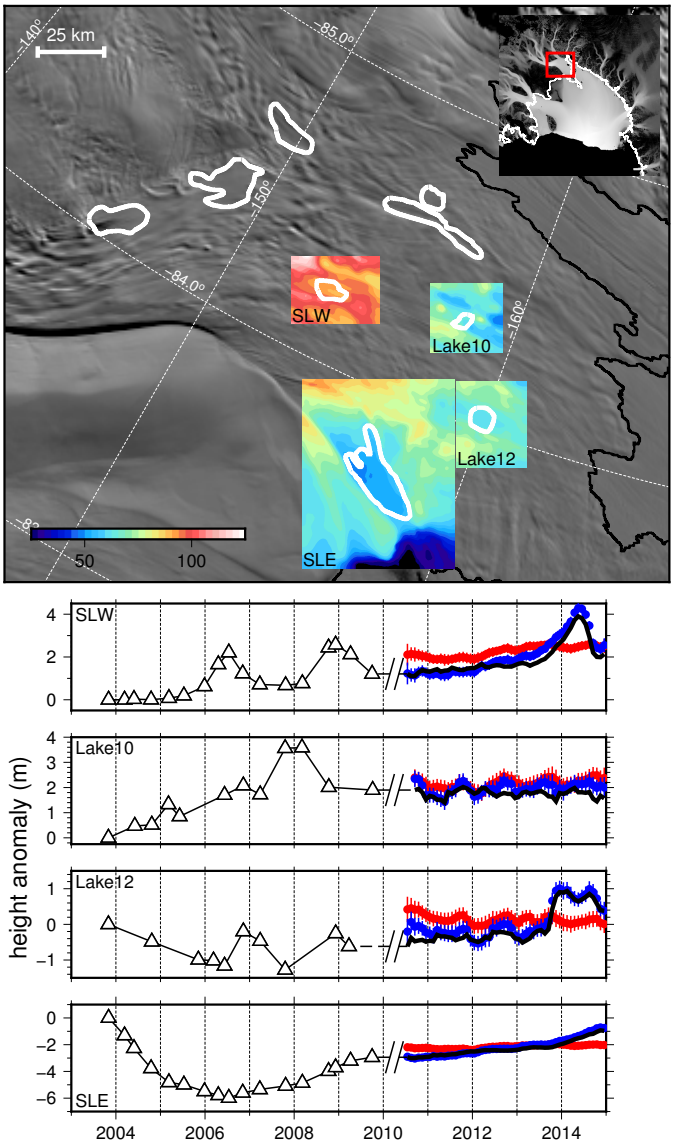

Figure 3.2: Top: Location of lakes on the northern and central regions of lower Whillans Ice Stream, with CryoSat-2-derived DEMs (color scale in meters) relative to lake outlines (*Fricker and Scambos*, 2009) and MODIS visual imagery (*Scambos et al.*, 2007). Inset shows location relative to ice velocity (*Rignot et al.*, 2011b) using the same colorscale as Figure 3.1. Bottom: Extended time series of subglacial lake height anomaly at SLW, Lake10, Lake12, and SLE. Triangles are the existing ICESat-derived time series (*Smith et al.*, 2009), while new CryoSat-2 time series (with formal-errors bars) is shown in red (off-lake heights), blue (on-lake heights), and black (lake height accounting for regional trends).

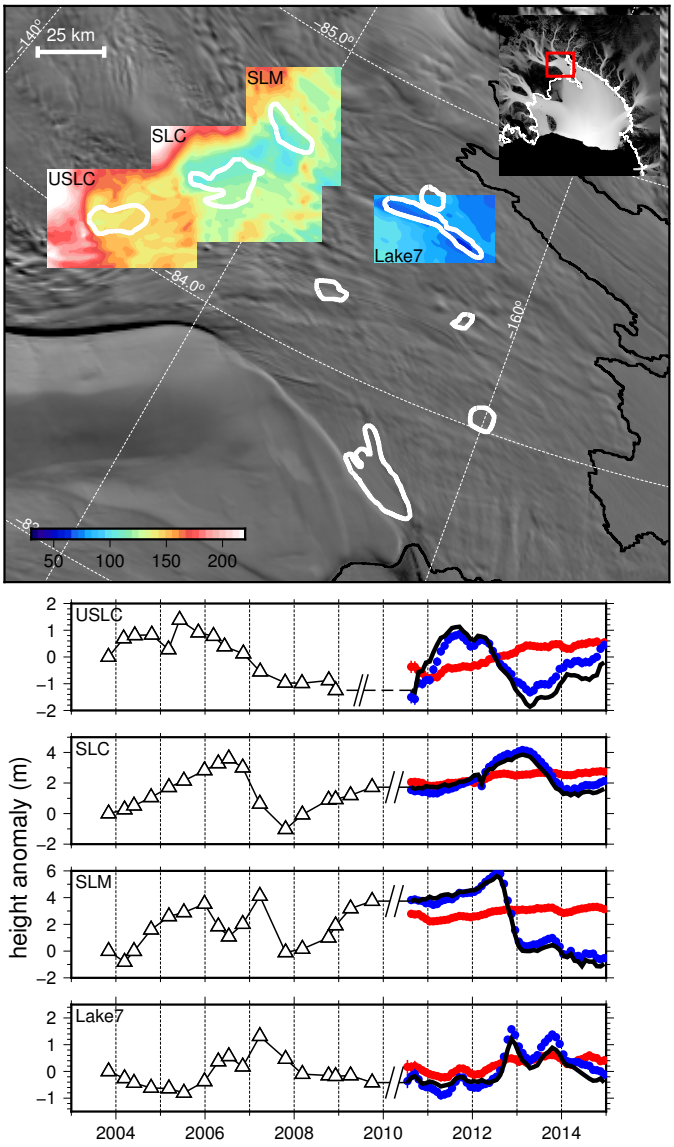

Figure 3.3: Top: Location of lakes on the southern region of lower Whillans Ice Stream, with CryoSat-2-derived DEMs (color scale in meters) relative to lake outlines (*Fricker and Scambos*, 2009) and MODIS visual imagery (*Scambos et al.*, 2007). Inset shows location relative to ice velocity (*Rignot et al.*, 2011b) using the same colorscale as Figure 3.1. Bottom: Extended time series of subglacial lake height anomaly at USLC, SLC, SLM, and Lake7. Triangles are the existing ICESat-derived time series (*Smith et al.*, 2009), while new CryoSat-2 time series (with formal-errors bars) is shown in red (off-lake heights), blue (on-lake heights), and black (lake height accounting for regional trends).

2004 and late 2007 (Figure 3.4). From CryoSat-2 observations heights steadily increased from mid 2010 to mid 2013 at a rate of 0.25 m yr^{-1}. Between mid 2013 and the end of 2014, heights increased by 1.5 m over four months, were sustained at the anomalously high level for seven months, and then decreased by 1.4 m over the last eight months of the time series. $Whillans_7$ exhibited little change over the ICESat period and, situated at the edge of the SARIn-mode region, had too sparse data to extend the record past the ICESat mission.

Institute Ice Stream Lakes

Beneath the Institute Ice Stream, $Institute_{E1}$ (441 km^2) and $Institute_{W1}$ (81 km^2) displayed similar activity during the ICESat period, both steadily increasing in height through the 4.5-year duration (1.1 m at $Institute_{E1}$ and 0.9 m at $Institute_{W1}$; Figure 3.5). These two lakes only were within the SARIn-mode mask starting in mid-2013. During the subsequent 1.5 years, $Institute_{E1}$ showed minimal activity, though there was a regional height-lowering signal of $\sim$0.4 m yr^{-1}. The time series at $Institute_{W1}$ suggests a surface lowering over the lake until early 2014, then a slight inflation, but the data over the lake itself were sparse.

$KambTrunk_1$

On the stagnated Kamb Ice Stream, $KambTrunk_1$ (67 km^2) generally had surface heights that decreased throughout the ICESat mission, with a maximum height-change of 0.8 m between early 2004 and late 2007 (Figure 3.6). During the CryoSat-2 period, there was minimal height change until mid-2012, when the average lake height increased by 2.4 m over 1.75 years. During the final seven months of the time series, the lake experienced a height change of -1.0 m.

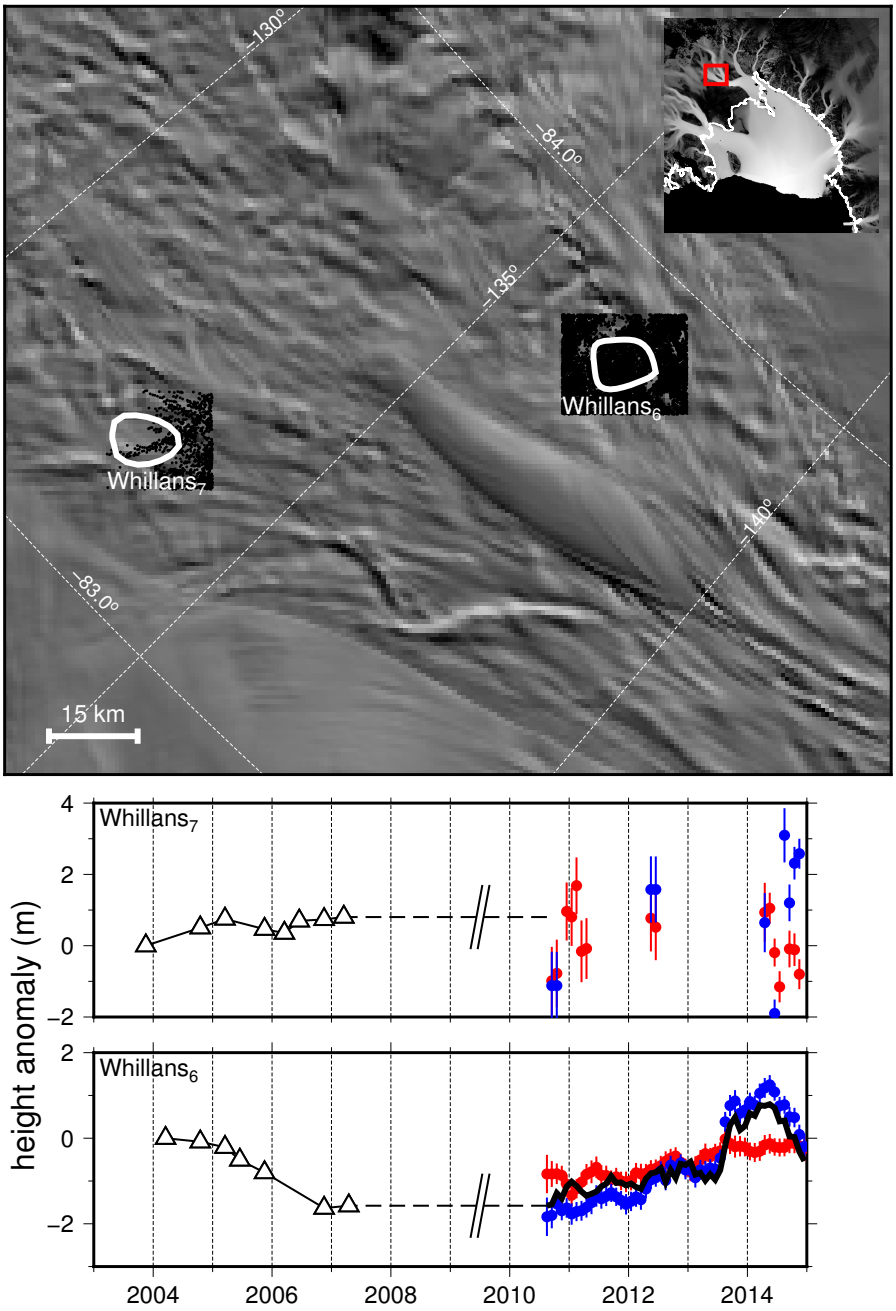

Figure 3.4: Top: Location of upper Whillans Ice Stream lakes, with CryoSat-2 SARIn footprints relative to lake outlines (*Smith et al.*, 2009) and MODIS visual imagery (*Scambos et al.*, 2007). Inset shows location relative to ice velocity (*Rignot et al.*, 2011b) using the same colorscale as Figure 3.1. Bottom: Extended time series of subglacial lake height anomaly at Whillans_6 and Whillans_7. Triangles are the existing ICESat-derived time series (*Smith et al.*, 2009), while new CryoSat-2 time series (with formal-errors bars) is shown in red (off-lake heights), blue (on-lake heights), and black (lake height accounting for regional trends).

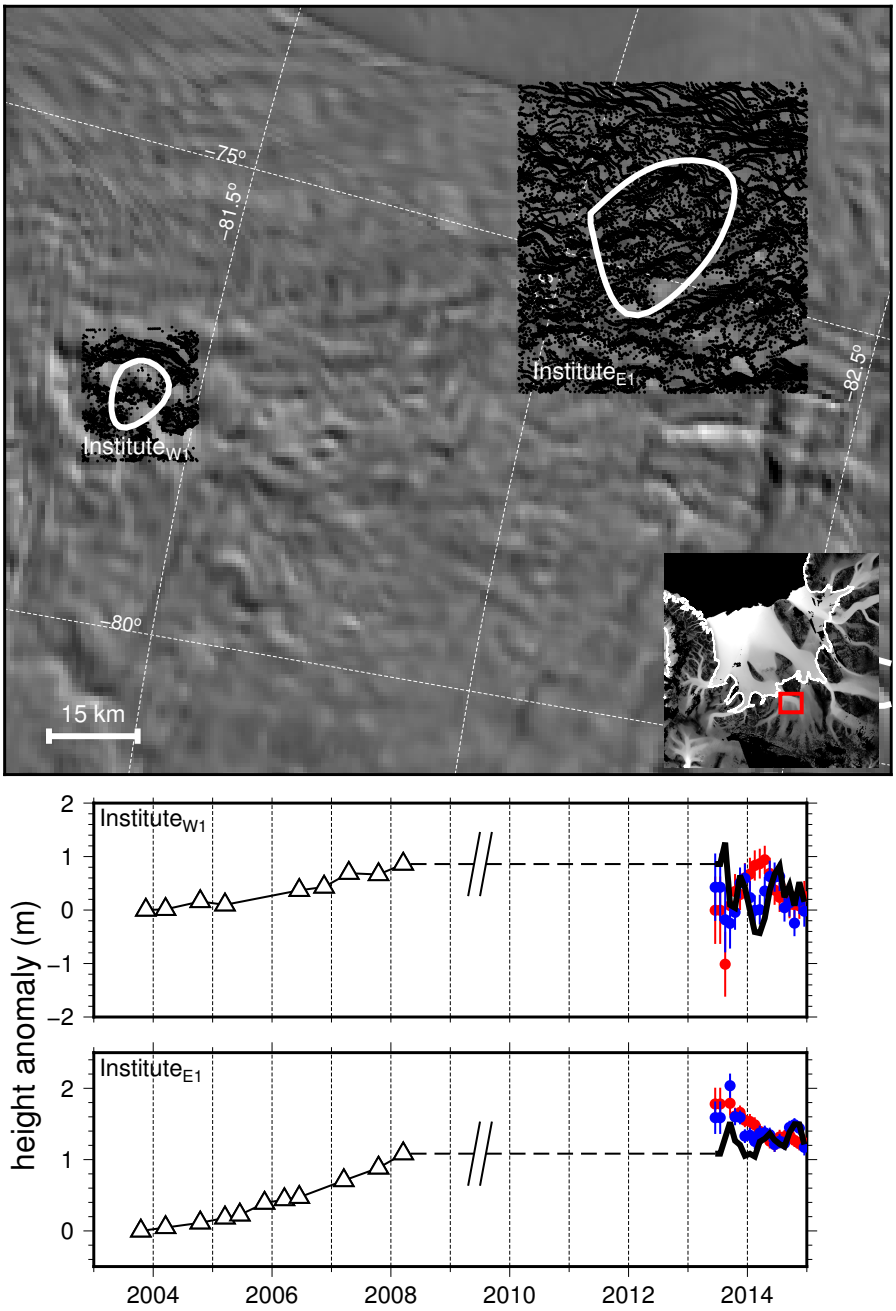

Figure 3.5: Top: Location of Institute Ice Stream lakes, with CryoSat-2 SARIn footprints relative to lake outlines (*Smith et al.*, 2009) and MODIS visual imagery (*Scambos et al.*, 2007). Inset shows location relative to ice velocity (*Rignot et al.*, 2011b) using the same colorscale as Figure 3.1. Bottom: Extended time series of subglacial lake height anomaly at Institute$_{W1}$ and Institute$_{E1}$. Triangles are the existing ICESat-derived time series (*Smith et al.*, 2009), while new CryoSat-2 time series (with formal-errors bars) is shown in red (off-lake heights), blue (on-lake heights), and black (lake height accounting for regional trends).

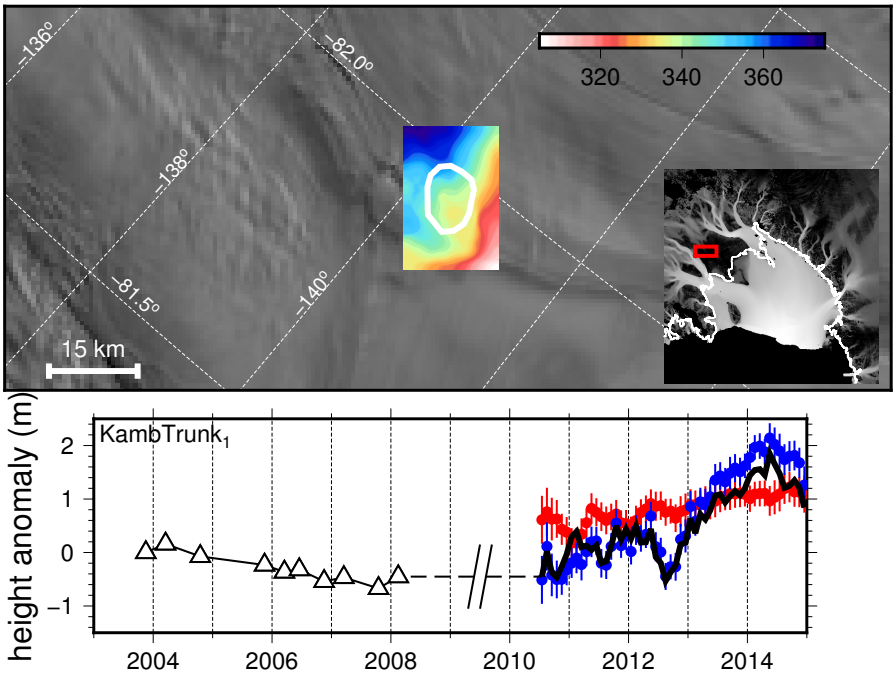

Figure 3.6: Top: Location of KambTrunk$_1$, with CryoSat-2-derived DEM (color scale in meters) relative to lake outlines (*Smith et al.*, 2009) and MODIS visual imagery (*Scambos et al.*, 2007). Inset shows location relative to ice velocity (*Rignot et al.*, 2011b) using the same colorscale as Figure 3.1. Bottom: Extended time series of subglacial lake height anomaly at KambTrunk$_1$. Triangles are the existing ICESat-derived time series (*Smith et al.*, 2009), while new CryoSat-2 time series (with formal-errors bars) is shown in red (off-lake heights), blue (on-lake heights), and black (lake height accounting for regional trends).

MacAyeal Lakes

During the ICESat period, the lakes beneath lower MacAyeal Ice Stream all exhibited periods of rapid height change punctuated by longer intervals of no change (Figure 3.7). Mac1 (150 km^2) had a height decrease in early 2004 ($\sim$6 m) and a height increase in mid 2007 ($\sim$4 m). Mac2 (140 km^2) only had one rapid change: an increase of $\sim$2.5 m during 2005. ICESat observations were more limited at Mac3 (144 km^2), but it appeared to have a subsidence event in early 2004 and late 2007/early 2008 with magnitudes of $\sim$2–4 m.

This lake system demonstrated the value of the increased temporal resolution of CryoSat-2 observations, revealing rapid switches from increasing heights to decreasing heights. The average surface height at Mac3 increased by 1.8 m over six months during 2011, sharply followed by a 3.5 m height decrease over 8 months. After this deflation event, heights steadily increased by 1.7 m over the final two years of the time series. The negative height-anomaly in late 2011 and early 2012 at Mac3 coincides with a large surface height anomaly at Mac1, located downstream, suggesting a hydrologic link. Here, surface heights increased by 5.9 m over 6 months, then decreased to the pre-event height over the following five months. There appeared to be a similar, though smaller (amplitude of 1.1 m) event peaking in late 2013. The time series ended with heights increasing, by 2.1 m over six months. This final event may be correlated to falling surface heights at Mac2 in mid to late 2014 (1.5 m over seven months). Mac2, which has a noisier time series than the other two subglacial lakes in the region, appeared to not display anomalous activity elsewhere in the CryoSat-2 record.

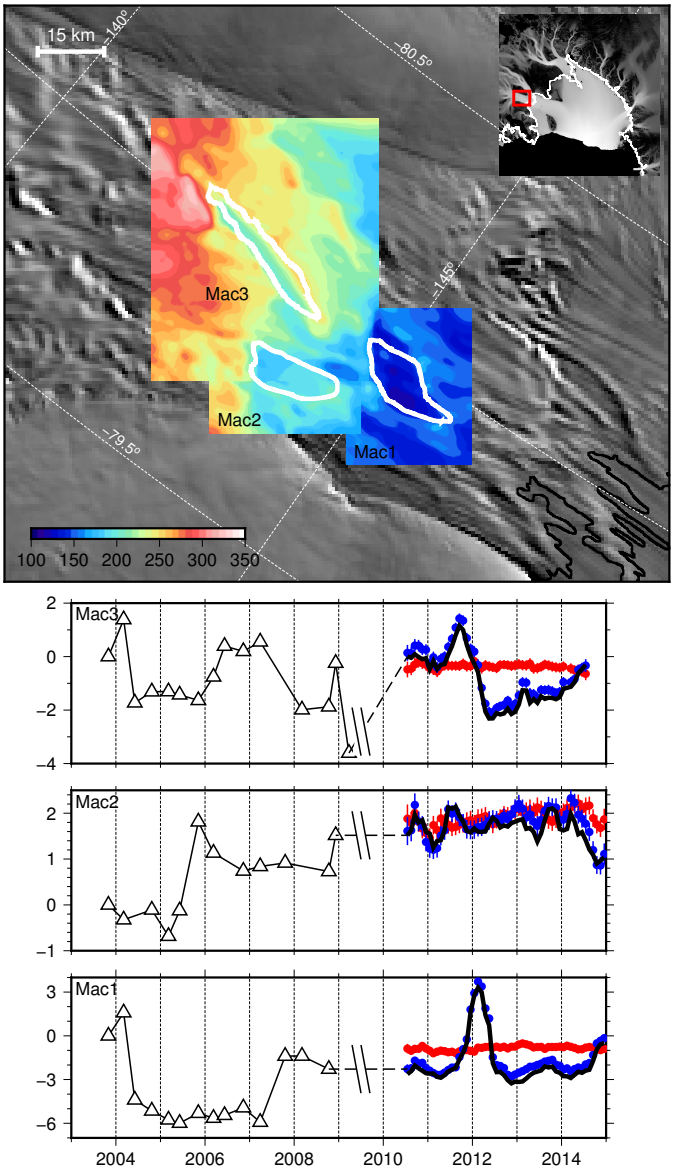

Figure 3.7: Top: Location of MacAyeal Ice Stream lakes, with CryoSat-2-derived DEMs (color scale in meters) relative to lake outlines (*Fricker et al.*, 2010) and MODIS visual imagery (*Scambos et al.*, 2007). Inset shows location relative to ice velocity (*Rignot et al.*, 2011b) using the same colorscale as Figure 3.1. Bottom: Extended time series of subglacial lake height anomaly at Mac1, Mac2, and Mac3. Triangles are the existing ICESat-derived time series (*Smith et al.*, 2009), while new CryoSat-2 time series (with formal-errors bars) is shown in red (off-lake heights), blue (on-lake heights), and black (lake height accounting for regional trends).

Rutford$_1$

Rutford$_1$ (111 km^2) is located near the grounding line of the Rutford Ice Stream (Figure 3.8). As observed by ICESat, the height of this lake increased by 1.4 m between mid-2005 and 2007, then decreased by 1.1 m over the subsequent year. As this lake is adjacent to the Ellsworth Mountains to the south, the rough terrain resulted in large uncertainties in the CryoSat-2 data both on and off the lake.

3.4.2 East Antarctic Subglacial Lakes

Byrd$_{s1}$

Of the 17 active subglacial lakes identified beneath Byrd Glacier, East Antarctica (*Stearns et al.*, 2008; *Smith et al.*, 2009) and later surveyed with airborne RES (*Wright et al.*, 2014), only Byrd$_{s1}$ is covered by CryoSat-2 SARIn-mode (Figure 3.9). Unfortunately, however, the switch between CryoSat-2 modes (from SARIn to LRM) occurs over this lake. Additionally, over the half of the lake that was covered by CryoSat-2 SARIn-mode, the spatial sampling is poor due to rough surface topography (as evidenced by the data gaps over features in the optical imagery), thus yielding a noisy time series. The long-term trend of the CryoSat-2 height is slightly negative at -0.09 m yr^{-1} between Jul. 2010 and Dec. 2014. During the ICESat period, this lake experienced a nearly linear surface height increase of 0.4 m over four years (early 2004 to early 2008), a positive trend of the same magnitude (though opposite sign) later seen in the CryoSat-2-derived dataset.

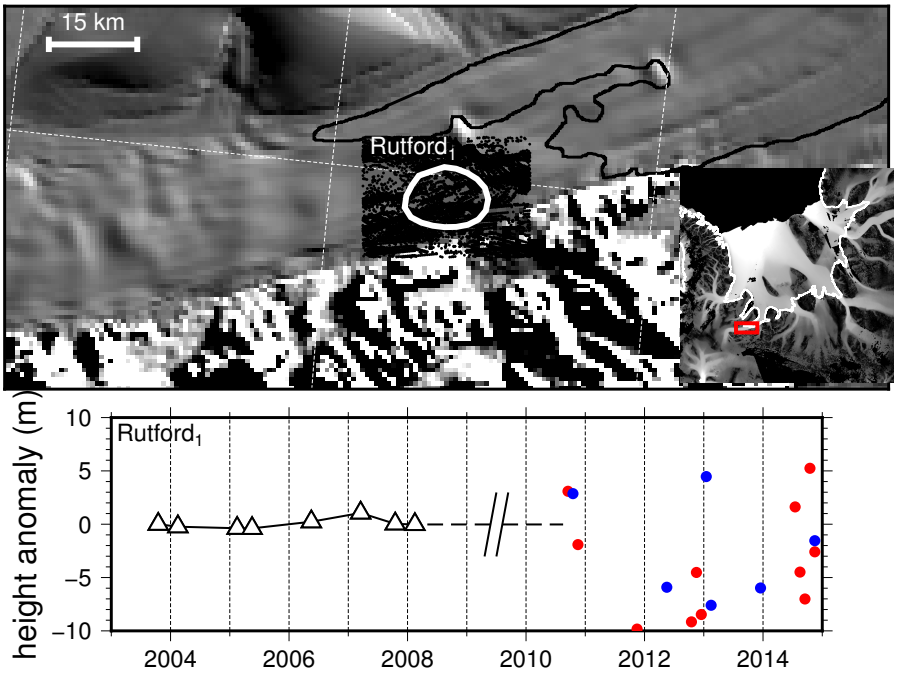

Figure 3.8: Top: Location of Rutford$_1$, with CryoSat-2 SARIn footprints relative to lake outlines (*Smith et al.*, 2009) and MODIS visual imagery (*Scambos et al.*, 2007). Inset shows location relative to ice velocity (*Rignot et al.*, 2011b) using the same colorscale as Figure 3.1. Bottom: Extended time series of subglacial lake height anomaly at Rutford$_1$. Triangles are the existing ICESat-derived time series (*Smith et al.*, 2009), while new CryoSat-2 time series (with formal-errors bars) is shown in red (off-lake heights), blue (on-lake heights). Lake heights accounting for regional trends are not shown due to noise.

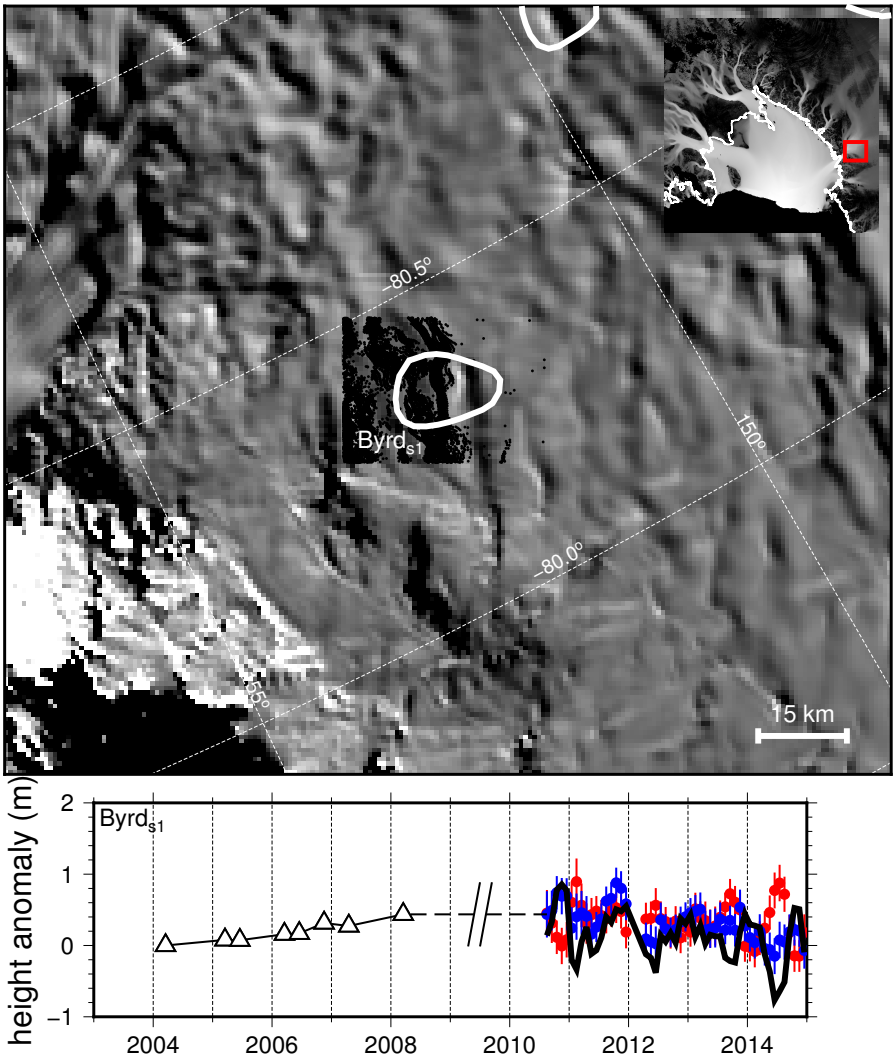

Figure 3.9: Top: Location of Byrd$_{s1}$ on Byrd Glacier, with CryoSat-2 SARIn footprints relative to lake outlines (*Smith et al.*, 2009) and MODIS visual imagery (*Scambos et al.*, 2007). Inset shows location relative to ice velocity (*Rignot et al.*, 2011b) using the same colorscale as Figure 3.1. Bottom: Extended time series of subglacial lake height anomaly at Byrd$_{s1}$. Triangles are the existing ICESat-derived time series (*Smith et al.*, 2009), while new CryoSat-2 time series (with formal-errors bars) is shown in red (off-lake heights), blue (on-lake heights), and black (lake height accounting for regional trends).

Cook Lakes

Cook_{E1} (263 km^2) and Cook_{E2} (145 km^2) are located in George V Land, East Antarctia, in the eastern catchment of the Cook Ice Shelf (Figure 3.10). These two lakes showed activity during the ICESat period, with the surface height of Cook_{E2} lowering by 18.6 m over 16 months beginning in late 2006 and correlated surface height increase of 0.7 m at Cook_{E1} over the same period. Steep slopes around the surface depression that define the boundary of Cook_{E2} resulted in poor spatial sampling (and a noisy time series) during the CryoSat-2 period, with a height change trend of 0.5 m yr^{-1}, an order of magnitude smaller than the previously-documented trend (*McMillan et al.*, 2013). Cook_{E1} showed a consistent and small decreasing surface-height trend of -0.06 m yr^{-1} for the duration of CryoSat-2 observations.

David Glacier Lakes

Similar to Byrd_{s1}, David_1 (939 km^2) and David_{s1} (189 km^2; named David_2 in *Smith et al.* (2009)) have rough ice-surface topography, resulting in stripes of poorly-sampled locations (Figure 3.11). David_1 showed a rapid increase in surface height early in the ICESat period followed by a more moderate increase (0.3 m) between 2005 and 2008, while the more upstream lake, David_{s1}, showed a similar pattern, with the opposite sign (rapid decrease in height, followed by a more moderate 0.2 m loss between 2005 and 2008). Observations during the CryoSat-2 period were noisy, but show in-phase changes both on and off the lakes.

Foundation Ice Stream Lakes

Foundation_1 (187 km^2) and Foundation_2 (68 km^2) showed anti-correlated activity during the ICESat period, with a surface height decrease of 0.7 m over two years at Foundation_2 and an increase of 0.5 m at Foundation_1 over the same time

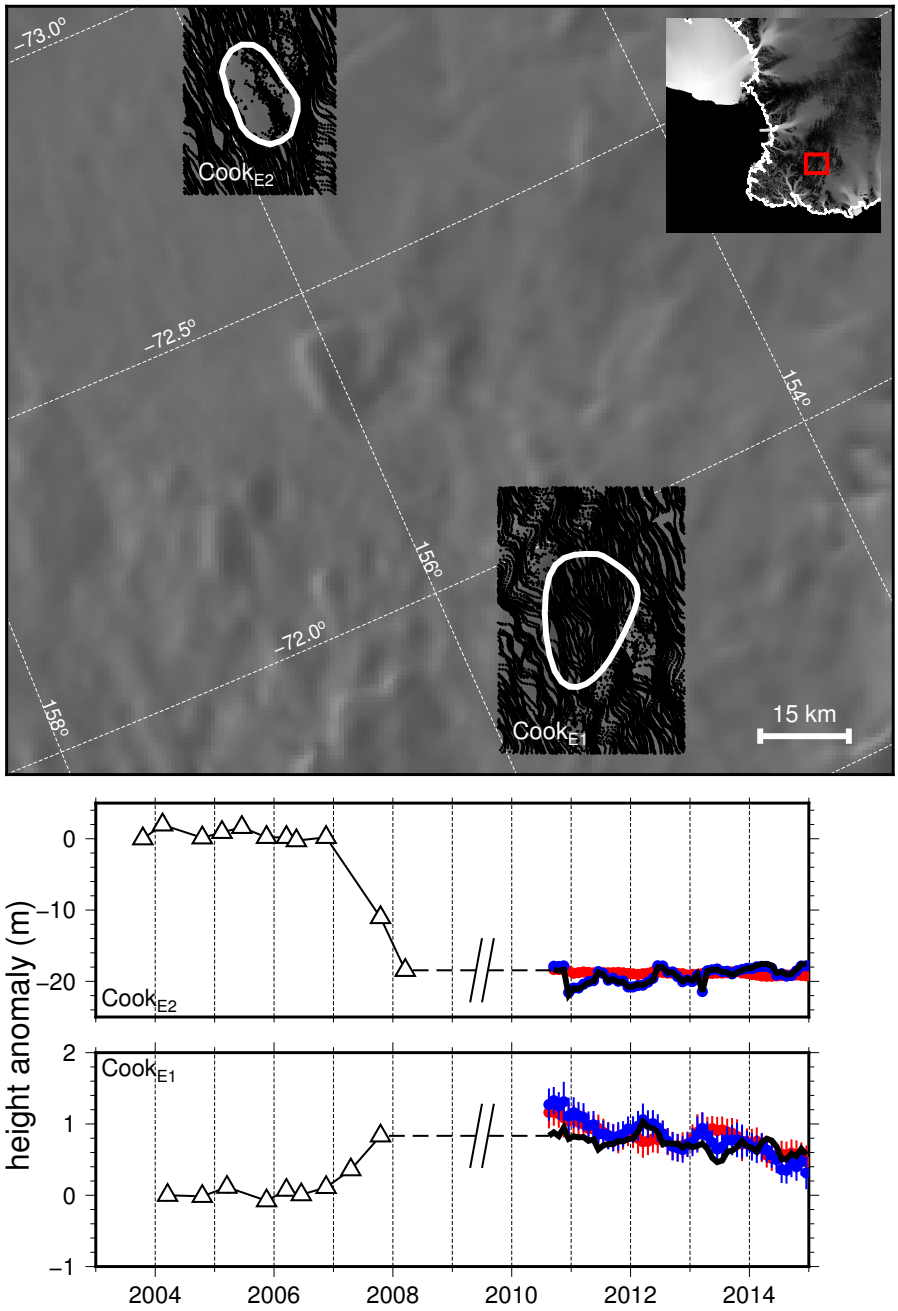

Figure 3.10: Top: Location of Cook_{E1} and Cook_{E2}, with CryoSat-2 SARIn footprints relative to lake outlines (*Smith et al.*, 2009) and MODIS visual imagery (*Scambos et al.*, 2007). Inset shows location relative to ice velocity (*Rignot et al.*, 2011b) using the same colorscale as Figure 3.1. Bottom: Extended time series of subglacial lake height anomaly at Cook_{E1} and Cook_{E2}. Triangles are the existing ICESat-derived time series (*Smith et al.*, 2009), while new CryoSat-2 time series (with formal-errors bars) is shown in red (off-lake heights), blue (on-lake heights), and black (lake height accounting for regional trends).

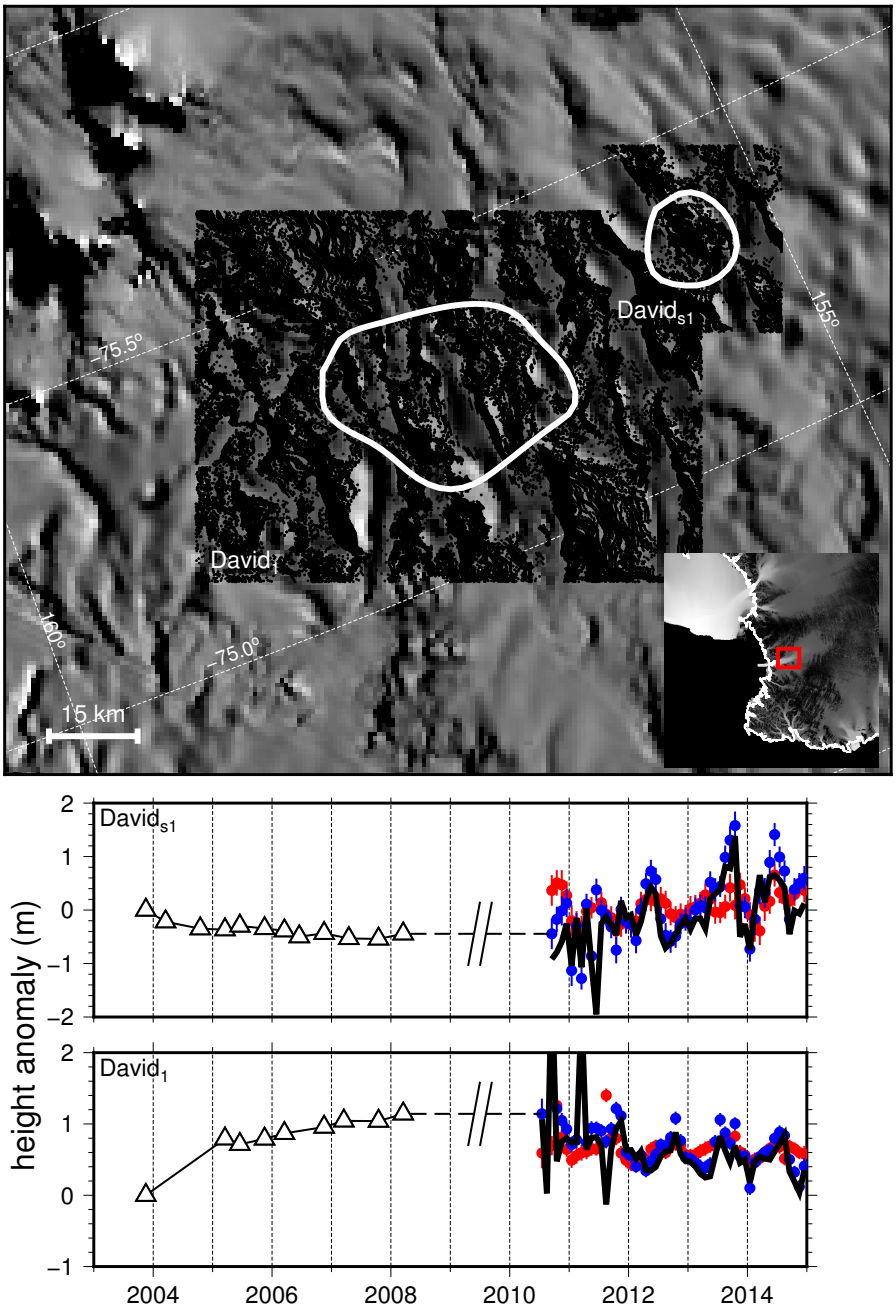

Figure 3.11: Top: Location of David Glacier lakes, with CryoSat-2 SARIn footprints relative to lake outlines (*Smith et al.*, 2009) and MODIS visual imagery (*Scambos et al.*, 2007). Inset shows location relative to ice velocity (*Rignot et al.*, 2011b) using the same colorscale as Figure 3.1. Bottom: Extended time series of subglacial lake height anomaly at David$_{s1}$ and David$_1$. Triangles are the existing ICESat-derived time series (*Smith et al.*, 2009), while new CryoSat-2 time series (with formal-errors bars) is shown in red (off-lake heights), blue (on-lake heights), and black (lake height accounting for regional trends).

period (Figure 3.12). After 2006, however, surface heights at both lakes increased until the end of 2007. CryoSat-2 SARIn-mode only covers these two lakes during 2014. At Foundation$_1$, small anomalies ($O(0.1)$ m) were correlated on and off the lake, while data were too sparse at Foundation$_2$ to assess any change.

Lambert$_1$

Under the main trunk of the Lambert Glacier, heights beneath Lambert$_1$ (615 km^2) decreased by 1.3 m over the first three years of the ICESat mission (Figure 3.13). The region outside the lake boundary is rough, resulting in a time series too noisy to assess regional height changes during the CryoSat-2 period. Therefore, we did not perform the correction for regional ice dynamics. Within the lake boundary, the heights increased at an average rate of 0.2 m yr^{-1} over the duration of the CryoSat-2 mission. Between early 2012 and early 2013, there was a short period of faster inflation (0.8 m over 4 months) followed by a period of rapid deflation (0.6 m over 4 months), with the elevated heights sustained for 2 months.

LennoxKing$_1$

LennoxKing$_1$ is a small lake (35 km^2) in the upstream catchment of the Lennox-King Glacier (Figure 3.14). During the ICESat period, the surface height of this lake decreased by 1.0 m over three years (2005 to 2008). During the CryoSat-2 period, heights both on and off the lake had small fluctuations on the order of 0.5 m, with no clear trend. The sign of these fluctuations were in-phase, with higher magnitudes occurring over the lake compared to outside the lake boundary.

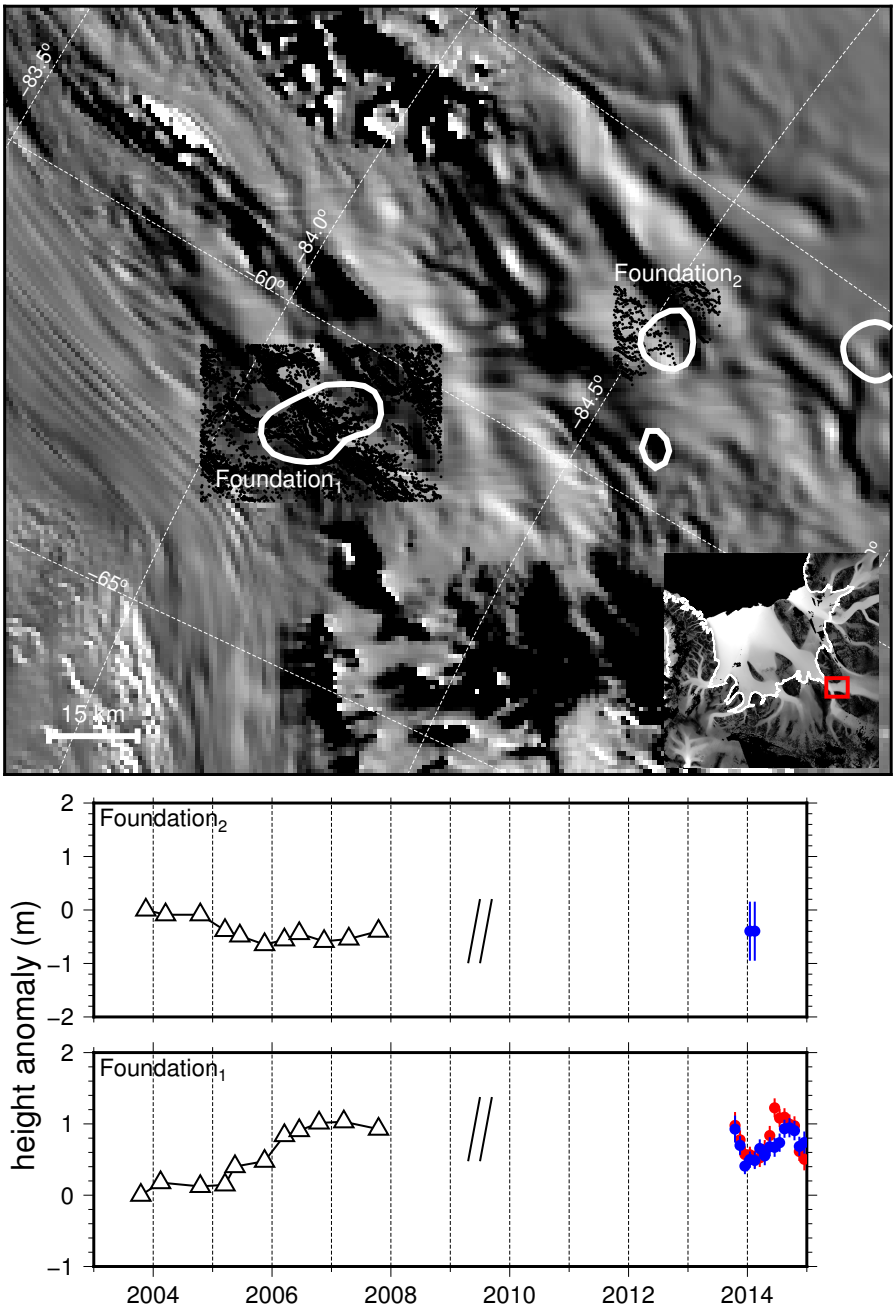

Figure 3.12: Top: Location of Foundation Ice Stream lakes, with CryoSat-2 SARIn footprints relative to lake outlines (*Smith et al.*, 2009) and MODIS visual imagery (*Scambos et al.*, 2007). Inset shows location relative to ice velocity (*Rignot et al.*, 2011b) using the same colorscale as Figure 3.1. Bottom: Extended time series of subglacial lake height anomaly at Foundation$_1$ and Foundation$_2$. Triangles are the existing ICESat-derived time series (*Smith et al.*, 2009), while new CryoSat-2 time series (with formal-errors bars) is shown in red (off-lake heights), blue (on-lake heights). Lake heights accounting for regional trends are not shown due to small signal-to-noise ratio.

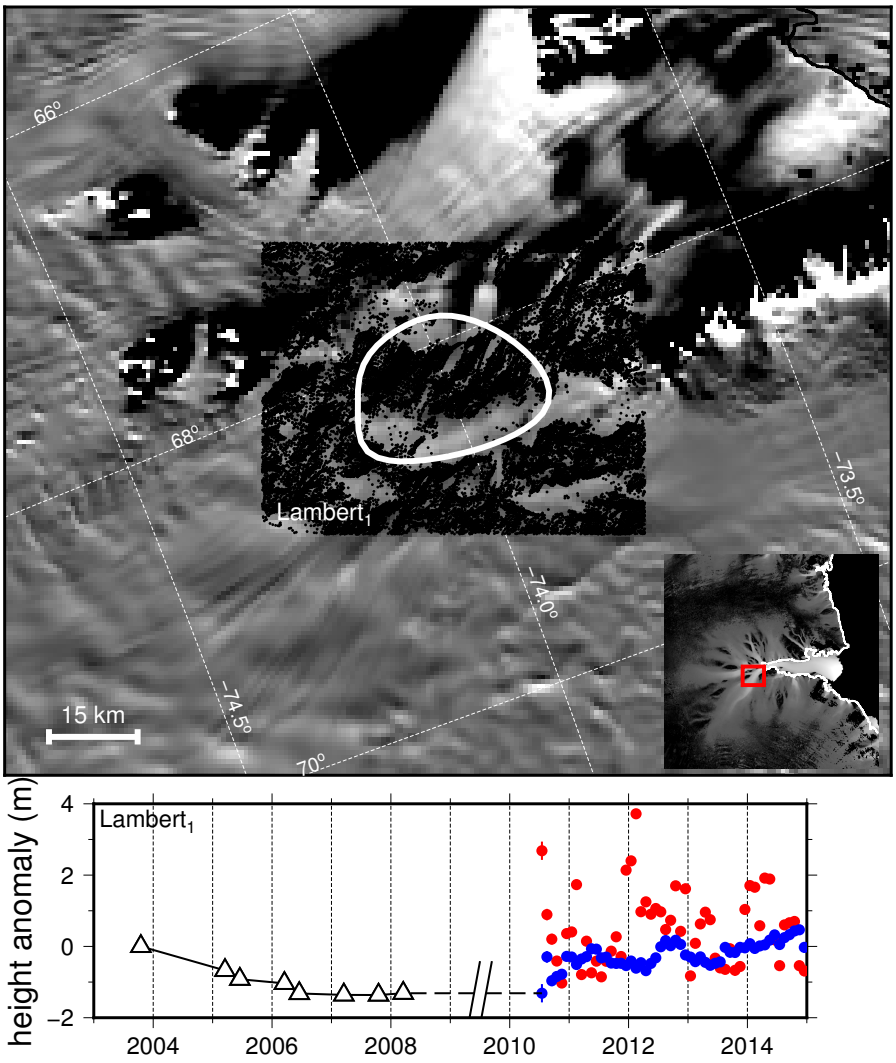

Figure 3.13: Top: Location of Lambert$_1$, with CryoSat-2 SARIn footprints relative to lake outlines (*Smith et al.*, 2009) and MODIS visual imagery (*Scambos et al.*, 2007). Inset shows location relative to ice velocity (*Rignot et al.*, 2011b) using the same colorscale as Figure 3.1. Bottom: Extended time series of subglacial lake height anomaly at Lambert$_1$. Triangles are the existing ICESat-derived time series (*Smith et al.*, 2009), while new CryoSat-2 time series (with formal-errors bars) is shown in red (off-lake heights), blue (on-lake heights). Lake heights accounting for regional trends are not shown due to noise in the off-lake data.

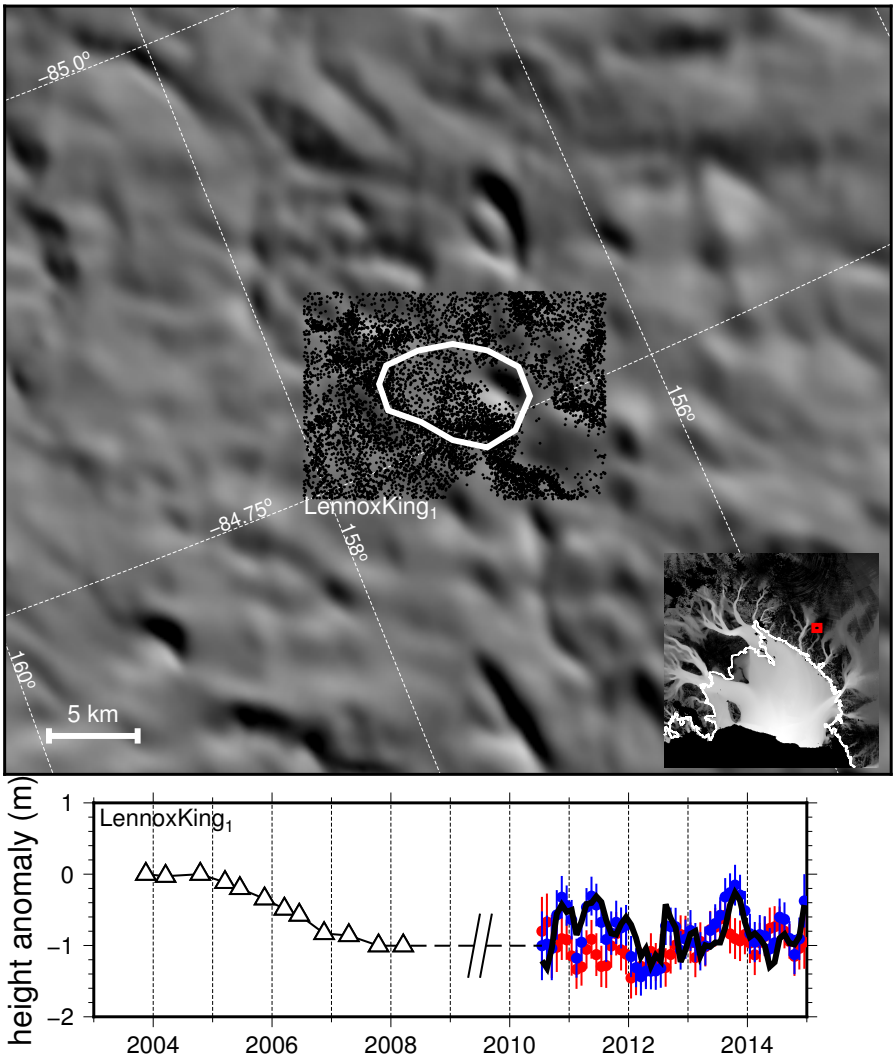

Figure 3.14: Top: Location of LennoxKing$_1$, with CryoSat-2 SARIn footprints relative to lake outlines (*Smith et al.*, 2009) and MODIS visual imagery (*Scambos et al.*, 2007). Inset shows location relative to ice velocity (*Rignot et al.*, 2011b) using the same colorscale as Figure 3.1. Bottom: Extended time series of subglacial lake height anomaly at LennoxKing$_1$. Triangles are the existing ICESat-derived time series (*Smith et al.*, 2009), while new CryoSat-2 time series (with formal-errors bars) is shown in red (off-lake heights), blue (on-lake heights), and black (lake height accounting for regional trends).

Ninnis Lakes

There are two lakes beneath Ninnis Glacier, East Antarctica: Ninnis_1 (190 km^2; named Cook_{W1} in *Smith et al.* (2009); lake named Ninnis_1 in *Smith et al.* (2009) was renamed to Mertz_1 for the deposited NSIDC inventory) and Ninnis_2 (227 km^2; named Cook_{W2} in *Smith et al.* (2009)). The ice surface fell by 0.7 m between 2004.5 and 2006.5 at Ninnis_1 and fell by 0.3 m between 2003.5 and 2006.5 at Ninnis_2, before increasing by 0.3 m over the last 1.75 years of the record (Figure 3.15). During the CryoSat-2 period, there was a negative height trend both on and off the lake, with the heights averaged over the lake decreasing at -0.3 m yr^{-1} after correcting for the regional signal. At Ninnis_2, heights remained constant over the 4.5-year time-period, both on and off the lake.

Recovery Ice Stream Lakes

Only the two lowermost subglacial lakes of the Recovery Ice Stream were within the SARIn-mode mask: Rec1 (1002 km^2) and Rec2 (680 km^2) (Figure 3.16). *Fricker et al.* (2014) discussed this connected lake system in detail. Briefly, surface height at Rec1 increased by 3.7 m between the beginning of the ICESat mission in late 2003 and Sep. 2008, while surface height at Rec2 increased by $\sim$1.6 m between Mar. 2006 and Mar. 2007, then decreased by 1.1 m between Mar. 2007 and Nov. 2009. Subsequent OIB data revealed a $\sim$2 m and $\sim$3 m drop in height at Rec1 and Rec2, respectively, between 2011 and 2012. CryoSat-2 SARIn-mode only covered Rec1 and Rec2 starting in mid 2013, with Rec2 lying on the edge of the mode-change boundary between SARIn and LRM (similar to Byrd_{s1}). Rec1 showed no significant change in surface height during the 1.5-year period, while the average height at Rec2 decreased by 1.0 m over the period, with the rate of change decreasing through time.

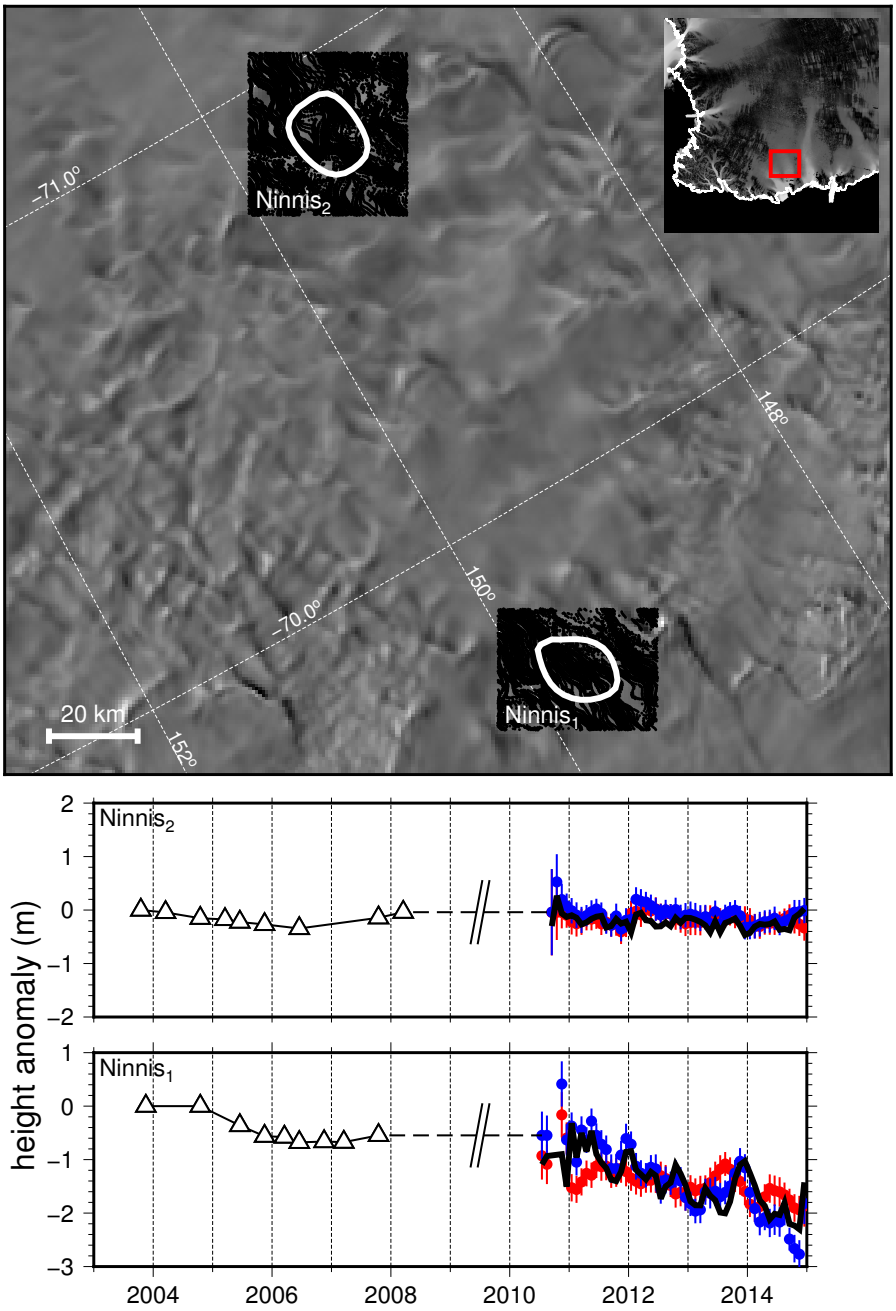

Figure 3.15: Top: Location of Ninnis Glacier lakes, with CryoSat-2 SARIn footprints relative to lake outlines (*Smith et al.*, 2009) and MODIS visual imagery (*Scambos et al.*, 2007). Inset shows location relative to ice velocity (*Rignot et al.*, 2011b) using the same colorscale as Figure 3.1. Bottom: Extended time series of subglacial lake height anomaly at Ninnis_1 and Ninnis_2. Triangles are the existing ICESat-derived time series (*Smith et al.*, 2009), while new CryoSat-2 time series (with formal-errors bars) is shown in red (off-lake heights), blue (on-lake heights), and black (lake height accounting for regional trends).

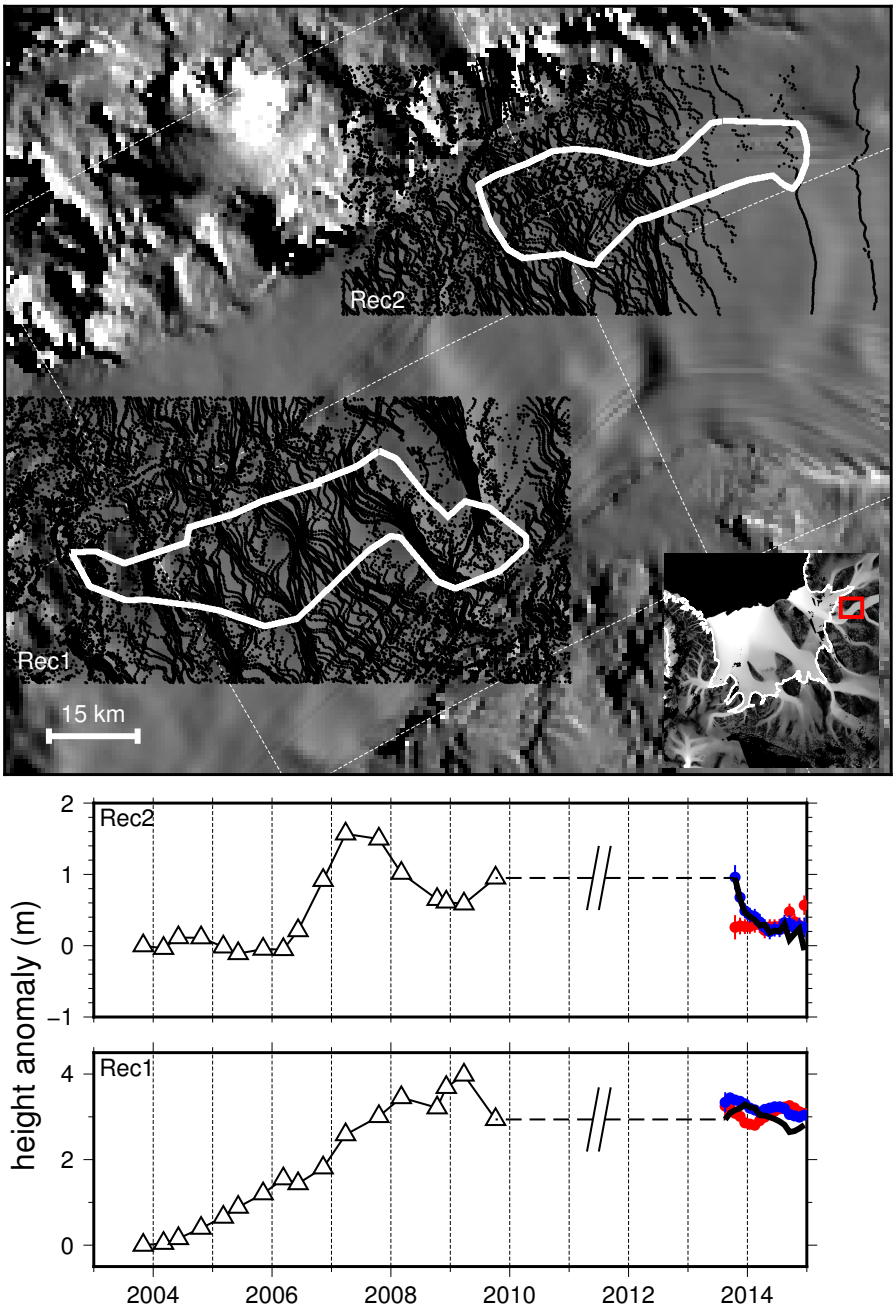

Figure 3.16: Top: Location of Recovery Ice Stream lakes, with CryoSat-2 SARIn footprints relative to lake outlines (*Fricker et al.*, 2014) and MODIS visual imagery (*Scambos et al.*, 2007). Inset shows location relative to ice velocity (*Rignot et al.*, 2011b) using the same colorscale as Figure 3.1. Bottom: Extended time series of subglacial lake height anomaly at Rec1 and Rec2. Triangles are the existing ICESat-derived time series (*Fricker et al.*, 2014), while new CryoSat-2 time series (with formal-errors bars) is shown in red (off-lake heights), blue (on-lake heights), and black (lake height accounting for regional trends).

Slessor Lakes

Located adjacent to the Recovery Ice Stream, Slessor Glacier had three lakes from the *Smith et al.* (2009) inventory covered by CryoSat-2 SARIn-mode: Slessor_1 (245 km^2), Slessor_2 (137 km^2), and Slessor_3 (107 km^2) (Figure 3.17). During the ICESat mission, Slessor_1 and Slessor_3 showed similar height changes, with height markedly decreasing from the start of the ICESat period (late 2003) to late 2005 (-0.9 m and -1.3 m at Slessor_1 and Slessor_3, respectively) followed by minimal changes to early 2008. The ice-surface height at Slessor_2 monotonically increased by 5.6 m over the ICESat period. Interestingly, Slessor_2 and Slessor_3, which abut each other, exhibited changes of opposite sign.

CryoSat-2 coverage only started in late 2013 for the upper two lakes, yielding slightly over one year of additional data. During the end of this period, Slessor_2 experienced a rapid height decrease of 10.7 m over four months. Because of this large dynamic signal in the region surrounding Slessor_3, we could not apply the correction for regional ice dynamics. Data from within the boundary of Slessor_3, however, showed a height-change signal that correlated with, though smaller in magnitude than, height changes at Slessor_2. This correlated behavior contrasted with the anti-correlated behavior observed between these two lakes during the ICESat period. Data at Slessor_1 were noisy with a large data gap in the middle of the lake, but there was no indication of a corresponding increase in surface height related to the decrease at Slessor_2.

Totten Lakes

Subglacial lakes Totten_1 (567 km^2) and Totten_2 (711 km^2) are both large subglacial lakes in the upstream catchment of Totten Glacier, East Antarctica (Figure 3.18). From late 2003 to late 2005, heights decreased by 1.5 m at Totten_1,

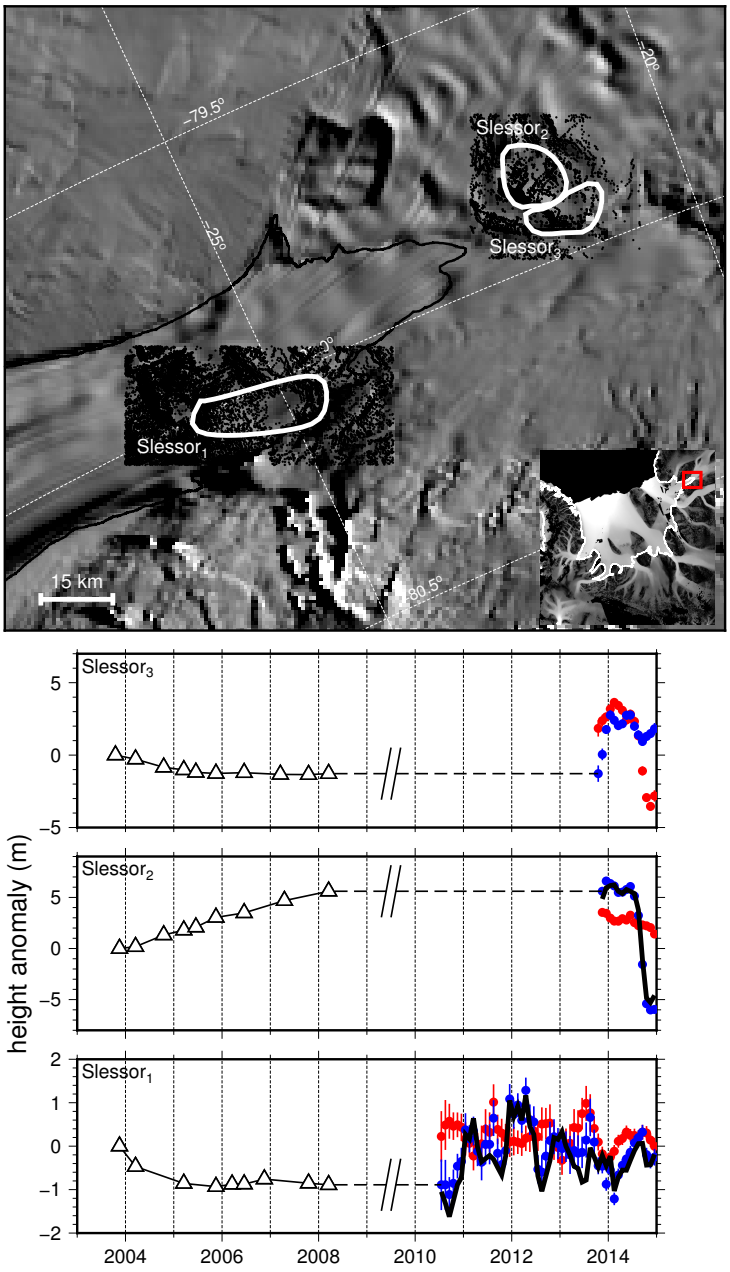

Figure 3.17: Top: Location of Slessor Glacier lakes, with CryoSat-2 SARIn footprints relative to lake outlines (*Smith et al.*, 2009) and MODIS visual imagery (*Scambos et al.*, 2007). Inset shows location relative to ice velocity (*Rignot et al.*, 2011b) using the same colorscale as Figure 3.1. Bottom: Extended time series of subglacial lake height anomaly at Slessor_1, Slessor_2, and Slessor_3. Triangles are the existing ICESat-derived time series (*Smith et al.*, 2009), while new CryoSat-2 time series (with formal-errors bars) is shown in red (off-lake heights), blue (on-lake heights), and black (lake height accounting for regional trends).

then increased by 0.7 m from 2006 to early 2008. Height changes at Totten_2, decreasing by 0.8 m between early 2004 and mid-2005, increasing by 0.6 m for the next 1.5 years, and decreasing again by 0.5 m until 2008. During the CryoSat-2 mission, both lakes experienced small height fluctuations, which appear to be in-phase with the regional fluctuations exhibited outside the lake boundaries.

Wilkes Lakes

Wilkes_1 (596 km^2; Figure 3.19) and Wilkes_2 (179 km^2; Figure 3.20) both increased in surface height throught the duration of the ICESat mission (Wilkes_1 by 0.7 m and Wilkes_2 by 0.4 m). Wilkes_1 showed no height changes during the CryoSat-2 mission, while the smaller Wilkes_2 had a more variable time series, which also suggested no significant dynamic changes in height over the lake. While these two lakes are both in Wilkes Land (hence their name), they are separated by over 600 km.

3.5 New Insights into Antarctic Subglacial Hydrology from CryoSat-2

Many subglacial lakes investigated in this study, especially those in East Antarctica, were located in areas of steep or rough surface topography, which significantly impacts the effectiveness of CryoSat-2 SARIn-mode altimetry. Previous work has established that, in areas of steep terrain, the SARIn-mode waveform can be unwrapped yielding a swath of height data (e.g., *Hawley et al.*, 2009). Applying swath mapping to this subset of lakes, which requires building a robust unwrapper program for processing raw CryoSat-2 waveforms, will likely provide a more precise time series of subglacial lake activity during the CryoSat-2 period.

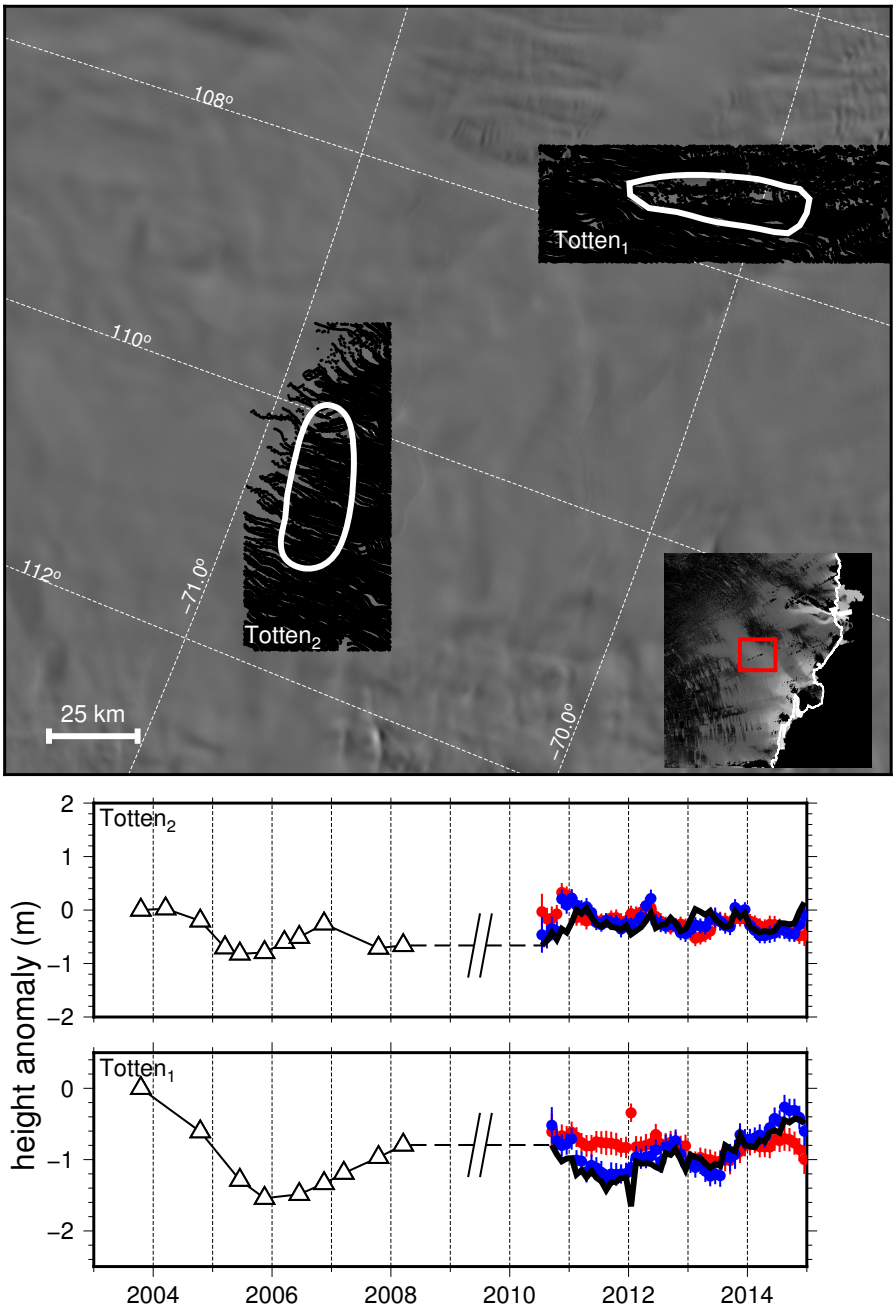

Figure 3.18: Top: Location of Totten Glacier lakes, with CryoSat-2 SARIn footprints relative to lake outlines (*Smith et al.*, 2009) and MODIS visual imagery (*Scambos et al.*, 2007). Inset shows location relative to ice velocity (*Rignot et al.*, 2011b) using the same colorscale as Figure 3.1. Bottom: Extended time series of subglacial lake height anomaly at Totten_1 and Totten_2. Triangles are the existing ICESat-derived time series (*Smith et al.*, 2009), while new CryoSat-2 time series (with formal-errors bars) is shown in red (off-lake heights), blue (on-lake heights), and black (lake height accounting for regional trends).

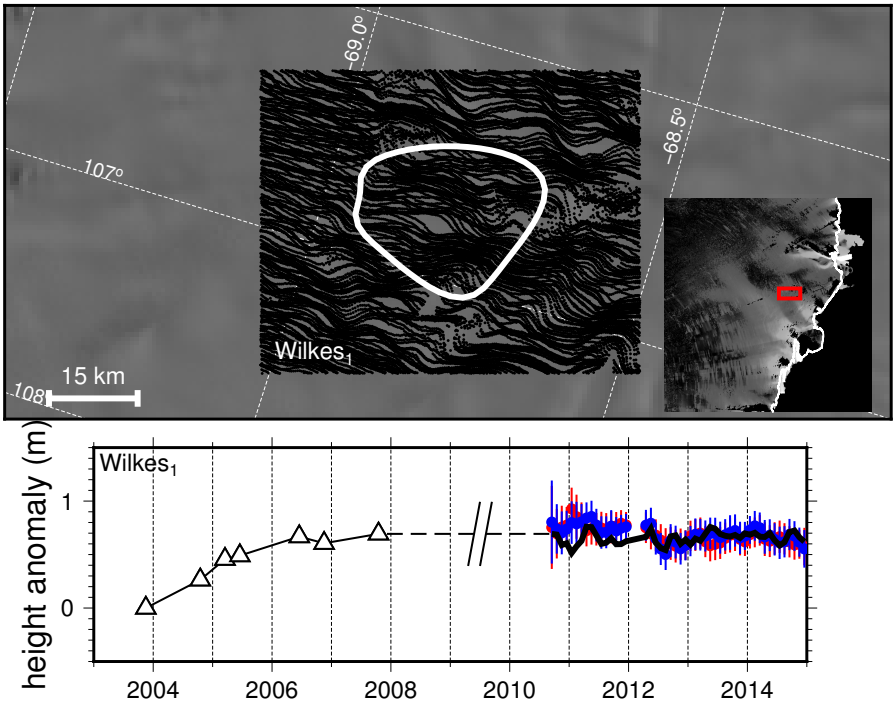

Figure 3.19: Top: Location of Wilkes_1, with CryoSat-2 SARIn footprints relative to lake outlines (*Smith et al.*, 2009) and MODIS visual imagery (*Scambos et al.*, 2007). Inset shows location relative to ice velocity (*Rignot et al.*, 2011b) using the same colorscale as Figure 3.1. Bottom: Extended time series of subglacial lake height anomaly at Wilkes_1. Triangles are the existing ICESat-derived time series (*Smith et al.*, 2009), while new CryoSat-2 time series (with formal-errors bars) is shown in red (off-lake heights), blue (on-lake heights), and black (lake height accounting for regional trends).

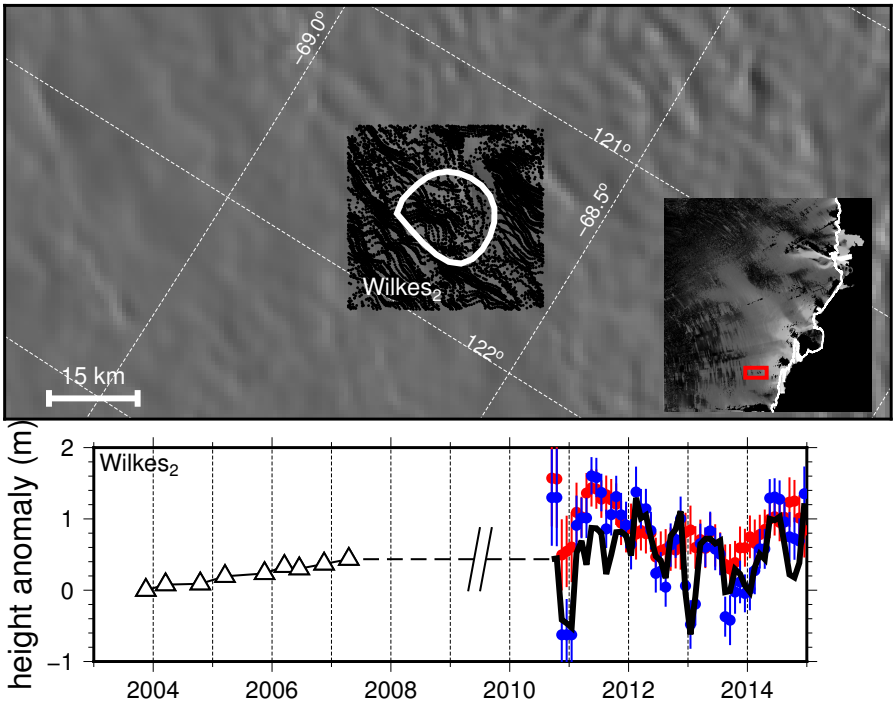

Figure 3.20: Top: Location of Wilkes_2, with CryoSat-2 SARIn footprints relative to lake outlines (*Smith et al.*, 2009) and MODIS visual imagery (*Scambos et al.*, 2007). Inset shows location relative to ice velocity (*Rignot et al.*, 2011b) using the same colorscale as Figure 3.1. Bottom: Extended time series of subglacial lake height anomaly at Wilkes_2. Triangles are the existing ICESat-derived time series (*Smith et al.*, 2009), while new CryoSat-2 time series (with formal-errors bars) is shown in red (off-lake heights), blue (on-lake heights), and black (lake height accounting for regional trends).

Future work should revisit these lakes after building and testing tools to unwrap the SARIn-mode phase data. Even with data sampling and precision limitations, we recorded large height-change events at nine subglacial lakes, which provide new insight into the basal hydrology system of Antarctica. We highlight three notable aspects of Antarctic subglacial hydrology revealed by the new, extended active subglacial lake records: the large event on Slessor Glacier, the inter-connected dyanmics of MacAyeal Ice Stream, and insights into the spatiotemporal variability of active lakes.

3.5.1 Slessor$_{23}$ Drainage

To better assess the full magnitude of the surface height anomaly near Slessor$_2$, we followed the methods of **Chapter 2** for creating a DEM-difference before and after a surface height anomaly. The resulting map of height differences (Figure 3.21) showed that the published outlines for both Slessor$_2$ and Slessor$_3$ were slightly offset relative to the height changes in the 2014 event and that the two lakes were likely actually one larger lake. We drew a new outline for this combined lake (which we call Slessor$_{23}$) and reprocessed the CryoSat-2 data to generate a time series of height anomalies. The newly-defined lake, with an area of 253 km^2, showed an average height change of -7.0 m over 6 months, with a peak one-month height-change of -2.9 m (equivalent to -35.0 m yr^{-1}).

The anomaly at Slessor$_{23}$ represents one of the largest observed by any technique, with over 1.8 km^3 of ice displaced over 6 months. The peak rate of ice displacement (-281 m^{3}s^{-1}) exceeds that of the largest subglacial lake drainage event in the inventory at Cook$_{E2}$ (*McMillan et al.*, 2013). The mean rate of volume-change is over 50% larger at Slessor$_{23}$ (-113 m^{3}s^{-1}) than the peak rate of change of the subglacial lake discharge event at Byrd Glacier, which caused a velocity increase of

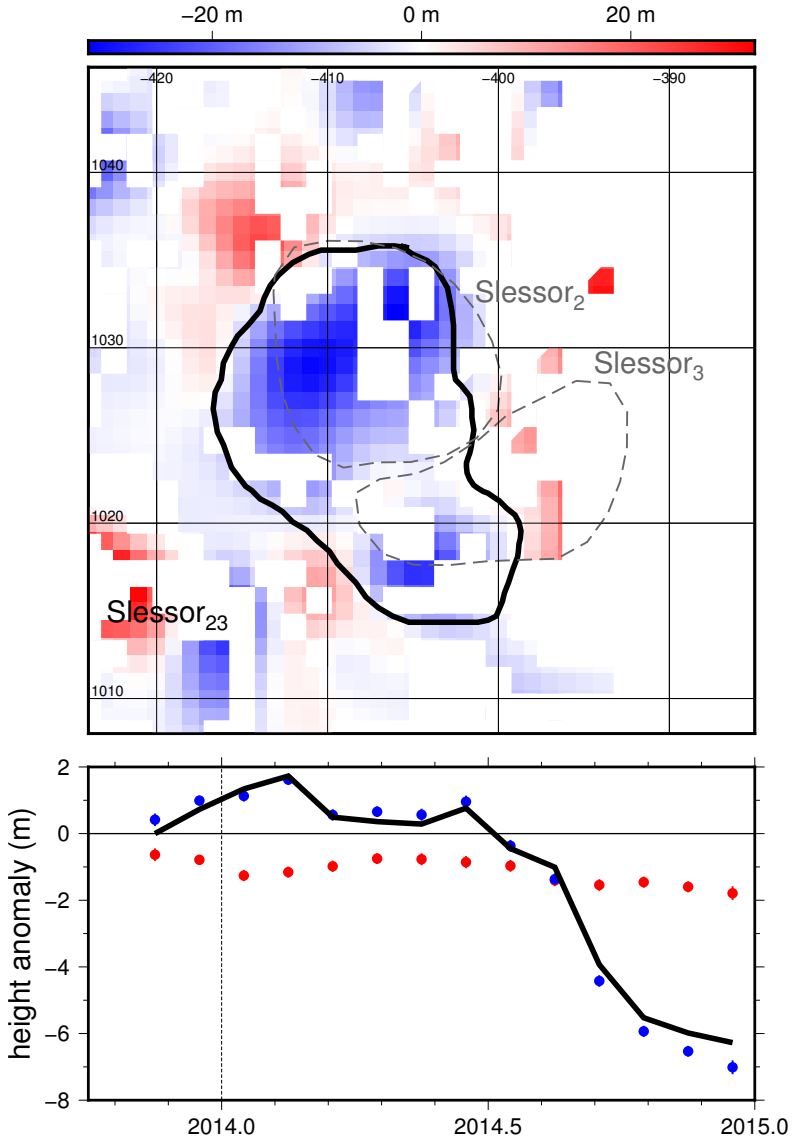

Figure 3.21: Top: Relative height change (in meters) between Jan.-Feb.-Mar. 2014 and Oct.-Nov.-Dec. 2014 at Slessor_2 and Slessor_3, masked to show only locations with CryoSat-2 observations during both periods. Previous ICESat-derived lake boundaries (dashed grey lines; *Smith et al.*, 2009) were offset relative to the extent of the large deflation event in 2014. Approximate outline for a combined lake, Slessor_{23}, shown in black. Bottom: Height-change time-series for the new lake outline, with on-lake average in blue, off-lake average in red, and the average lake height accounting for regional changes in black. ICESat data were not reprocessed to estimate 2003–2009 changes.

10% (*Stearns et al.*, 2008). Future work will investigate the impact of this large drainage event on the dynamics of Slessor Glacier.

3.5.2 Connected Hydrology on MacAyeal Ice Stream

On MacAyeal Ice Stream, CryoSat-2 analysis revealed a clearer picture of the connectivity between subglacial lakes. The coarse temporal resolution of ICESat compared to CryoSat-2 observations inhibited insight into the exact timing between lake activity (*Fricker et al.*, 2010). With the CryoSat-2 time series, the correlation between peak deflation rate at Mac3 and peak height at Mac 1 suggests that subglacial water drains directly from Mac3 into Mac1, bypassing Mac2. This relationship between discharge rate and heights is similar to that seen using GPS observation of surface heights on the Whillans/Mercer ice streams (**Chapter 4**). Moreover, the increased spatial resolution of CryoSat-2 DEMs in the area show a clear path of low hydropotential (i.e., lower elevation given relatively flat basal slopes) for subglacial water drainage from Mac3 to Mac1 (Figure 3.7). Future work will use these DEMs to more precisely map subglacial water transport routes to better understand the connected hydrology, especially in the context of other geophysical observations suggesting subglacial water movement (*Winberry et al.*, 2009).

3.5.3 Spatiotemporal Variability of Active Lakes

The new extended record of surface anomalies demonstrated that several, but not all, locations identified as active subglacial lakes continued to exhibit behavior after the end of the ICESat time series. On Whillans, Kamb, MacAyeal, Recovery, and Slessor ice streams, there were nine locations that had large (>1 m) surface height anomalies during the CryoSat-2 mission, in addition to the six events

previously reported using CryoSat-2 data (*McMillan et al.*, 2013, **Chapter 2**, and **Chapter 4** of this dissertation). Following existing literature, we interpret these events as the surface expression of moving subglacial water. The location of these features appeared to be stationary on Mercer, Whillans, Kamb, MayAyeal, and Recovery ice streams, with fill/drain cycles ranging generally between 1 and 5 years. The event at Slessor_{23} likely has a recurrence interval of a decade or longer, as do the large, previously documented events at SLE (*Fricker et al.*, 2007) and Cook_{E2} (*McMillan et al.*, 2013), demonstrating that active subglacial lakes operate on long timescales as well as short. The distribution of lakes across this continuum of recurrence intervals, but especially at long intervals, remains unknown. Moreover, because the time series of height change only spans one drainage event for each of these three large lakes, it is difficult to ascertain whether these features will in the future repeat similarly to the documented cases. Nevertheless, these events highlight the need to develop methods for identifying active subglacial lake locations using datasets collected before and after the ICESat mission because our existing inventory only includes lakes that exhibited change during a limited time window (especially compared to the long timescales of ice-sheet variability).

Some of the subglacial lakes that continued to show dynamic behavior had strong activity punctuated by periods of inactivity (e.g., SLW, L7, Mac1, and Cook_{E1}). These lakes seem to not store (and later release) significant quantity of basal water and consequently are not the main drivers of subglacial hydrologic variability; rather, these lakes seemed to react to upstream discharge events or regional shifts in hydropotenial and throttled the flow of water downstream. We conclude that care must be taken when analyzing a location as an "active" subglacial lake since it may actually be a "reactive" lake for which the regional hydrological context is paramount in understanding the individual lake's impact on the ice sheet.

There were also many locations identified as active subglacial lakes in the *Smith et al.* (2009) inventory that did not exhibit any dynamic behavior between 2010 and 2015. In multiple cases, including lakes on Byrd Glacier, Totten Glacier and Institute and Foundation ice streams, ICESat had observed small (<1 m) anomalies over large areas (resulting in relatively large volume changes given the low signal-to-noise ratio). This type of lake with fluctuations of 10s of cm in surface height during the ICESat mission may be related to basal water features as originally hypothesized, but also may be related to variability in surface processes, variability in the stress regime, or even noise in the original ICESat data. In some cases, including at David Glacier, Totten Glacier, and Foundation and Whillans ice streams, CryoSat-2 analysis, which has higher spatial resolution than ICESat (*Siegfried et al.*, 2014), revealed that the observed small-magnitude height-anomalies on these lakes were in-phase with small height-anomalies in the region outside the lake boundaries. This correlation suggests that these areas are in reality reflecting regional-scale changes rather than local hydrology. Although identifying the exact cause of such surface-height variation is difficult without coincident time-series observations of surface processes and ice velocity, interpreting future observations based on the previous identification of the area as an active subglacial lake from low-amplitude signals can result in flawed conclusions.

3.6 Summary

We reanalyzed 37 active subglacial lakes from the continent-wide *Smith et al.* (2009) inventory (2003–2008) using CryoSat-2 SARIn-mode data (2010–2015) to examine to what extent these locations have continued to exhibit anomalous surface-height change. Of these 37 locations, we found nine large height-change events that have occurred since July 2010, in addition to the six that have already

been identified by previous research (*McMillan et al.*, 2013, **Chapter 4**). One of these events has the highest rate of volume displacement ever recorded, peaking at over 280 m^3s^{-1}. We also found locations that likely are not areas of active subglacial hydrology, suggesting that our mapping and understanding of active subglacial lakes, a part of the basal water system only discovered in the last decade, are still immature.

To fully grasp the physical processes occurring beneath the ice sheet and how those processes affect ice dynamics requires continued monitoring of these locations with precise, time-resolved methods to estimate surface-height changes, surface-processes changes, and velocity changes. Furthermore, our existing inventory of subglacial lakes is limited by the duration for which we have precise, repeat altimetry measurements of the ice surface. In order to understand the co-evolution of active subglacial hydrology with the ice sheet, our collection of observations must be expanded in both time and space. Future polar-focused altimetry missions, with more technologically-advanced instrumentation (e.g., ICESat-2, scheduled for launch in 2017), will be essential for accomplishing these goals. We, however, must plan appropriately to ensure ice-focused cross-calibration experiments between missions to ensure the longest, most precise record of ice-surface height changes.

3.7 Acknowledgements

We thank the National Snow and Ice Data Center for access to the subglacial lake record, the European Space Agency for CryoSat-2 data, and NASA grant NNX11AQ78H for funding.

Chapter 3, in full, is currently being prepared for submission for publication of the material. The dissertation author was the primary investigator and author of this material.

Chapter 4

Rapid basal water system evolution triggered by a subglacial flood in West Antarctica

4.1 Abstract

Height-change anomalies in satellite-altimeter data have been interpreted as the surface expressions of basal water moving into and out of subglacial lakes on timescales of months to years. These signals have been mapped throughout Antarctica, but only broad connections between active lakes and ice dynamics have been made. We present the first high temporal-resolution observations of ice velocity evolution due to cascading subglacial lake drainage events using five years of Global Positioning System (GPS) data on Whillans and Mercer ice streams, West Antarctica. We identify three episodic ice velocity fluctuations of nearly 4% over two years correlated to lake drainage evolution and an eleven-month disruption of the tidally-modulated stick-slip cycle that dominates regional ice motion. These

observations reveal that basal conditions of an Antarctic ice stream can rapidly evolve and drive a dynamic ice response on sub-annual timescales, which can bias observations used to infer long-term ice-sheet changes.

4.2 Introduction

Water at the ice-bed interface controls the rate at which Antarctica's glaciers and ice streams flow towards the ocean, yet a calibrated, quantitative link between ice flow and subglacial hydrology remains elusive, primarily due to a lack of suitable observations to constrain models (*Flowers*, 2015). Observing the Antarctic basal water system, especially on large spatial-scales, is challenging due to its inaccessibility under thick ice, so information that we have is indirect, based on either: (i) airborne radio-echo sounding, which images the ice-bed interface based on its dielectric contrast (e.g., *Oswald and Robin*, 1973; *Vaughan et al.*, 2007; *Schroeder et al.*, 2013); or (ii) inferences from repeat-pass satellite altimetry of the ice surface (e.g., *Gray et al.*, 2005; *Wingham et al.*, 2006b; *Fricker et al.*, 2007). These ice-surface measurements identified spatially-coherent height anomalies that change on timescales of months to years and have been interpreted as the surface expression of the filling and draining of subglacial lakes (*Gray et al.*, 2005; *Wingham et al.*, 2006b; *Fricker et al.*, 2007; *Smith et al.*, 2009). On ice streams, these "active" lakes can perturb ice dynamics by sequestering and episodically releasing up to cubic kilometers of subglacial meltwater generated in the upstream catchment. Simultaneous observations of surface-height anomalies and ice-velocity changes would, therefore, provide important constraints to the current generation of process-based subglacial hydrology models.

There have been only two documented cases of a direct connection between subglacial lake discharge and ice dynamical changes in Antarctica (*Stearns et al.*,

2008; *Scambos et al.*, 2011). These studies both used subglacial-lake activity records derived from satellite laser altimetry with 3–4 month temporal resolution and ice velocities derived from optical-image feature-tracking at episodic and typically infrequent intervals (generally one year or longer). This limited availability of velocity-change measurements may alias other dynamic signals occurring in the region and prevents a better understanding of how subglacial hydrological systems co-evolve with the overlying ice sheet on shorter timescales.

The lower confluence of Whillans and Mercer ice streams (WIS/MIS) is a unique location to study the interaction between subglacial hydrology and ice dynamics due to the presence of a well-studied system of interconnected subglacial lakes (*Fricker et al.*, 2007; *Fricker and Scambos*, 2009; *Carter et al.*, 2013; *Siegfried et al.*, 2014; *Tulaczyk et al.*, 2014) on a sensitive ice-bed interface (i.e., low (<10 kPa) driving and basal stresses) over an area of ∼20,000 km^2 (*Bindschadler et al.*, 2003; *Joughin et al.*, 2004a). On diurnal timescales, ice here moves via tidally-paced "stick-slip" motion, in which minor tidal-amplitude changes (±1 m) cause velocity fluctuations of more than an order of magnitude (*Bindschadler et al.*, 2003). This stick-slip motion arises from a delicate balance between driving and resistive stresses at the bed (*Winberry et al.*, 2014): when the accumulated stress exceeds a failure threshold, typically occurring twice daily at high- and low-tide, the ice rapidly slides downstream by 10s of centimeters in <1 hour. The failure threshold, however, is not always met at low tide due to a combination of the regional deceleration (*Beem et al.*, 2014) and amplitude variations of tidal constituents with greater than diurnal periods (e.g., fortnightly, semi-annual). When the threshold is not exceeded, there is no slip event until the following high tide, resulting in an inter-event duration of ∼24–28 hours (*Winberry et al.*, 2014). While long-term rates of ice flux to the ocean likely are not sensitive to stick-slip motion specifics, understanding stick-slip

dynamics can reveal clues about basal properties that are otherwise only available through direct sampling of the ice-bed interface (*Goldberg et al.*, 2014).

4.3 Data and Methods

4.3.1 GPS Array and Processing

Shortly after the initial discovery of WIS/MIS lakes (*Fricker et al.*, 2007), we began to install a semi-continuous, evolving array of up to 23 GPS stations that operated until 2015 (Figure 4.1a). We collected GPS data with Trimble NetRS or NetR9 receivers equipped with Trimble Zephyr Geodetic or Zephyr Geodetic II antennas and recording at either 15 s or 30 s intervals. Due to both the long baseline to the nearest fixed GPS base station (upwards of 200 km at some sites) and gaps in the base station data collection due to equipment failure, we processed the GPS data using a precise point positioning (PPP) technique implemented by Natural Resources Canada's online tool Canadian Spatial Reference System-Precise Point Positioning (CSRS-PPP). In this analysis, we used data between 1 January 2010 and 1 January 2015, as we had at least one GPS continuously collecting data during this time period.

4.3.2 Subglacial Lake Time Series

We followed the methods of *Siegfried et al.* (2014) to generate a self-consistent record of surface height anomalies across WIS/MIS subglacial lakes using ICESat laser altimetry (release 633, applying the Gaussian-Centroid correction following *Borsa et al.* (2014)), CryoSat-2 SARIn-mode radar altimetry (Baseline B release), and local GPS height data (Figures 4.1b-d). We performed this analysis from the start of the ICESat mission (late 2003) to the end of the GPS record (1 January

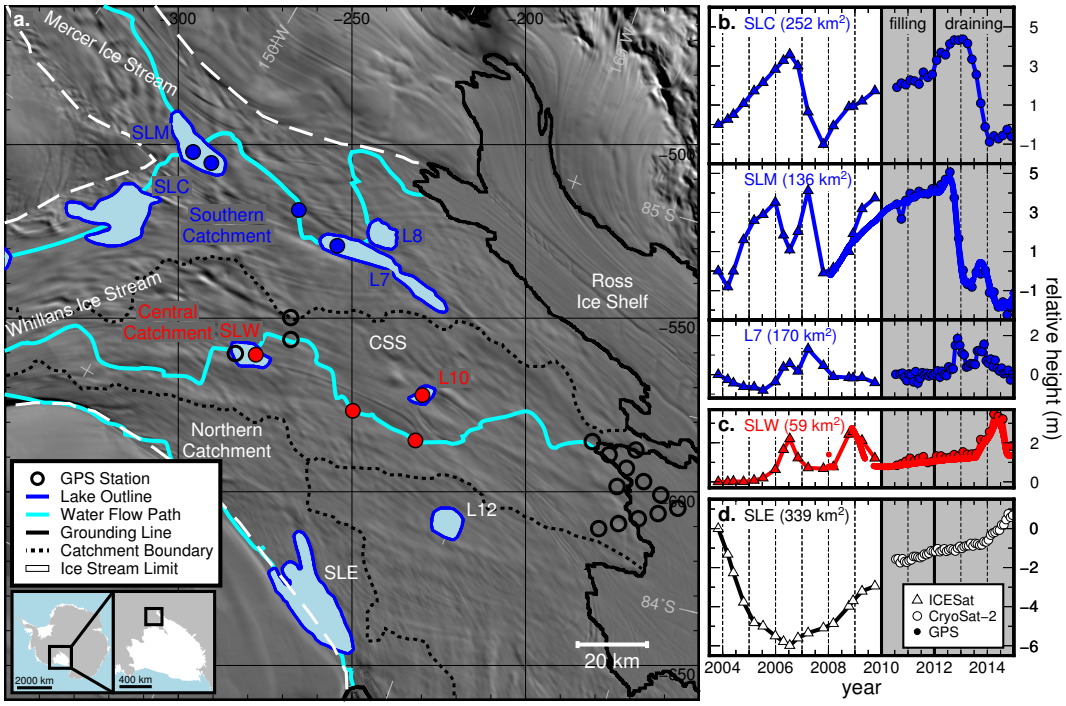

Figure 4.1: Map of WIS/MIS subglacial lakes, instrumentation, and record of lake activity. (a) Imagery mosaic of WIS/MIS (*Scambos et al.*, 2007), with locations of GPS sites, subglacial lakes (*Fricker and Scambos*, 2009), inferred subglacial water flow paths (*Carter et al.*, 2013), and subglacial hydrological catchment boundaries. The eight GPS stations used in this study are colored by catchment. CSS marks approximate location of the "central sticky spot" (*Winberry et al.*, 2014). Time-series of surface height anomalies for lakes in the (b) southern catchment, (c) central catchment, and (d) northern catchment. Grey shading (2010–2015) indicates period of GPS coverage shown in Figure 4.2 and 4.3, with identified phases of filling and draining marked.

2015) for the five largest subglacial lakes in the region: Subglacial Lake Conway (SLC), Subglacial Lake Mercer (SLM), Subglacial Lake 7 (L7), Subglacial Lake Whillans (SLW), and Subglacial Lake Engelhardt (SLE).

We converted lake-averaged height change to ice volume displacement (i.e., the volume of ice vertically displaced relative to October 2003) by multiplying height-change anomalies by lake areas from *Fricker and Scambos* (2009). This volume has previously been reported as the volume of subglacial water in the lake (e.g., *Fricker et al.*, 2007; *Fricker and Scambos*, 2009; *Smith et al.*, 2009); because surface-height changes are the result of a combination of subglacial water movement and dynamic changes within the ice column due to stress-regime changes (e.g., *Sergienko et al.*, 2007), we prefer this change in nomenclature. We also differentiated the ice volume displacement ($\frac{\mathrm{d}(vol)}{\mathrm{dt}}$) to use as a proxy for subglacial water discharge (Figure 4.2b). While $\frac{\mathrm{d}(vol)}{\mathrm{dt}}$ values are likely not the exact rates of hydrologic activity, we believe they represent upper limits for these rates as ice dynamical changes generally will act with the same sign as hydrologic changes (i.e., dynamic thickening due to reduced downstream lubrication during lake filling and dynamic thinning due enhanced downstream lubrication during lake drainage).

4.3.3 Velocity

Because lower WIS/MIS moves via stick-slip motion, velocities on sub-daily timescales can vary by over two orders of magnitude, complicating analysis of longer-term (i.e., >30 day) velocity changes. To mitigate this issue, we developed methods to remove the stick-slip signal while still accurately estimating velocity over sub-annual intervals. We first estimated a daily position from the processed GPS data. We then differentiated the time-series of positions in wavelet space, transformed back to the time-domain to calculate velocities, and low-pass filtered

the results with an eight-week window to remove short-term, periodic signals (e.g., variations due to fortnightly tides). We verified this method for deriving velocities in a stick-slip regime using synthetic GPS data (see Auxiliary Material).

4.3.4 Slip Detection and Statistics

From our 2010–2015 GPS position data, we manually picked approximate times of each slip event for the complete GPS dataset. We cross-referenced the approximate slip catalogue with every GPS station to ensure no slips were missed and no erroneous slips were picked. After coarse manual picking, we applied a semi-automated picking scheme based on velocity thresholds to select slip-event start and end points. We applied this scheme at the GPS station closest to the central sticky spot (CSS in Figure 4.1a) (*Winberry et al.*, 2014) that reliably recorded the slip event. Comparing to an existing catalogue of WIS/MIS slip events picked via more accurate seismic methods (*Pratt et al.*, 2014), we found the uncertainty of our method to be 2.0 ± 2.6 (1σ) minutes, which is accurate enough to assess the ocean tidal state at the initiation of the slip event as well as inter-event durations on the scale of hours. We estimated slip event statistics (Figure 4.3) over 28-day windows (nominally two fortnightly tidal cycles), centered every seven days.

4.3.5 Inter-event Strain Rate

We estimated inter-event strain-rates approximately along ice-flow (between GPS stations on SLM and L7) and approximately across ice-flow (between GPS stations on L7 and SLW). Due to imprecision resulting from inconsistent slip-event start and stop times, individual GPS mid-winter data gaps, and variability with tidal-height, we could not calculate the strain accumulated between each pair of slip events, which is $O(0.01\text{m})$. Instead, we converted long-term ice velocities to

inter-event velocities by multiplying by the fraction of annual motion at each GPS station that occurred during inter-event periods (0.85 at SLM, 0.40 at L7, 0.40 at SLW). We then estimated inter-event axial and lateral strain-rates from velocity differences between pairs of GPS stations.

4.4 Results and Discussion

4.4.1 Regional Hydrology

Our GPS-derived height-change record captured two distinct phases of the regional subglacial hydrologic system (Figures 4.1b-d, 4.2a): (i) a two-year period (January 2010 to December 2011) during which heights across each lake increased monotonically as they had since mid-2008 (*Siegfried et al.*, 2014), indicative of subglacial lakes slowly filling (the "filling phase"); and (ii) a three-year period (January 2012 to December 2014) during which the height of one or more of the subglacial lakes markedly decreased (the "draining phase"). We interpret the two-year filling phase as the "baseline state" in order to understanding how the discharge of water from subglacial lakes affects ice dynamics.

SLC, SLM, and L7 are thought to be hydrologically connected based on the filling patterns evident in the ICESat record, which suggest that subglacial water moves from SLC to SLM to L7 (*Fricker and Scambos*, 2009). Our patterns of GPS- and CryoSat-2-derived ice volume change during the draining phase are consistent with this hypothesis: values at SLM and L7 fluctuate simultaneously in response to upstream changes at SLC. In the Central Catchment, the extended time-series captured a third fill/drain cycle at SLW. When converted to volumes of ice displacement (Figure 4.2a), the changes the Central Catchment (red) were over an order of magnitude smaller than those in the Southern Catchment (blue). In the

Northern Catchment, the monotonic height increase of SLE, the largest WIS/MIS lake, that had started in late 2006 (*Fricker et al.*, 2007) continued until the end of the record in December 2014, for a total change of 6.7 m (2.3 km^3).

4.4.2 Velocity Changes

Our velocity estimates from GPS observations across WIS/MIS (Figure 4.2c) revealed distinctly different dynamic behavior between the filling and draining phases. During the filling phase, GPS-derived ice velocities were consistent with long-term deceleration (*Beem et al.*, 2014). Overall, we estimated an average velocity slow-down for the years 2010–2011 of 1.9–2.7% yr^{-1} across WIS/MIS (Figure 4.2c). During the draining phase, there was a broad departure from this deceleration, and in the Southern Catchment the regional signal was temporarily reversed and there was slight ice-stream acceleration. To highlight this change from the background state, we calculated the velocity anomaly after removing the long-term trend (Figure 4.2d). The detrended velocity anomalies revealed a clear semi-annual velocity cycle with amplitude of 0.32%, which we also removed (see Auxiliary Material for velocity anomalies without this signal removed).

In the detrended velocity anomalies, we observed two years (2012–2013) of enhanced ice flow, when velocities across the region were up to 3.8% higher than a baseline of continued deceleration at 2010–2011 rates. The period of speed-up began in January 2012, when the height at SLM briefly stopped increasing ($\frac{\mathrm{d}(vol)}{\mathrm{dt}} \sim 0$), and ended in December 2013 when SLC reached low-stand (Figure 4.2a). We observed three distinct periods of acceleration leading up to velocity peaks (v_{P1}, v_{P2}, and v_{P3} in Figures 4.2, 4.3), and each correlated to specific features of the height-change time series:

- v_{P1} occurred in early 2012 amidst a rapid increase of $\frac{\mathrm{d}(vol)}{\mathrm{dt}}$; velocities were

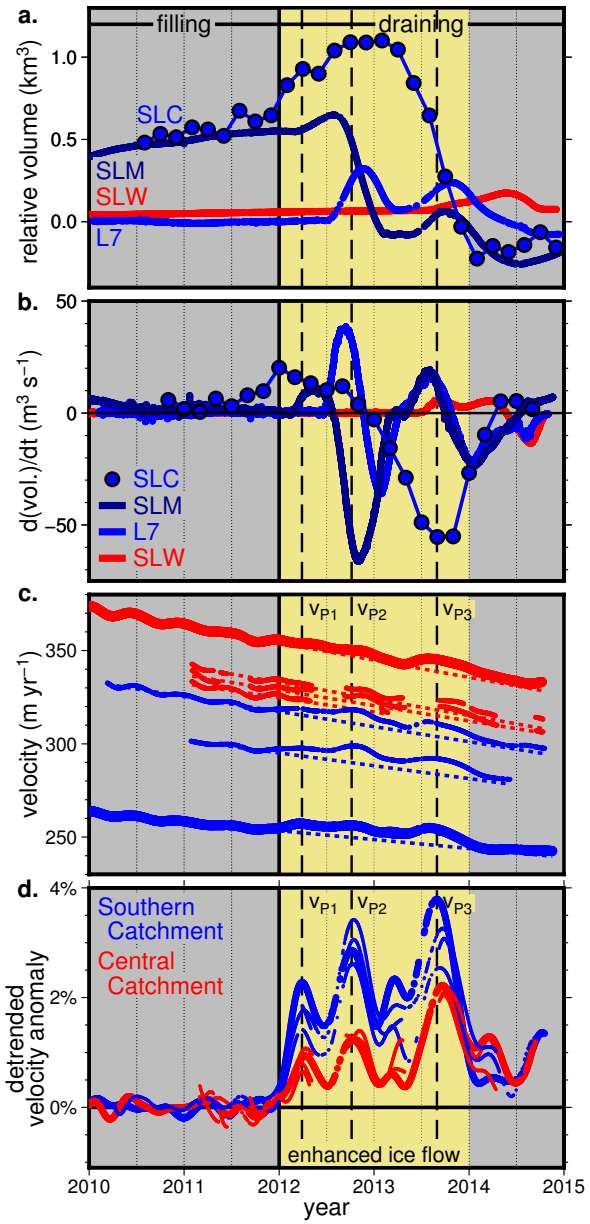

Figure 4.2: Time series of ice-volume displacement with coincident ice-velocity changes. (a) Ice volume displacement at SLM, L7, and SLW (GPS-based) and SLC (CryoSat-2-based), colored by subglacial hydrologic catchment (Figure 4.1). Vertical dashed lines correspond to velocity peaks. (b) Rate of volume change for time-series in (a). (c) Surface ice velocity at four GPS stations in each catchment (locations indicated in Figure 4.1a). SLM and SLW GPS represented by thicker lines, and extrapolated velocities based on 2010-2011 deceleration shown as dashed lines. (d) Velocity anomalies shown as percent difference from dashed line in (c). Yellow-shaded region indicates the period of enhanced ice velocities. Filling and draining phases separated by solid vertical line.

2.3% higher than the baseline at SLM and only 0.9% higher at SLW.

- v_{P2} was in late 2012, when heights at SLM were decreasing and heights at L7 were increasing. The peak occurred 31 days after the maximum $\frac{\mathrm{d}(vol)}{\mathrm{dt}}$ at L7, 18 days before the minimum $\frac{\mathrm{d}(vol)}{\mathrm{dt}}$ at SLM, and 35 days before the peak in surface height at L7. At v_{P2} the maximum velocity increase at the GPS station between SLM and L7 (3.4%) was nearly three times greater than that at SLW (1.2%).

- v_{P3} occurred in late 2013, 27 and 19 days after peak $\frac{\mathrm{d}(vol)}{\mathrm{dt}}$ at SLM and L7, respectively, and 37 and 50 days before peak heights at SLM and L7, respectively. Due to the coarse temporal resolution of CryoSat-2 data compared to GPS, it is hard to assess where the timing of peak velocity compared to $\frac{\mathrm{d}(vol)}{\mathrm{dt}}$ at SLC, but it appears that the $\frac{\mathrm{d}(vol)}{\mathrm{dt}}$ minimum continued while ice velocities decrease. Velocity was 3.8% higher than the baseline at SLM, almost twice as large as the velocity increase at SLW (2.2%). The magnitude of v_{P3} may also have been influenced by SLW activity.

After v_{P3}, surface heights of SLC, SLM, and L7 decreased and ice flow in both catchments rapidly decelerated, with ice in the southern catchment decelerating at a higher rater than that in the central catchment (sustained >10% yr^{-1} (>25.6 m yr^{-2}) for nearly six weeks at SLM compared to a peak deceleration of 5.9% yr^{-1} (21.4 m yr^{-2}) at SLW).

We propose that these three transient acceleration events are related to the dynamic ice-stream response to subglacial water moving through the Southern Catchment. The pause in ice-surface inflation (i.e., $\frac{\mathrm{d}(vol)}{\mathrm{dt}} \sim 0$) during the first acceleration event in early 2012 could represent the first release of water from SLM, a hypothesis based on previous modeling studies which indicate that, given constant

inflow, significant outflow from a subglacial lake initiates before surface heights decrease (*Carter et al.*, 2013). The velocity peak itself (v_{P1}) occurred just after an abrupt switch from heights slowly decreasing to rapidly increasing (Figure 4.2a, Auxiliary Material). We propose that the timing of v_{P1} may correspond to a local switch from outflow through an inefficient, distributed drainage system (in which water flux is correlated to ice velocity) to an efficient, channelized system (in which water flux is anti-correlated to ice velocity). The switch in drainage regime would siphon water from the distributed system to the channelized system, increasing basal traction downstream of SLM. This change in basal lubrication could cause a dynamic ice-thickness change, explaining the sudden increase in surface height. Alternative explanations for the rapid inflection in surface-height rate-of-change include increased flow of subglacial water into SLM from changes to upstream hydrology and geometric changes that temporarily increased SLM's capacity. While we cannot rule out alternative hypotheses, the velocity observations are generally consistent with the proposed drainage system evolution.

The second and third acceleration events could represent transient episodes of decreased basal traction resulting from the discharge of up to $\sim$0.8 km^3 water over 8 months from SLM into L7 and the discharge of up to $\sim$1.3 km^3 of water over 12 months from SLC into SLM and L7. Broadly, the correlation between v_{P2} and v_{P3} with large, negative $\frac{\mathrm{d}(vol)}{\mathrm{dt}}$ values at SLM and SLC, respectively, drives this hypothesis. If the elevated ice velocities were driven by subglacial hydrology, a closer examination of the relationship between the evolution of volume displacement and velocity may reveal additional information about the nature of the basal water system (see also, *Magnússon et al.*, 2007; *Moon et al.*, 2014).

There are two end-member cases of the relationship between basal water and velocities: (1) sliding velocity increases due to increased bed separation, and

(2) sliding velocity increases due to effective stress. In the first case, ice-bed contact area, which likely correlates with $\frac{\mathrm{d}(vol)}{\mathrm{dt}}$, would primarily control velocity (e.g., *Alley*, 1989; *Creyts and Schoof*, 2009). Therefore velocities should reach a maximum when $\frac{\mathrm{d}(vol)}{\mathrm{dt}}$ reaches a minimum. In the second case, a maximum in subglacial storage volume, which is determined by subglacial water pressure, corresponds to a minimum in effective stress and high velocities (e.g., *Tulaczyk et al.*, 2000; *Truffer et al.*, 2001). In this case, velocities should reach a maximum when $\frac{\mathrm{d}(vol)}{\mathrm{dt}}$ also reaches a maximum.

In our observations of WIS/MIS, however, both velocity peaks occurred after maxima in $\frac{\mathrm{d}(vol)}{\mathrm{dt}}$ of downstream lakes and before minima in $\frac{\mathrm{d}(vol)}{\mathrm{dt}}$ of upstream lakes. We then suggest that, if the accelerations were driven by subglacial hydrology, neither of these end-member cases is sufficient to explain the impact of subglacial lake drainages on this region's ice dynamics. Moreover, SLM had two episodes of highly negative $\frac{\mathrm{d}(vol)}{\mathrm{dt}}$ (i.e., two drainages of subglacial water out of the lake). In the first case (late 2012), increasing drainage correlated to increasing velocity, while in the second case (late 2014), increasing drainage correlated to decreasing velocity. These observations highlight that the coupled subglacial-glacial system may rapidly evolve in such a way that observations from a single location provide data to support contradictory inferences.

4.4.3 Stick-Slip Changes

Monitoring of the region's stick-slip motion throughout an active subglacial hydrologic period provides additional information about ice-bed interface dynamics. Again, we used the filling phase to define the "normal" baseline dynamics and analyzed changes during the draining phase to understand the impact of subglacial drainage events. During the filling phase, the timing of stick-slip events was related

to ocean tidal height, as previously observed (*Bindschadler et al.*, 2003; *Winberry et al.*, 2014) (Figure 4.3a). The average number of slip events per year steadily decreased over the two years (2010–2011; Figure 4.3b), while the mean interval between slip events increased (Figure 4.3c). The median inter-event interval was highly correlated with the difference between the number of high-tide and low-tide slip events (Figure 4.3c), consistent with a model of deceleration accommodated by skipped low-tide events. Previous work by *Winberry et al.* (2014) hypothesized that skipped slips and consequent ice deceleration are related to decreased lubrication of the ice-bed interface; this inference agrees with our surface-height observations which show that large subglacial lakes impound water during this period.

Normal ice stream stick-slip behavior (*Bindschadler et al.*, 2003; *Winberry et al.*, 2014) was disrupted for the first ∼11 months of the draining phase. This manifested as a shift in slip-event timing (Figure 4.3), with no measurable change in slip-event magnitude or velocity (Figure 4.4). Coinciding with the initial acceleration to v_{P1} (Jan.–Feb. 2012), this shift began with a switch to more slip events occurring at high tide relative to low tide (Figures 4.3a, 4.3b). During the filling phase, such a relative increase in high-tide slip events corresponded to more skipped slip events and a higher median inter-event duration; during the draining phase, however, the increased number of high-tide slip events corresponded to a decrease in median inter-event duration and slip events occurring more frequently. This change can clearly be seen in the shift to anti-correlation between median inter-event duration and difference in number of high- and low-tide slip events (Figure 4.3c).

Between v_{P1} and v_{P2} (Apr.–Aug. 2012), the balance between high-tide and low-tide events switched again, this time to progressively more low-tide slip events. As L7 began filling in August 2012, slip events no longer regularly occurred near tidal extremes, suggesting that tidal modulation of the basal stress-cycle became

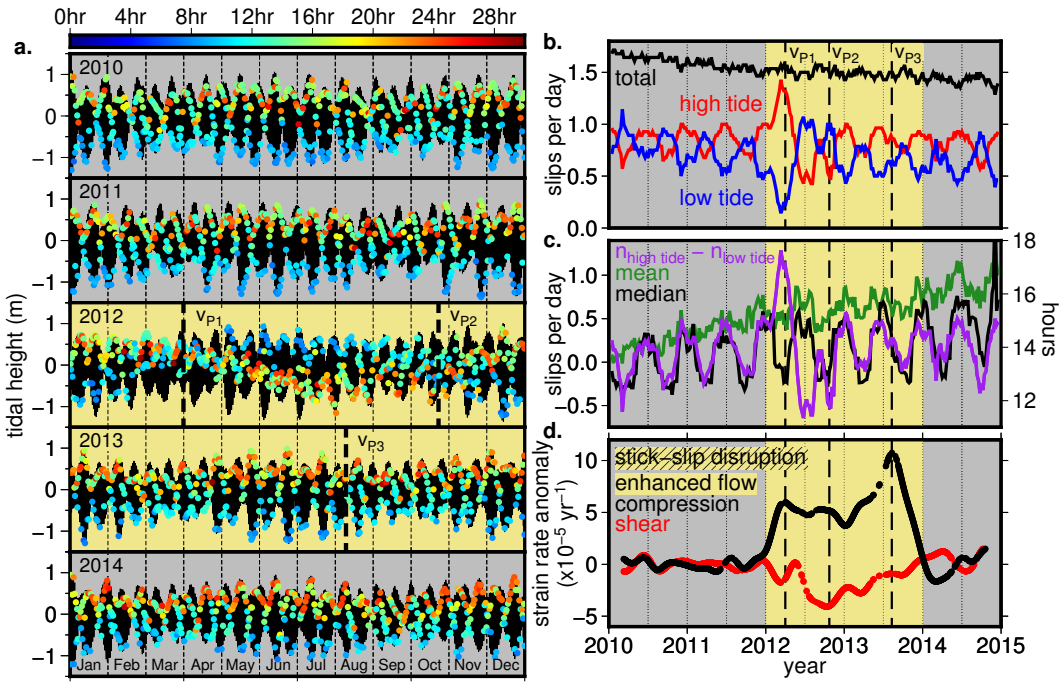

Figure 4.3: Slip event timing, statistics, and corresponding strain-rate anomalies. (a) Time-series of 2,777 slip events (circles) color-coded by time since previous slip event, plotted relative to Circum-Antarctic Tidal Simulation tidal predictions (*Padman et al.*, 2002) (black). Dashed vertical lines denote velocity maxima (Figure 4.2). (b) Time-series of slip events per day (black: total; high-tide: red; low-tide: blue). (c) Time-series of the difference between high- and low-tide slip events per day (purple; left axis) and mean and median inter-event duration (green and black, respectively; right axis). (d) Inter-event compressional (black) and shear (red) strain-rate anomalies. Yellow-shading indicates enhanced ice flow period; hatching indicates stick-slip disruption period.

less important than glaciological and hydrological factors. Soon after L7 reached its maximum surface-height, however, the stick-slip cycle abruptly reverted to its normal timing-pattern, concluding the 11-month timing disruption. This switch occurred over a few days during neap tide in early December 2012, demonstrating how rapidly ice dynamics can react to transient forcings from active subglacial hydrology. Although subglacial hydrologic activity continued (Figure 4.2a) and ice velocities fluctuated (Figure 4.2d), the normal stick-slip cycle persisted through the end of 2014 (Figure 4.3).

4.4.4 Correlation to Inter-event Strain-rate

GPS-derived inter-event strain-rates provide further insight into the dynamic response of the ice stream. While the period of enhanced ice velocities corresponded to a marked increase in along-flow compressional strain-rates, the slip-event timing disruption corresponded to a decrease in inter-event lateral shear strain-rates (Figure 4.3d). This relationship was highlighted by the period of slip-event/tidal-height decoupling occurring with reductions in shear strain-rate, suggesting that cross-flow variations in ice motion may be important for the ocean control of WIS/MIS basal dynamics (and therefore stress transmission inland from the grounding line (e.g., *Rosier et al.*, 2014; *Thompson et al.*, 2014)). Consequently, models striving to capture basal dynamics effectively may need to explicitly resolve along- and across-flow stresses.

Because slip-event magnitude and velocity did not measurably change during our five-year observation period, we hypothesize that these subglacial floods did not overcome the steep hydropotential gradients to lubricate localized areas of high basal-resistance that rupture at slip-event onset (*Winberry et al.*, 2014; *Walter et al.*, 2011). Instead, given increased inter-event compressional strain-rates from

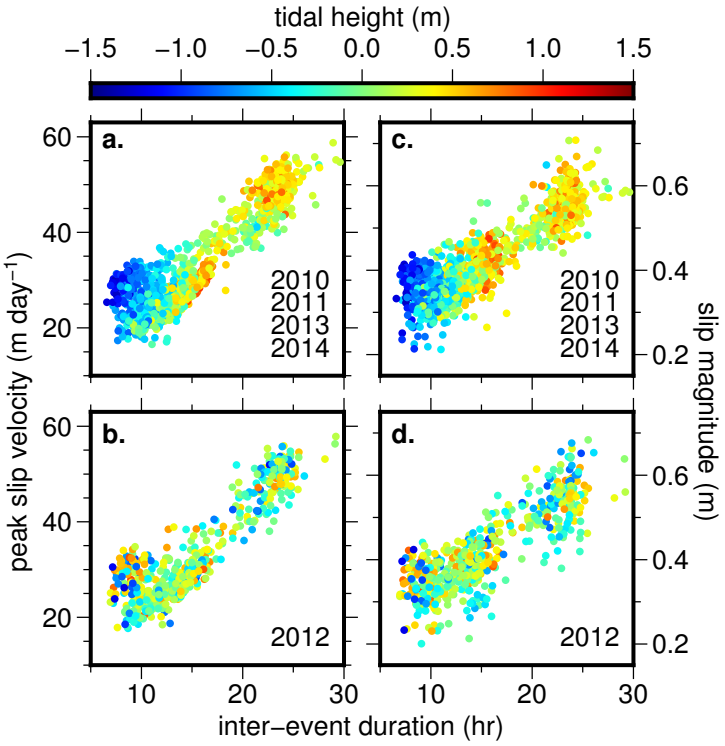

Figure 4.4: Slip event characteristics during normal and disrupted states. (a, b) Peak slip velocity and (c, d) slip magnitude for each slip event at the farthest-field, grounded GPS station during time intervals of (a, c) the normal stick-slip cycle state and (b, d) the stick-slip cycle disrupted by subglacial hydrology. Color scale indicates the CATS tidal height (*Padman et al.*, 2002) at the time of slip initiation. The slip velocity and magnitude as a function of inter-event duration (a proxy for accumulated stress (*Winberry et al.*, 2014)) did not measurably change during the stick-slip timing disruption, suggesting that resistive areas of the basal interface were not affected by the discharge from subglacial lakes.

upstream, we believe that the stress-loading of these resistive areas changed by increasing lubrication of surrounding regions that move via basal sliding. Our data therefore illustrate how a subglacial flood can rapidly alter ice dynamics in regions of polar ice sheets characterized by low basal-traction (e.g., *Joughin et al.*, 2004a, 2006; *Andrews et al.*, 2014); stick-slip dynamics, in this case, were a convenient window through which we can interrogate the stress-loading at the bed.

4.5 Summary

We have used five years of continuous GPS data from stations on and between lakes on WIS/MIS to suggest that subglacial activity does affect ice dynamics. In one of the few regions of Antarctica where ice velocity is decelerating, a subglacial flood coincided with a sustained, two-year period of enhanced ice flow of large enough magnitude to reverse the regional slowdown. During this event, normal stick-slip behavior was also interrupted, which was associated with reduced shear strain rates. This correlation may indicate that lateral shearing of resistive basal areas plays an important role in tidal triggering of slip events on WIS/MIS. As shear-strain rates began increasing toward background levels, normal stick-slip timing was restored within days. This "normal" state persisted even though the basal hydrology system continued to evolve and drive even higher compressive strain-rates, highlighting the complexity between inland transmission of stresses, basal dynamics, and subglacial hydrology.

Similar ice accelerations from variable ice-bed lubrication have been observed on temperate mountain glaciers and in Greenland, where changes are related to external factors such as air temperature and melt magnitude (e.g., *Bartholomaus et al.*, 2008; *Andrews et al.*, 2014; *Moon et al.*, 2014). The modified ice stream dynamics we detected, however, were likely driven by internal variability unrelated

to climate and are therefore more difficult to identify as non-steady-state without the context of multi-year, continuous observation. Internal variability of Antarctic subglacial hydrology is hypothesized to regulate millennial-scale fluctuations in ice stream dynamics (and therefore ice flux to the ocean) (e.g., *Alley et al.*, 1994; *Anandakrishnan and Alley*, 1997; *Vaughan et al.*, 2008; *Catania et al.*, 2012), yet the recurrence interval of subglacial drainage events can be orders of magnitude shorter. While our five-year time series was sufficient to capture the dynamics of one complete cycle of the particular system we studied, continued long-term, high-frequency observations are needed to fully understand the role of episodic subglacial hydrology events in past and future Antarctic ice sheet evolution.

4.6 Auxiliary Material

4.6.1 Sensitivity Test for Velocity Estimation

We created a synthetic GPS dataset for testing our methods for estimating velocity. Our synthetic experiment consisted of an ice stream with two, 0.4 m slips per lunar day, with a GPS station recording at 1/15 Hz. We tested (a) whether the calculation of a daily position aliased the beating between lunar and solar days into the velocity measurement and (b) the uncertainty of the velocity calculation given noisy 15 s GPS data. When slip events occurred with exactly a 12-hour inter-event interval and with no added noise, there was a small overall bias (with respect to the pre-determined velocity) of 0.05 m yr^{-1} (0.01–0.02% of the velocities of WIS/MIS) and no obvious aliasing at periods longer than 30 days. When we added uniform noise of up to 1 meter to each GPS measurement, the standard deviation of velocity residuals increased to up to 0.03 m yr^{-1}, an order of magnitude lower than the signals in which we are interested (i.e., velocity changes of 0.1% and greater).

When we allowed the inter-event duration to vary randomly between 6 and 12 hours (still with exactly two slips per lunar day), the velocity measurement maintained its small bias, but there is an additional uncertainty of ± 0.10 m yr^{-1} (1σ). Given added noise 0.01 m, 0.05 m, 0.1 m, 0.5 m, and 1 m to the position measurement, the uncertainty did not appreciably change over 100 iterations, yielding standard deviations of 0.14 ± 0.02 , 0.14 ± 0.01, 0.14 ± 0.01, 0.14 ± 0.01, 0.14 ± 0.02 m yr^{-1}, respectively for each noise level. These noise levels (0.03-0.05% of WIS/MIS velocities) still remained below the signals in which we are interested. Correlated uncertainties in GPS data (flicker, white, random walk, etc.) operate on the 0.001 m yr^{-1} level (e.g., *Langbein*, 2008), well below the 0.1–1 m yr^{-1} changes we analyze.

4.6.2 Supplemental Figures

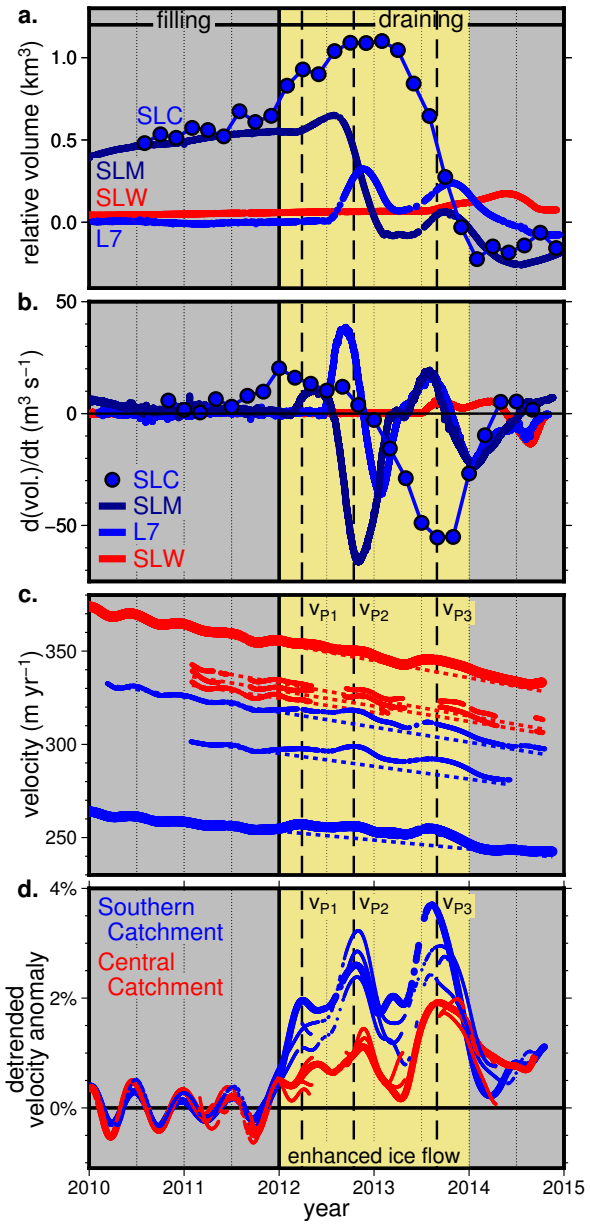

Figure 4.5: Figure 4.2 without the semi-annual velocity cycle removed from panel (d).

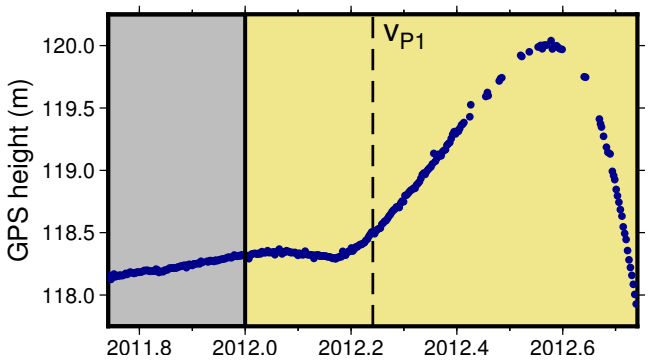

Figure 4.6: Relationship between v_{P1} and surface height changes at SLM GPS station. v_{P1} occurs just after a rapid change from $dh/dt < 0$ to $dh/dt >> 0$. Background colors are the same as Figure 4.2 (gray for filling phase, yellow for enhanced ice flow).

4.7 Acknowledgements

NASA supported M.R.S.'s contribution to this manuscript through their Earth and Space Science Fellowship (grant NNX11AQ78H). GPS data collection was supported by NSF grants to H.A.F. and S.T. (grants ANT-0838885, ANT-0839142, and ANT-0636970) as part of the interdisciplinary WISSARD project. We thank the 2010-2015 WISSARD Field Team members for data collection assistance, UNAVCO, Raytheon Polar Services, Antarctic Support Contract (ASC), Kenn Borek Air, and the New York Air National Guard for logistical support; the European Space Agency for CryoSat-2 data; and A. Borsa and K. Christianson for helpful discussion.

Chapter 4, in full, has been submitted for publication of the material as it may appear in Geophysical Research Letters: Siegfried, M. R., Fricker, H. A., Carter, S. P., Tulaczyk, S., "Rapid basal water system evolution triggered by subglacial floods in West Antarctica", *Geophysical Research Letters*, 2015. The dissertation author was the primary investigator and author of the paper.

Chapter 5

Investigating interactions between the subglacial water system and seawater near an ice-stream grounding line using GPS and elastic modeling

5.1 Abstract

The discharge of subglacial water from beneath the Antarctic ice sheet across the grounding line and into the sub-ice-shelf cavity has been hypothesized to influence both grounding-line dynamics, through modulation of basal-melt rates, and ocean dynamics, through modification of local to regional circulation patterns. The grounding line is the triple-juncture between ice, rock, and water and governed by many complex processes that can alter where, and how intensely, cold, fresh subglacial water and warm seawater mix. Here, we use Global Positioning System (GPS) data and an elastic-beam model to investigate the strength of two such processes that can affect subglacial water transport near the grounding line: (1)

tidally-induced flexure of the ice stream as the ice goes afloat and (2) mechanical ice-bed decoupling at high-tide. We find that the magnitude of ice flexure that could drive seawater upstream of the grounding line is damped in regions where subglacial water is inferred to discharge into the ocean cavity. This mechanism is then unlikely to impact local mixing dynamics. Our GPS experiments over three years did not indicate significant ice-bed decoupling or grounding-line migration over tidal timescales and we therefore could not investigate the importance of this process on the the mixing of subglacial and ocean water. Instead, we used these GPS experiments to map the landward limit of ice flexure and find that it is upstream of both the limit of flexure determined by InSAR and the inland extent of seawater imaged by an active seismic survey. Overall, our results demonstrate that our grounding-line embayment site, where subglacial water is hypothesized to discharge into the ocean, is complex and inferring time-variable ice-water-rock interactions in the region requires significant improvement to the precision of our measurements.

5.2 Introduction

Water beneath ice streams and glaciers in Antarctica is hypothesized to flow from the ice sheet interior to the margins. After traveling distances up to 100s of kilometers (*Wingham et al.*, 2006b; *Carter et al.*, 2009; *Flament et al.*, 2014) subglacial water flow continues to the grounding line, discharging into the Southern Ocean (*Goodwin*, 1988; *Fricker et al.*, 2007; *Carter and Fricker*, 2012; *Le Brocq et al.*, 2013). Here, it both contributes directly to sea level rise with its additional mass of $\sim$65 Gt yr^{-1} (*Pattyn*, 2010) and, perhaps more importantly, mixes with the ocean in what has been termed an "estuarine" environment (*Horgan et al.*, 2013a). Subglacial water flux to the ocean can alter the local freezing and melting

patterns at the grounding line and in the sub-ice-shelf cavity as well as impact ocean circulation through the release of significant volumes of freshwater (e.g., *Payne et al.*, 2007; *Jenkins*, 2011). Constraining the poorly-understood processes that control mixing of water bodies at the ice-ocean interface is therefore necessary for modeling of ice-sheet grounding-line dynamics and ice discharge at present and in the future.

There are two tidally-driven processes that can alter subglacial water pressures near to the grounding line, with potentially significant impacts on the location and vigor of mixing of fresh and saline water: (1) flexure as the ice transitions from grounded to floating, and (2) mechanical ice-bed decoupling during high tide. In the first case, the ice shelf, which is in hydrostatic equilibrium, moves up and down with ocean tides, while the ice upstream of the grounding line does not. This transition is accommodated by a several-kilometer wide zone of flexure between the grounding line and ice downstream. Due to the elastic properties of ice, bending downstream of the grounding line also causes bending upstream in the opposing direction (i.e., deflection up at low tide, down at high tide), which has been observed up to $\sim$1 km inland using tiltmeters (*Smith*, 1991; *Jacobel et al.*, 1994; *Heinert and Riedel*, 2007). Motion of this "flexural bulge" through tidal cycles has been hypothesized to be a grounding-line-stabilizing process by dewatering and compacting subglacial sediments through cyclic loading (*Christianson et al.*, 2013) or, alternatively, a destabilizing process by driving subglacial pressure changes of large enough magnitude to draw relatively-warm seawater upstream beneath grounded ice (*Walker et al.*, 2013).

The second process of ice-bed decoupling during periods of high tide is a function of tidal amplitude and basal slopes. In regions of high tidal amplitudes and low basal slopes, this process causes the ungrounding of large areas of "lightly

grounded" ice (i.e., near its floatation height), increasing the surface area of basal ice available for melt through exposure to ocean processes and moving the location of seawater-freshwater interaction further upstream. This type of grounding-line migration has been observed with satellite altimetry at the mouth of Institute and Möller ice streams, where tidal amplitudes are fairly large (*Brunt et al.*, 2011). In areas with lower tidal amplitude or higher basal slopes, grounding-line migration over tidal periods is much less extensive, yet can still appreciably impact subglacial pressure and modify subglacial water-flow routes (*Sayag and Worster*, 2013).

In this chapter, we use Global Positioning System (GPS) surveys collected between 2011 and 2015, and two-dimensional flexure modeling to assess the relative importance of these two processes at Whillans Ice Stream (WIS), West Antarctica. WIS is a region with active subglacial hydrology, which controls the rate and timing of subglacial water transfer across the grounding line (*Fricker et al.*, 2007; *Fricker and Scambos*, 2009; *Carter et al.*, 2013; **Chapter 4**). Models of regional subglacial hydrology suggest that water is discharged into the Ross Sea at grounding-line embayments (*Carter and Fricker*, 2012), making this a key geometry for understanding the interaction between subglacial and ocean water. Here, we investigate the relevance of these ice-ocean processes at an embayment in the WIS grounding line.

We first use GPS data across the flexure zone of a nearby grounding-line peninsula to constrain parameters for our flexure model, then use results from this model to estimate the magnitude of upstream flexural-bending across a larger region of the WIS grounding line, including both embayments and peninsulas. We use GPS arrays over a grounding-line embayment characterized by low surface and basal slopes (*Christianson et al.*, 2013) to test whether GPS is sensitive enough to observe grounding-line migration over tidal periods in a low-slope environment.

Finally, we discuss the implications of these observations on the interaction between the subglacial and sub-ice-shelf systems.

5.3 Methods

5.3.1 Continuous GPS

We carried out four different continuous GPS (cGPS) experiments in the WIS flexure zone during the 2011–2012, 2013–2014, and 2014–2015 austral summers (Figure 5.1). These experiments were performed across two different geometries of the grounding line. The first geometry, which we use as our control site, is a grounding-line peninsula, where the grounding line is convex in the along-flow sense. We performed one cGPS experiment at this location during the 2011–2012 austral summer. The second site is a grounding-line embayment, where the grounding line is concave in the along-flow sense. Subglacial hydrology models have shown that subglacial water tends to discharge into the sub-ice-shelf cavity at embayments (*Carter and Fricker*, 2012), implying that embayments are central to mixing dynamics. We performed three cGPS experiments in the grounding-line embayment: a permanent cGPS deployment from 2011 to 2015 and two summer-only experiments, one in 2013–2014 and one in 2014–2015. The peninsula and embayment sites are ∼37 km apart (Figure 5.1).

Peninsula Site

Our cGPS experiment at the peninsula site consisted of an ice-flow-parallel, grounding-line-perpendicular array of stations through the flexure zone deployed for 29 days in 2011–2012. We installed five dual-frequency Trimble NetR9 GPS receivers with Zephyr Geodetic II antennas, equally-spaced at ∼1.8 km within the

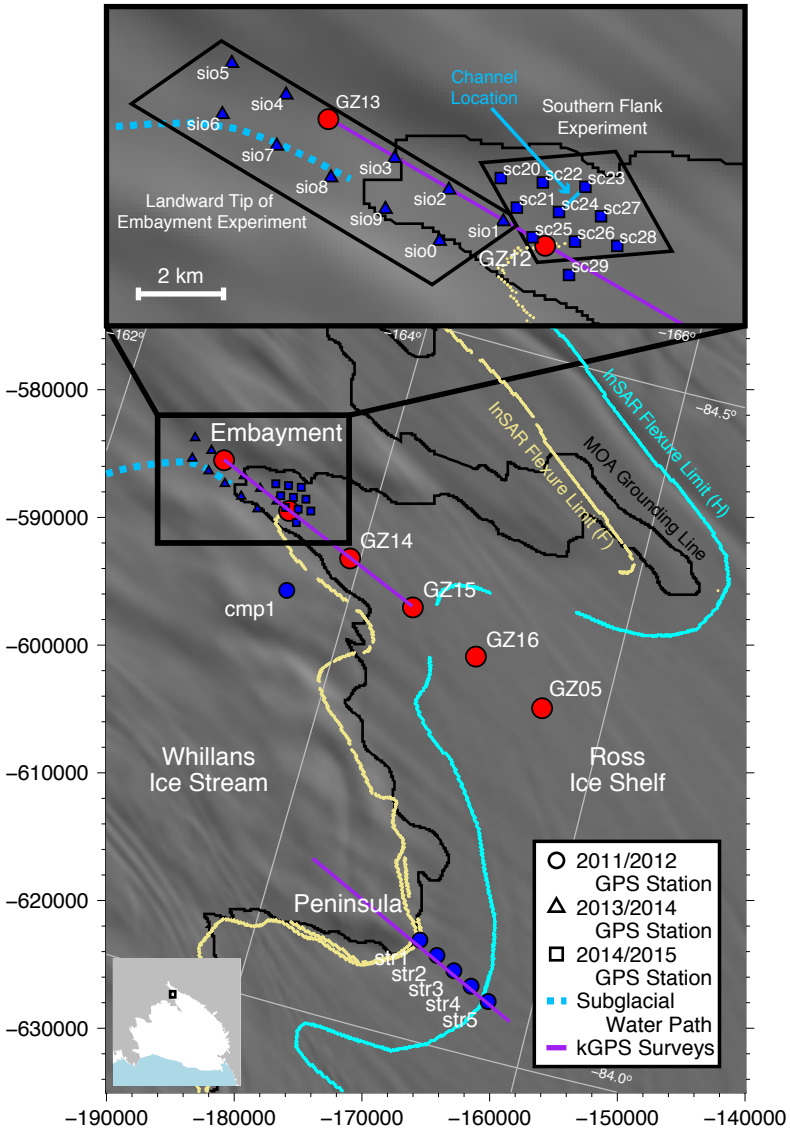

Figure 5.1: Map of the Whillans Ice Stream grounding line and location of GPS experiments in the peninsula and the embayment. Red fill represents year-round installations, and blue fill represents stations deployed during the austral summer only. Purple lines show the locations of the 12-hour kGPS survey transects in the embayment and peninsula regions of the grounding line. Dashed light blue line is the hypothesized subglacial water flow path (*Carter and Fricker*, 2012); solid light blue line indicates the location of a channel eroded into ocean-bottom sediment (*Horgan et al.*, 2013a). Black line is the MODIS Mosaic of Antarctica (MOA) grounding line (*Scambos et al.*, 2007). Yellow and cyan lines are the inland (F) and seaward (H) limits of flexure from InSAR (F from *Rignot et al.*, 2011a, H from E. Rignot, *pers. comm.*, 2011). Background imagery is from MOA (*Scambos et al.*, 2007). Projection is polar stereographic (in meters) with standard parallel at 71°S.

flexure zone (blue circles in Figure 5.1). While four of the units recorded data at 15 seconds, one unit recorded at 30 seconds, requiring us to downsample all cGPS data at the peninsula to the lower 30-second data rate for comparison. We used the most seaward station (STR5) as our local tide gauge to quantify the tidal response at the four other cGPS stations. We compared STR5 to the Circum-Antarctic Tidal Simulation (CATS2008a, an update of *Padman et al.*, 2002) to validate the use of this station as a tide gauge.

Embayment Site

Our first experiment at the embayment site was the installation of six cGPS stations in an ice-flow-parallel, grounding-line-perpendicular array in the flexure zone. These stations were equally-spaced at ∼6 km, covering a 30 km long transect (red circles in Figure 5.1) and collected data from 2011 to 2015. All embayment cGPS units were Trimble NetR9 receivers with Zephyr Geodetic II antennas and recorded at 15-second intervals. Two stations in this array (GZ16 and GZ05) were located past the seaward limit of flexure, so either could be used as our local tide gauge. While we would prefer to be consistent and only choose one station as our reference, instrumental issues required us to use both.

We carried out one additional cGPS experiment in the embayment in each of the 2013–2014 and 2014–2015 austral summers. In 2013–2014, we deployed 10 Trimble NetR9 GPS receivers with Zephyr Geodetic II antennas for 20 days in two flow-parallel lines separated by ∼1.4 km across the landward tip of the embayment (GPS sites SIO[0-9] in Figure 5.1). Along-flow station spacing was ∼1.6 km, or nominally two ice-thicknesses. In 2014–2015, we deployed 9 Trimble NetR9 GPS receivers with Zephyr Geodetic II antennas for 16 days, in a diamond pattern (∼1 km spacing) that straddled the (geographic) southern flank of the embayment

(GPS sites SC2[0-8] in Figure 5.1). This array was centered on channel eroded into the ocean-bottom sediment that potentially focuses sub-ice-shelf tidal circulation (*Horgan et al.*, 2013a).

5.3.2 Kinematic GPS

While our cGPS data have sufficiently high temporal resolution to investigate individual tidal cycles, the dataset only samples at discrete locations. In the 2011–2012 field season, we complemented the cGPS data with coincident, repeat kinematic GPS (kGPS) surveys along the cGPS transects in both the embayment and the peninsula. For these surveys, we mounted a Zephyr Geodetic II GPS antenna to the frame of a snowmobile, and recorded data on a Trimble NetR9 receiver at 5Hz. Driving the snowmobile at ∼20–25 km hr^{-1} resulted in about 1-m spacing between GPS measurements, which limited the aliasing of surface topographic features (e.g., *Siegfried et al.*, 2011). To ensure we sampled the transect approximately once an hour, we limited the transect length to 18 km at both locations. While this length transect covered the entire flexure zone at the peninsula, we did not reach the full hydrostatic limit of flexure at the embayment, where the flexure zone is wider due to two-dimensional effects. We drove each transect for 12 hours (i.e., capturing the entire tidal range), resulting in 12 flexure-zone surveys at the peninsula and 11 flexure-zone surveys at the embayment.

5.3.3 GPS Processing

For data collected during the 2011–2012 field season, we post-processed both cGPS and kGPS data using differential carrier-phase processing, implemented by Track v1.27 (*Chen*, 1998). We used a summer-only, high-rate base station located near our field camp (CMP1 in Figure 5.1), resulting in baseline lengths (i.e.,

distance from base station to GPS sites within each experiment) of 29–36 km for peninsula GPS stations and 11–21 km for embayment GPS stations. We processed both cGPS and kGPS data relative to this base station with loose constraints on kinematic motion, generally following the methods of *King* (2004).

We estimated a realistic uncertainty that includes inherent uncertainty in GPS data as well as uncertainty in the data collection methods (e.g., engine noise, vertical motion from the snowmobile suspension, multipath, axial deviations of the frame, etc.) by calculating the standard deviation of residuals in GPS data (after removing the mean ice-surface topography) within a 1-km section of our survey transect on grounded ice. This value is more representative of the actual uncertainty of our experiment rather than a formal uncertainty estimate provided by the GPS processing tools. The residuals were normally distributed with a standard deviation of <0.07 m (Figure 5.2). For the later experiments, logistical constraints prevented us from deploying a local GPS base station. Therefore, we processed the data using a precise point positioning (PPP) method implemented by Natural Resources Canada's online tool Canadian Spatial Reference System-PPP (CSRS-PPP).

To analyze the tidal signal in GPS-derived heights, we converted both cGPS and kGPS data to normalized tidal amplitudes following *Vaughan* (1995):

$$d = \frac{h_1 - h_2}{p_1 - p_2} \tag{5.1}$$

where d is the normalized tidal amplitude, h_1, h_2 are the GPS heights at t_1 and t_2, and p_1, p_2 are tidal heights at t_1 and t_2. An amplitude of $d = 0$ means the ice is fully grounded and an amplitude of $d = 1$ means the ice is hydrostatically floating. At the peninsula we used observed heights from station STR5 for p_1 and p_2, while at the embayment, we used observed heights from station GZ05.

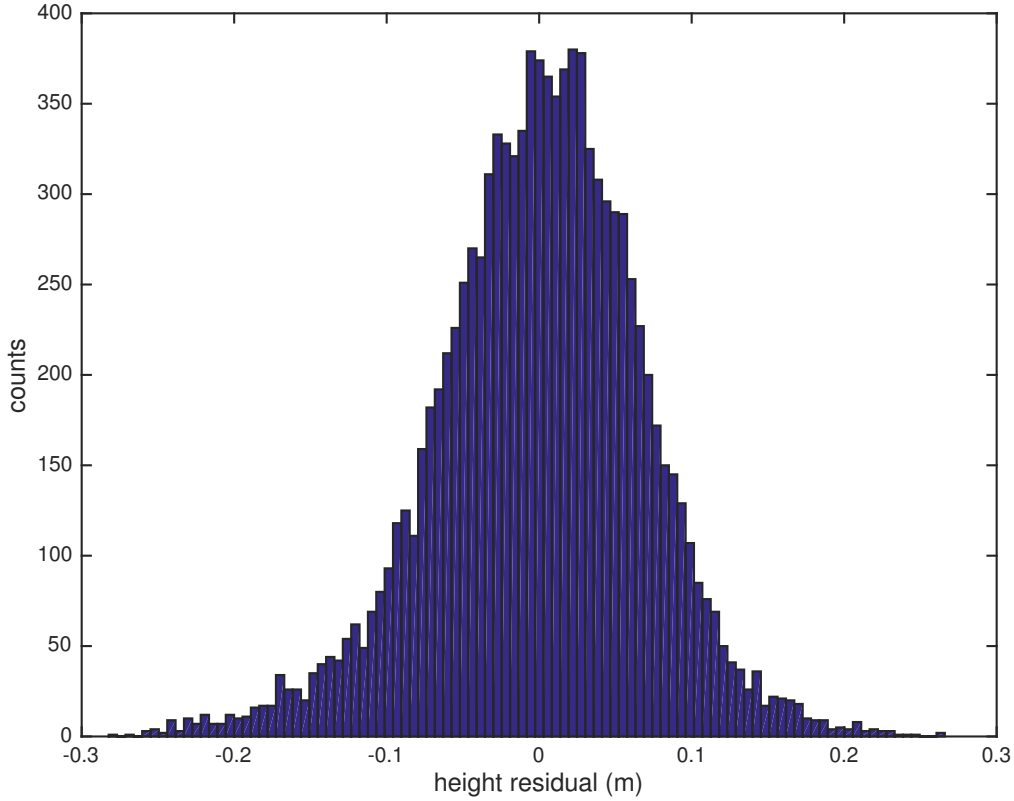

Figure 5.2: Histogram of GPS residuals over a 1 km section of grounded ice used to the estimate kGPS precision of our experimental setup. Standard deviation of these residuals is 0.068 m ($N = 10,637$).

For kGPS data, we defined a profile collected at mean tide as the tidal-reference height-profile (i.e., h_2 corresponds to $p_2 = 0$) and calculated average along-profile normalized tidal amplitudes in 100 m segments, with segments centered every 10 m. For cGPS, we removed the mean height over the data collection period (two weeks for summer-only stations, five months for permanent stations) in order to define t_2 as a mean tide when $h_2 = p_2 = 0$. Because the cGPS dataset is much longer than the kGPS dataset, we were able to select times for t_1 that maximized the signal-to-noise ratio (i.e., at peak high-tides and low-tides). We calculated the mean height over a 90-minute window centered on these times of peak tide and calculated normalized tidal amplitudes following Eq. 5.1. We then compared these tidal amplitudes to values predicted by the ice-flexure model. Additionally, we cross-correlated vertical GPS signals with the local GPS tide gauge to assess the amplitude and any phase delay in the tidal signal across the flexure zone. A phase lag in ice response to tidal height changes may indicate that a viscoelastic flexure model would be more appropriate (*Reeh et al.*, 2000).

5.3.4 Ice Flexure Model

After verifying the suitability of an elastic model for predicting flexure over tidal periods through analysis of GPS-derived height data at the peninsula, we used the two-dimensional (2D), thin-plate elastic flexure model of *Garcia et al.* (2014), which extends the model of *Sandwell* (1984). This model takes an arbitrary, 2D forcing map and iteratively solves in Fourier-space for the resulting flexure of a thin elastic plate with spatially-variable rigidity over a fluid half-space. The benefit of this model is that it does not require the grounding line to be "clamped" to the substrate at or upstream of the grounding line; therefore, we can investigate flexure over grounded ice. The model requires a forcing ($f(\mathbf{x})$) and a rigidity value ($D(\mathbf{x})$)

at each grid cell. The variable flexural rigidity is needed to allow for changes in ice thickness across the model domain and is related to ice thickness, $h(\mathbf{x})$, by

$$D(\mathbf{x}) = \frac{Eh^3(\mathbf{x})}{12(1-\nu^2)} \tag{5.2}$$

where E is Young's modulus and ν is Poisson's ratio. We used ice thickness estimates from Bedmap2 (*Fretwell et al.*, 2013), which, as the coarsest dataset, set our model grid cells at 1 km $\times$ 1 km resolution. We set $\nu = 0.3$ (e.g., *Vaughan*, 1995) and estimate E by tuning the model to the data collected at the peninsula site, where we expect the flexure zone to have negligible bridging stresses. While we set ν and tune E, we recognize that neither value may be the "true" value for the elastic properties of ice as there is a trade-off in Eq. 5.2 between $h(\mathbf{x})$, E, and ν.

To simulate tidal forcing, we began by ascribing a binary (i.e., 0 or 1) force based on a 1-km resolution grounding line mask derived from combined InSAR, altimetry, and optical imagery data (*Depoorter et al.*, 2013). In this model experiment, we set the forcing to 0 upstream of the grounding line and 1 downstream of the grounding line. This binary forcing resulted in a grounding line that was displaced inland by a distance equivalent to half the width of the flexure zone because we do not prescribe zero-deflection at the grounding line as a boundary condition. To mitigate this mismatch, we could parameterize the ice-bed interface (e.g., a partially-supported beam similar to *Walker et al.*, 2013), but the spatial variation of this parameter is largely unconstrained by data. For this reason, we excluded a parameterization of ice-bed coupling strength. Instead, we adjusted the forcing grid to create a forcing ramp within the flexure zone based on the morphology of a 1D elastic model (e.g., *Vaughan*, 1995) in order to map the

grounding line appropriately, while still allowing investigations of upstream flexure. We verified the output against InSAR-mapped limits of flexure (landward limit, F, from *Rignot et al.*, 2011a, seaward limit, H, from E. Rignot, *pers.comm.*, 2011). We recognize that our forcing adjustment is an empirical workaround to avoid the complex and difficult to observe physics of the ice-bed interface near the grounding line. Future work will develop a more realistic elastic model that effectively captures limits of ice flexure, while neither prescribing zero-deflection/zero-tilt boundary conditions at the grounding line (e.g., *Holdsworth*, 1969; *Vaughan*, 1995; *Reeh et al.*, 2003; *Marsh et al.*, 2014) nor using minimally-constrained parameters to describe bed characteristics (e.g., *Sayag and Worster*, 2011; *Walker et al.*, 2013).

5.4 Results

5.4.1 Ice Flexure

Tidal Signal in GPS Data across the Flexure Zone

cGPS data at the peninsula (Figure 5.3a) and embayment (Figure 5.3b) showed a clear tidal signal that became increasingly damped with proximity to the grounding line. To determine any phase lag in the tidal signal through the flexure zone, we cross-correlated the GPS stations along each transect to the local tide gauge (STR5 at the peninsula; GZ05 at the embayment). Phase lags through the flexure zone relative to ocean tide have previously been identified as the reason to employ a viscoelastic constitutive equation for ice flexure at tidal frequencies (*Reeh et al.*, 2000). At long phase lags (days to weeks), both locations showed waxing and waning of the correlation coefficient with the daily and fortnightly tides (Figure 5.3). GZ13 in the embayment showed a low amplitude (correlation coefficient, R, of 0.2) signal that was almost 180° out of phase with the tides; this was likely due to

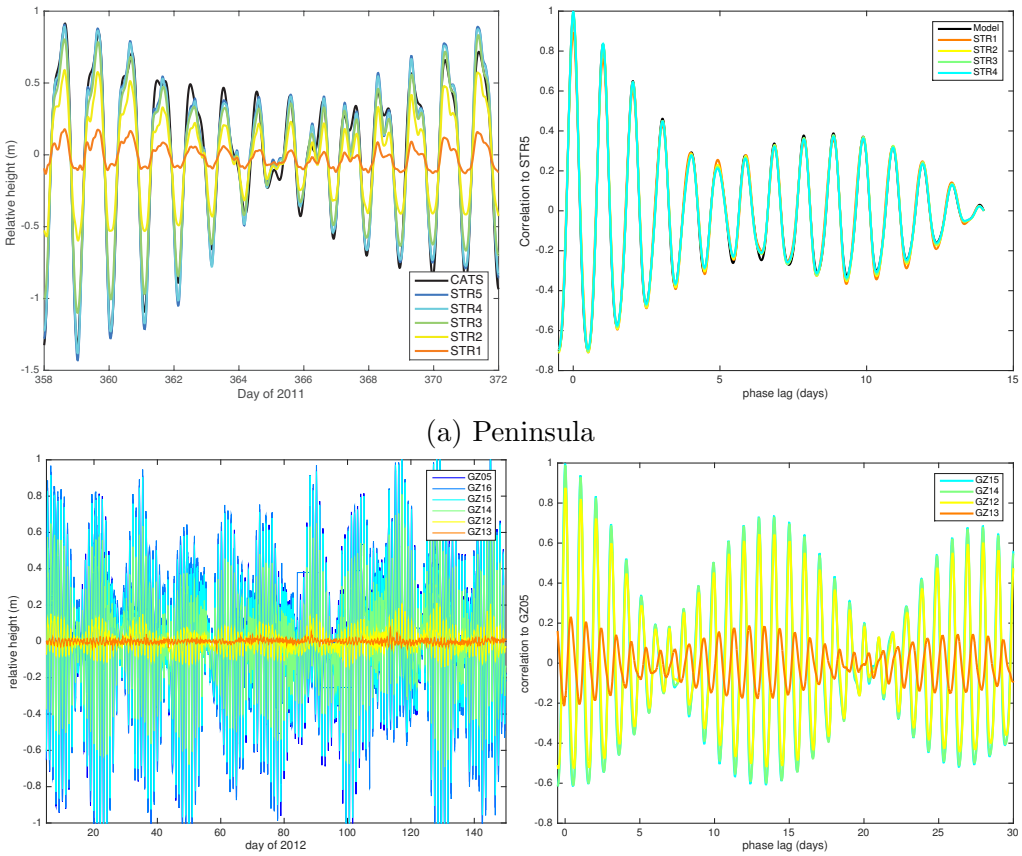

(a) Peninsula

(b) Embayment

Figure 5.3: cGPS height measurements and cross-correlation with most seaward station at the (a) peninsula and (b) embayment (see Figure 5.1 for locations). Left: Heights of GPS stations through the flexure zone along the peninsula transect for 14 days in late 2011 to early 2012 and along the embayment transect for the first 150 days of 2012. Panel (a) also shows the modeled tidal height from CATS2008a at the location of STR5. Right: Correlation coefficient as a function of phase lag for cross-correlations between the most seaward GPS station and other stations in the flexure zone. STR5 was used as the tidal station for the peninsula, where it was also cross-correlated with the CATS2008a model. GZ05 was used as the tidal station for the embayment transect. Figure 5.4 highlights the cross-correlation at short lags.

our decision not to apply an ocean-load tide correction. Future work will consider how to best apply load tide corrections in grounding line applications.

At shorter phase lags (<1 hour), peninsula stations STR1, STR3, and STR4 showed peak correlation at 0 phase lag, while STR2 had a peak correlation at an offset of 90 seconds (Figure 5.4a). The lack of phase lags across the flexure zone at the peninsula confirms that our choice of elastic model was appropriate. Embayment stations had peak correlation at 0 lag near the seaward limit of flexure at GZ15. Phase lags then increased landward (16.5 minute lag at GZ14; 32 minute lag at GZ12; Figure 5.4b).

kGPS Profiles

The kGPS-derived height profiles across the flexure zone at the two sites (peninsula and embayment) revealed that the grounding line has a different morphology at each location. At the peninsula site, the grounding line has relatively steep surface-slopes, with >4 m height change between the inland limit of flexure and the hydrostatic point at low tide, while the embayment flexure zone has lower slopes with <1 m difference (Figure 5.5). Our results estimating normalized tidal amplitude from kGPS illustrate the importance of the timing of data collection within a tidal cycle when investigating tidal processes: in the embayment, where profiles were collected at spring tide, tidal amplitudes from kGPS agreed well with those derived from cGPS point measurements; in the peninsula, where data were collected at neap tide, tidal amplitude estimates were noisy and inaccurate due to the lower signal-to-noise ratio. Normalized tidal amplitude profiles from kGPS and cGPS are shown in Figure 5.6.

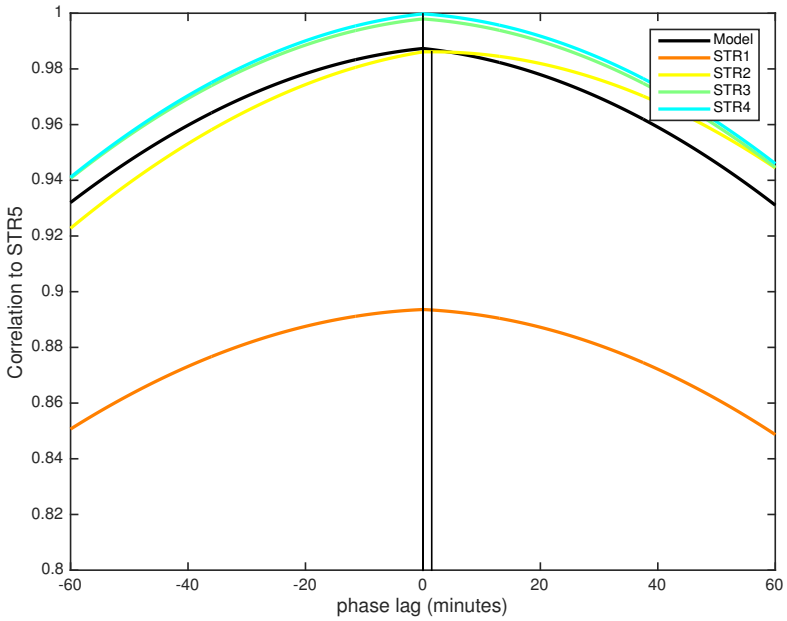

(a) Peninsula

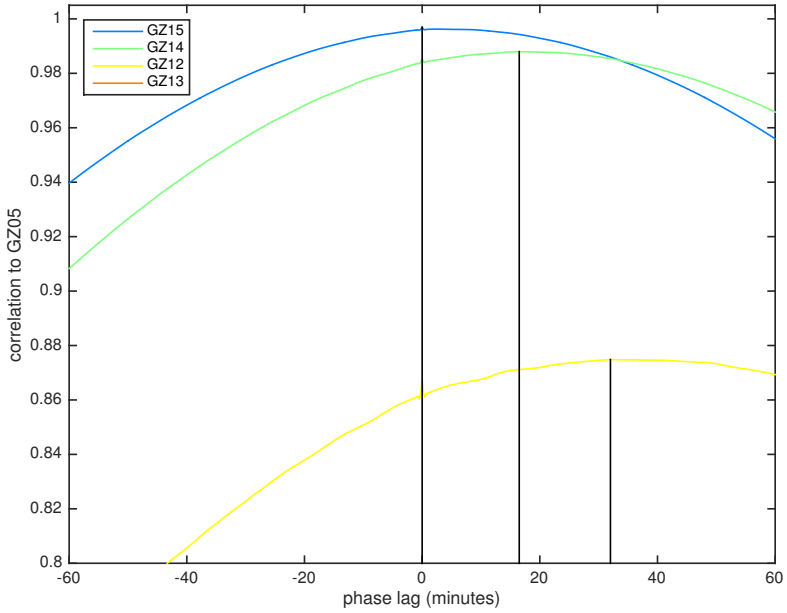

(b) Embayment

Figure 5.4: Cross-correlation at lags up to 1 hour from GPS data collected in the (a) peninsula and (b) embayment regions of the grounding line (see Figure 5.1 for profile locations). Sites in the peninsula region showed peak correlation with tides at zero phase lag for stations STR1, STR3, and STR4, with STR2 having a peak correlation 1.5 minutes later. Profile from the embayment showed peak correlation at increasing lags toward the grounding line.

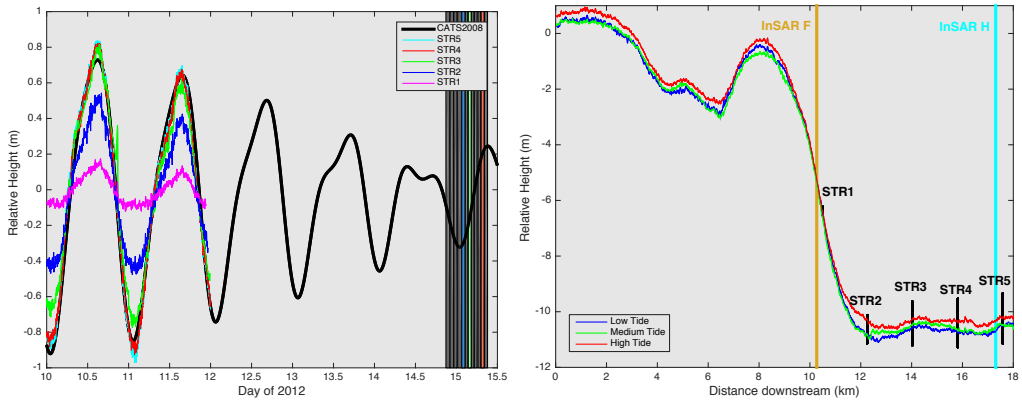

(a) Peninsula

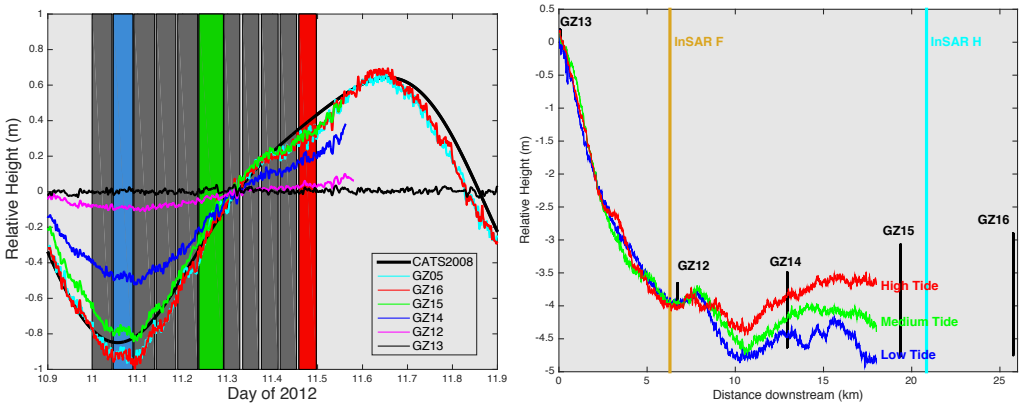

(b) Embayment

Figure 5.5: GPS height measurements as a function of time and of distance along transect at the (a) embayment and (b) peninsula regions of the grounding line (see Figure 5.1 for location). Left: Timing of kGPS surveys, where each vertical-shaded rectangle corresponds to a single survey of the kGPS transect. Blue, green, and red colored boxes represent the timing of profiles shown in right panels. Right: Surface profiles along the transects at high (red), medium (green), and low (blue) tide, with limits of flexure (F: landward limit, H: seaward limit) from InSAR indicated (*Rignot et al.*, 2011a, E. Rignot, *pers. comm.*, 2011). Vertical black bars show range of heights sampled at cGPS locations over the duration of the full cGPS experiments (>14 days).

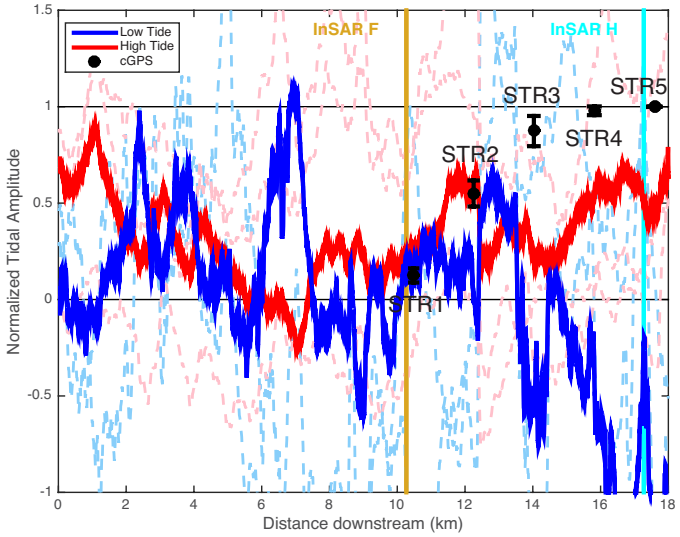

(a) Peninsula

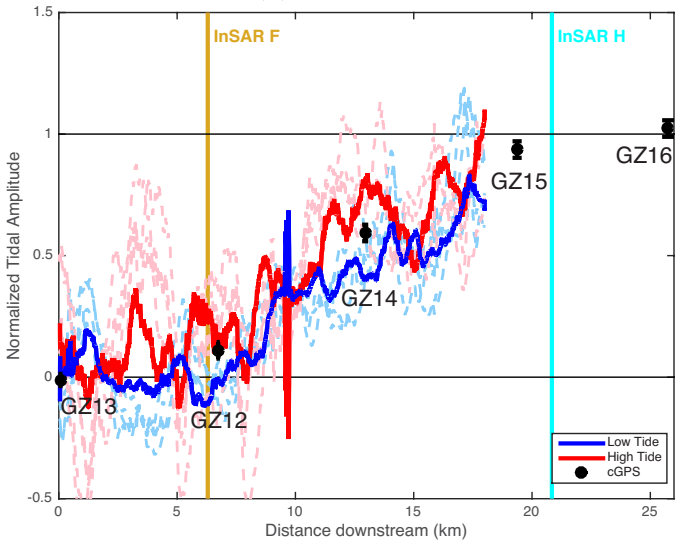

(b) Embayment

Figure 5.6: Normalized tidal amplitude profiles estimated from kGPS surveys at the (a) peninsula and (b) embayment regions of the grounding line (see Figure 5.1 for location). Dashed light red and light blue lines show individual profiles at low and high tide, respectively, while solid red and blue show the mean high-tide and mean low-tide profiles. Black dots represent the mean tidal amplitude at cGPS stations along the survey transect.

Elastic Modeling

We used the cGPS-derived flexure profile from the peninsula region to constrain the effective Young's modulus, E, that we then used in the 2D flexure model (Figure 5.7). The best fit to the cGPS data was achieved using $E = 1$ GPa, which is consistent with previous attempts at modeling the flexural ice response to ocean tides (e.g., 0.88 ± 0.35 from *Vaughan*, 1995). Also shown is the 1D flexure solution with the ice clamped at the grounding line to demonstrate that this location is mostly free of 2D effects in the flexure zone, making it a logical location to tune our model. Using this value for E, we modeled ice flexure across the whole domain, which included a large swath of the WIS grounding line (Figure 5.8).

Across the flexure profile at the embayment site, the 2D model captured both the structure and width of the flexure-zone profile when compared to cGPS- and kGPS-derived flexure profiles (Figure 5.9). We compared output from the 2D model with the output from the 1D model using both a realistic ice thickness ($h = 710$ m) and the thickness that would be required to simulate a flexure zone of the correct width ($h = 3550$ m, 5x thicker). This stresses the importance of using a 2D model instead of a 1D model when investigating flexural processes. Last, we compared the model's predictions at the inland and seaward limits of flexure determined by InSAR to assess the accuracy of the modeled output (Figure 5.10). The model accurately places the seaward limit of flexure, but estimates a normalized tidal amplitude of 0.14 ± 0.08 at the inland limit of flexure, which corresponds to a horizontal offset of the grounding line of about one ice thickness, which is less than one grid cell.

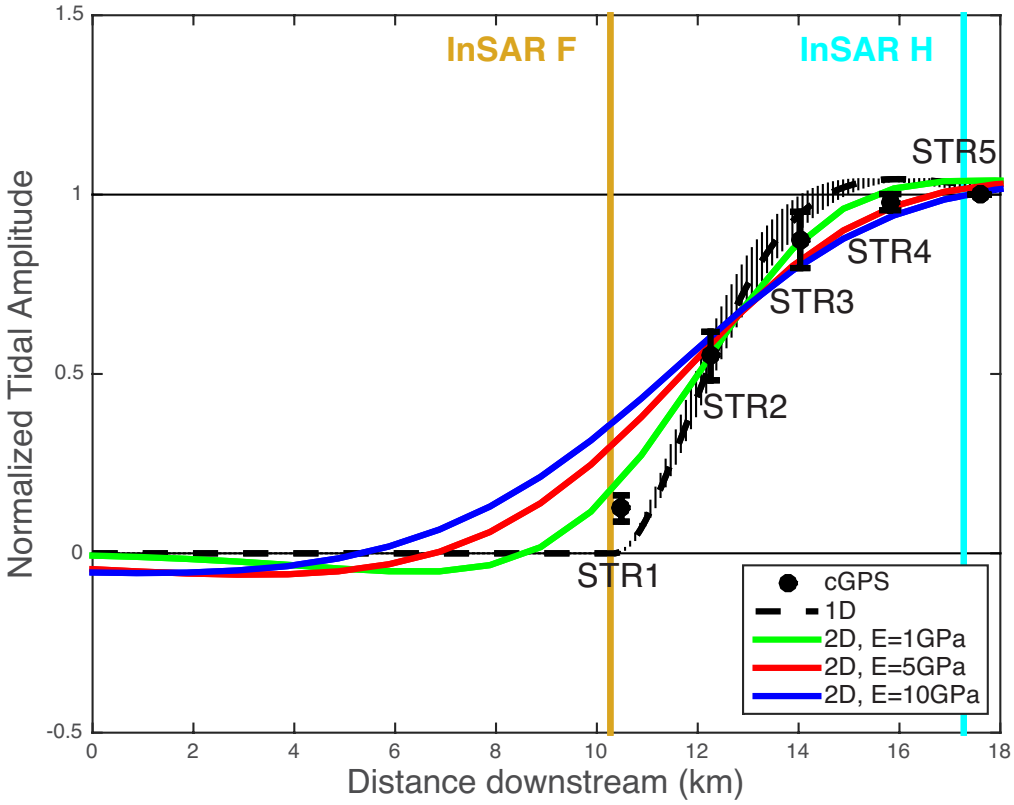

Figure 5.7: Comparison of the flexure profile derived from cGPS data in the peninsula region with model output from a 2D flexure model with various values for Young's modulus (E): 1 GPa (green), 5 GPa (red), 10 GPa (blue) and a 1D elastic flexure model clamped at the grounding line using constants from *Vaughan* (1995) and the local ice thickness of 690 m (dashed black line). Limits of ice flexure from InSAR (*Rignot et al.*, 2011a, E. Rignot, *pers. comm.*, 2011) indicated by colored vertical lines.

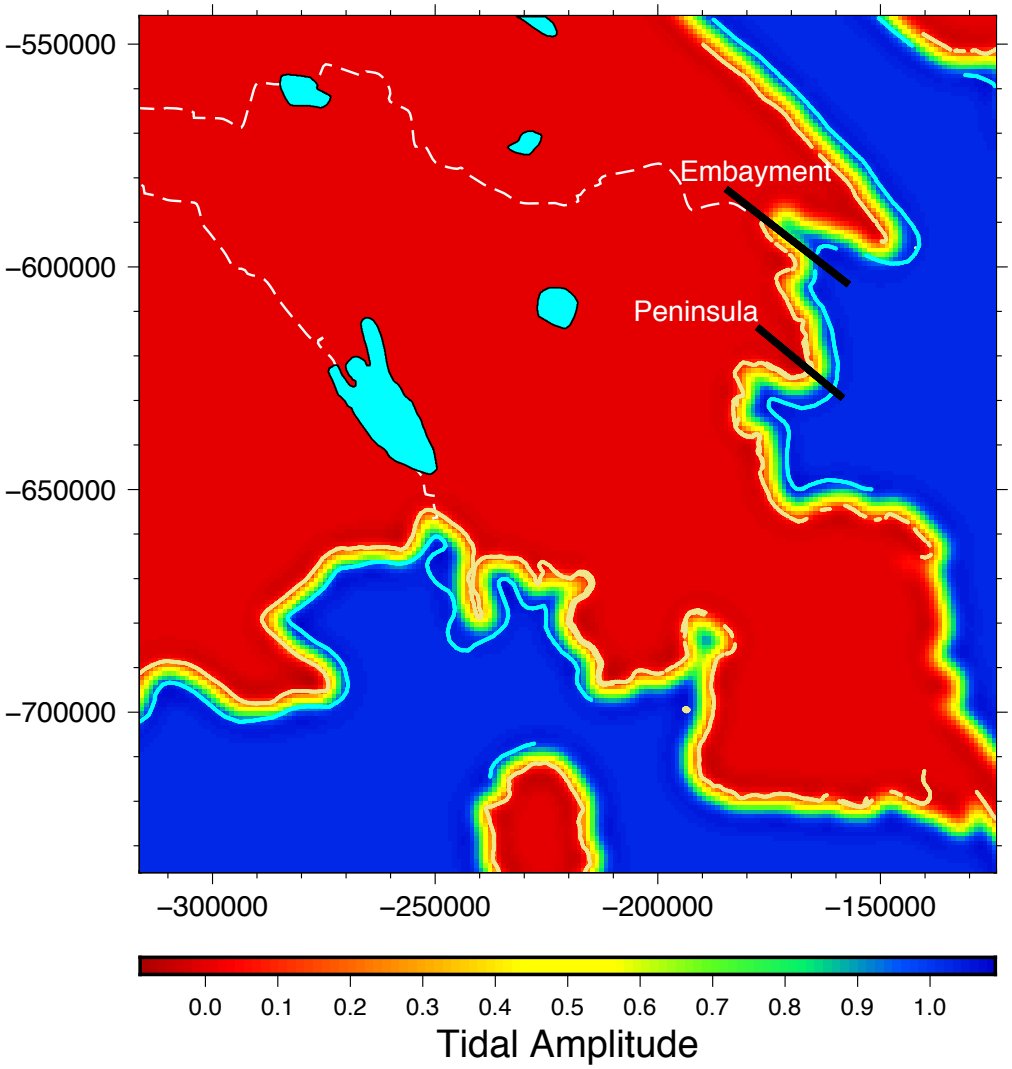

Figure 5.8: Modeled normalized tidal amplitude for the full domain using the 2D elastic model with variable rigidity from *Garcia et al.* (2014). Cyan polygons denote subglacial lakes of lower Whillans Ice Stream (*Fricker and Scambos*, 2009), with dashed white lines showing inferred subglacial water flow paths (*Carter and Fricker*, 2012). Black lines across the grounding line are the two survey transects across the peninsula and embayment sites. InSAR-derived limits of flexure (*Rignot et al.*, 2011a, E. Rignot, *pers. comm.*, 2011) shown in yellow and cyan.

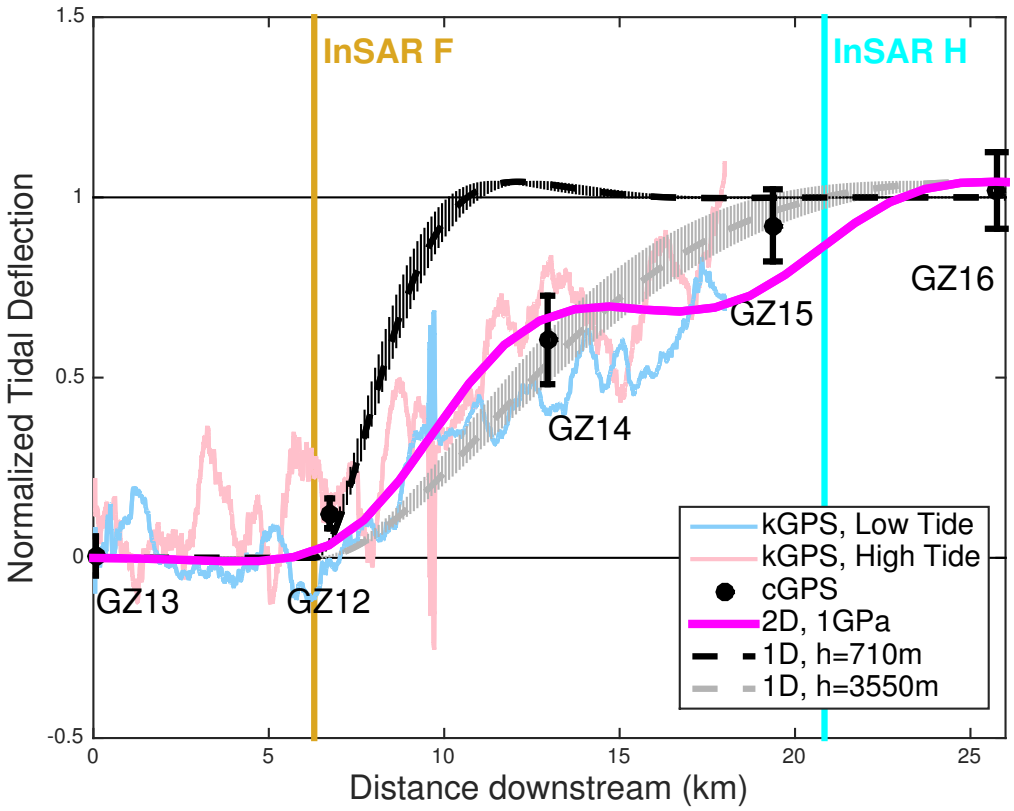

Figure 5.9: Comparison of cGPS and kGPS observations and elastic modeling along the embayment transect, with InSAR-derived limits of flexure from *Rignot et al.* (2011a) and E. Rignot, *pers. comm.* (2011) shown in yellow and cyan. 1D modeling requires using an ice thickness, h, 5 times greater than observed to capture the width of the flexure zone at the embayment, highlighting the need for employing a 2D model. 2D modeling using $E = 1$ GPa captures the width of the flexure zone and the resulting structure agrees well with data for most of the transect. Flexure upstream of the grounding line is highly damped compared to the peninsula site.

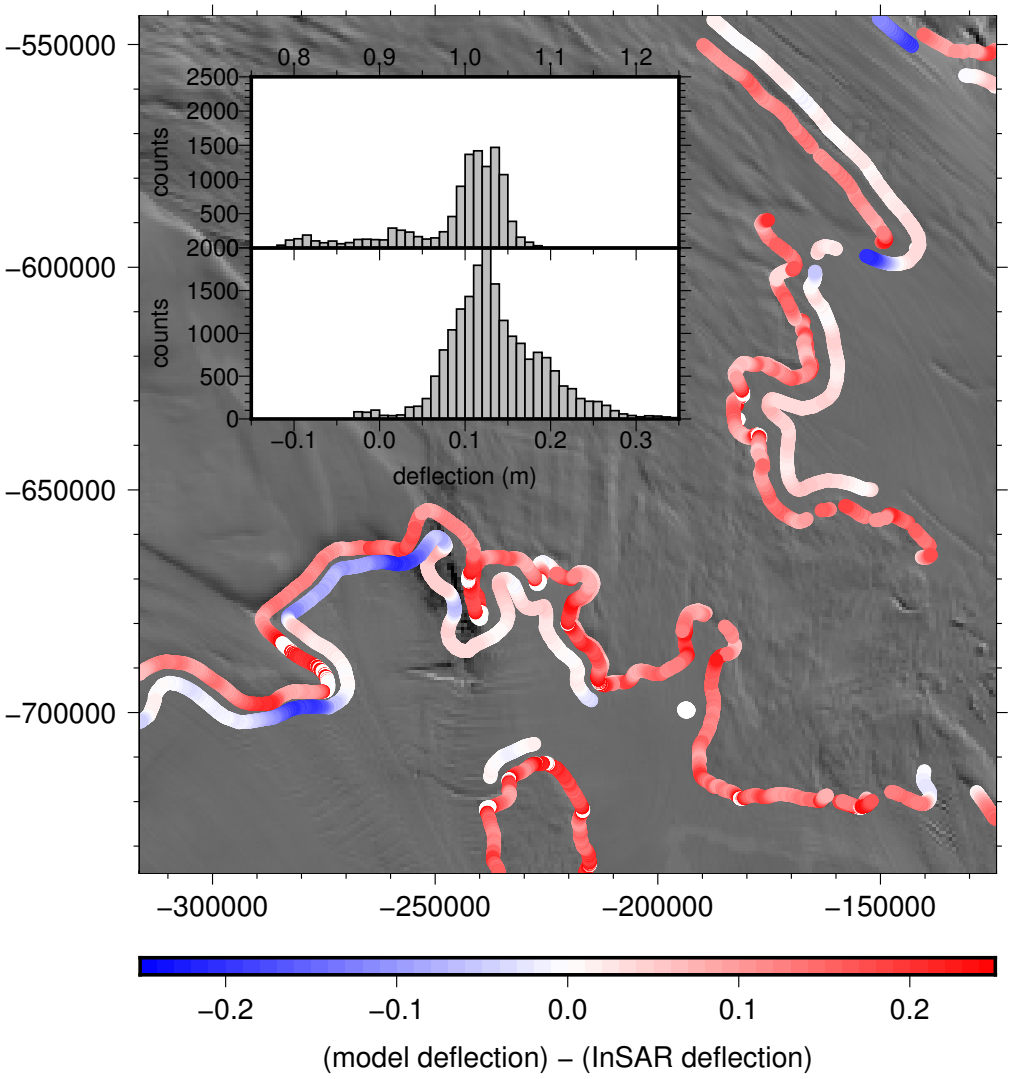

Figure 5.10: Accuracy assessment of flexure model using InSAR-derived limits of flexure (*Rignot et al.*, 2011a, E. Rignot, *pers. comm.*, 2011). Inset histograms show distribution of modeled values at the seaward (top) and landward (bottom) limits of flexure. Our model consistently recovers the correct seaward limit of flexure (0.99 ± 0.06), but estimates an amplitude of 0.14 ± 0.08 at the landward limit of flexure, where deflection should be 0. This difference corresponds to the model placing the grounding line ∼1 ice thickness too far inland.

5.4.2 Grounding Line Migration

We used all the cGPS data spanning 2011–2015 to assess whether we can use GPS methods to investigate tidally-driven grounding-line migration in the embayment, which has low surface slopes (Figure 5.5). To identify which stations contained tidal signals, we cross-correlated GPS data from stations at the landward tip of the embayment and on the southern flank of the embayment with the floating GPS site. Across the landward end of the embayment, GPS stations SIO0, SIO1, and SIO9 clearly showed correlations with the tidal signal, with increasing phase lag landward, i.e., toward grounded ice (Figure 5.11), similar to the permanent GPS stations further seaward in the flexure zone discussed earlier (Figure 5.4). Sites SIO2 and SIO4–SIO7 were anti-correlated with the tides, which is due to not implementing an ocean-load tide correction. Therefore, we conclude that these sites are grounded. Sites SIO3 (magenta in Figure 5.11) and SIO8 (cyan in Figure 5.11) showed peak phase lags between that of nearby floating and nearby grounded sites. On the southern flank of the embayment, the GPS stations behaved as expected: lines of stations parallel to the southern grounding line show an increasingly-damped tidal signal moving landward (Figure 5.12).

5.5 Discussion

5.5.1 Flexurally-Driven Tidal Pumping

We used our 2D model to assess locations where flexurally-driven tidal pumping of seawater upstream may be an important process by analyzing where anti-correlated flexure (i.e., deflection in the opposite direction of the tidal forcing) occurs (Figure 5.13). The 2D effect of flexure is clearly highlighted when looking at negative flexure upstream of the grounding line: deflections are focused upstream of

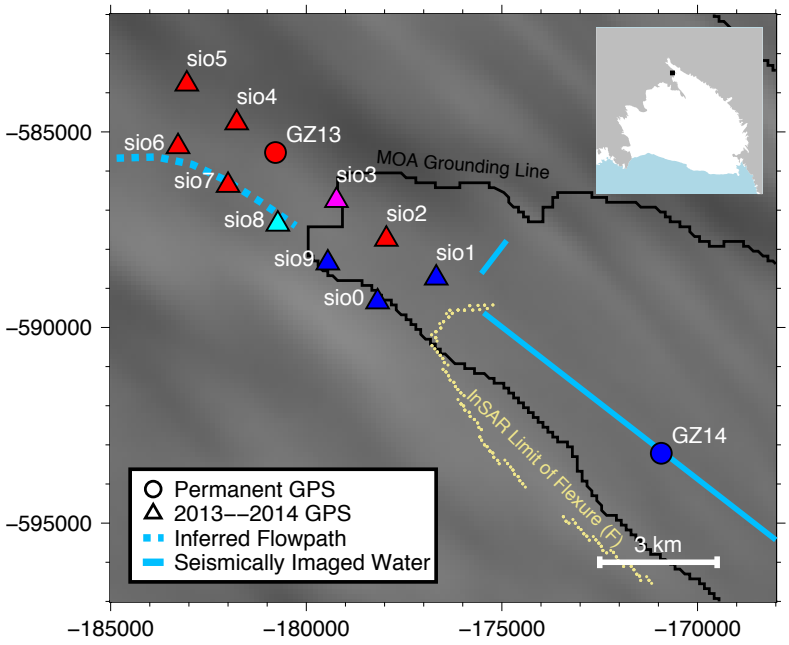

(a)

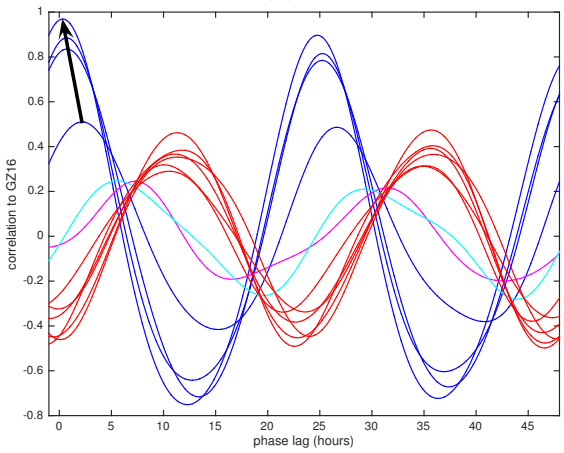

(b)

Figure 5.11: (a) Map of the cGPS experiment at the landward tip of the embayment in 2013–2014, with inferred subglacial water flowpath (*Carter and Fricker*, 2012), locations of a seismically-imaged water column in 2011–2012 (*Horgan et al.*, 2013a), inland limit of flexure from InSAR (*Rignot et al.*, 2011a), and MODIS Mosaic of Antarctica (MOA) grounding line (*Scambos et al.*, 2007). GPS station colors correspond to colors in panel (b). (b) Cross-correlations between cGPS stations and fully-floating site GZ16. Arrow points from SIO9 downstream to GZ14, showing the decreasing phase lag with distance. Red sites are likely grounded. Floatation of cyan and magenta stations cannot be assessed.

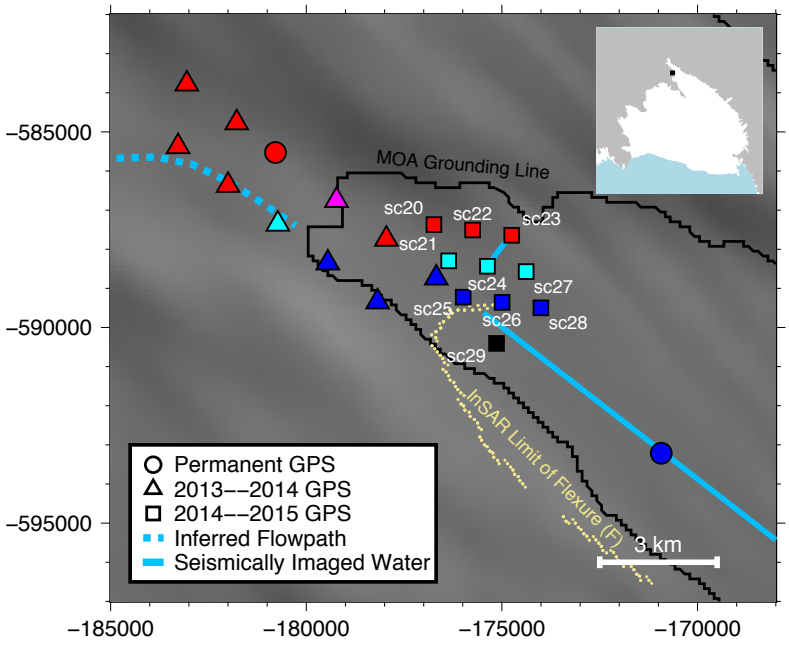

(a)

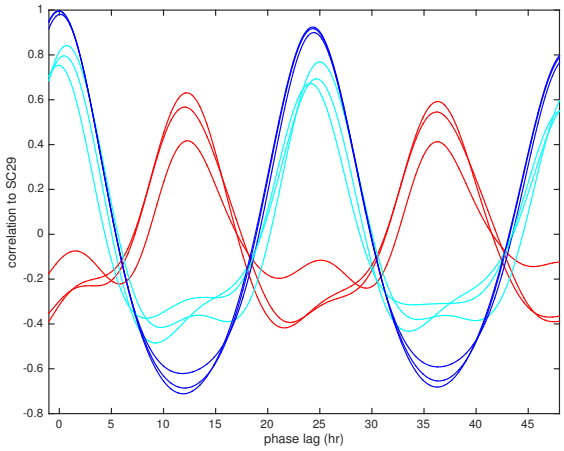

(b)

Figure 5.12: (a) Map of the cGPS experiment on the southern flank of the embayment in 2014–2015, with inferred subglacial water flowpath (*Carter and Fricker*, 2012), locations of a seismically-imaged water column in 2011–2012 (*Horgan et al.*, 2013a), inland limit of flexure from InSAR (*Rignot et al.*, 2011a), and MODIS Mosaic of Antarctica (MOA) grounding line (*Scambos et al.*, 2007). GPS from Figure 5.11 (circles/triangles with no labels) shown to provide context on location of floating (blue) and grounded (red) sites. Colors for labeled GPS stations correspond to colors in panel (b). (b) Cross-correlations between stations and SC29. Blue and cyan sites are likely floating. Red sites are likely grounded.

grounding-line peninsulas and are dispersed upstream of grounding-line embayments. The signal is weakest where subglacial water is proposed to discharge into the sub-ice-shelf cavity, leading us to suggest that the cyclic, vertical movement of an upstream flexural-bulge is not likely a grounding-line-destabilizing process.

Upstream flexure is focused behind grounding-line peninsulas. At least in this location the peninsula is characterized by steep surface slopes (Figure 5.5) and therefore steep hydropotential gradients. The seawater pumping mechanism requires shallow gradients for the dynamic subglacial pressure change due to flexure to reverse the static hydropotential gradient. Therefore, it is unlikely that seawater can be pumped upstream past the grounding line. While our modeling cannot ascertain whether or not the cyclic flexure at a peninsula locally stabilizes the grounding line via sediment strengthening, other evidence suggests that sediment compaction does occur in this geometry (*Christianson et al.*, 2013). Our modeling work suggests that the effect of this stabilization mechanism would be magnified by the geometry.

The model we employ is limited by its required forcing adjustment to shift the grounding line to a more realistic location. However, any model that does not set a grounding-line boundary-condition requires prescribing basal conditions, either through an ice-bed coupling parameterization or through defining the elastic properties of the substrate (e.g., *Walker et al.*, 2013; *Sayag and Worster*, 2013). These avenues require assumptions about the basal interface that are largely unconstrained by observation, especially in terms in the spatial variability of the interface properties. One approach to mitigate this issue is to assign bed properties at a location we are confident in their value (i.e., an area with extensive geophysical or *in situ* observations) and compare the resulting limits of flexure over a broader region to the InSAR-derived locations, similar to how we assessed our model's

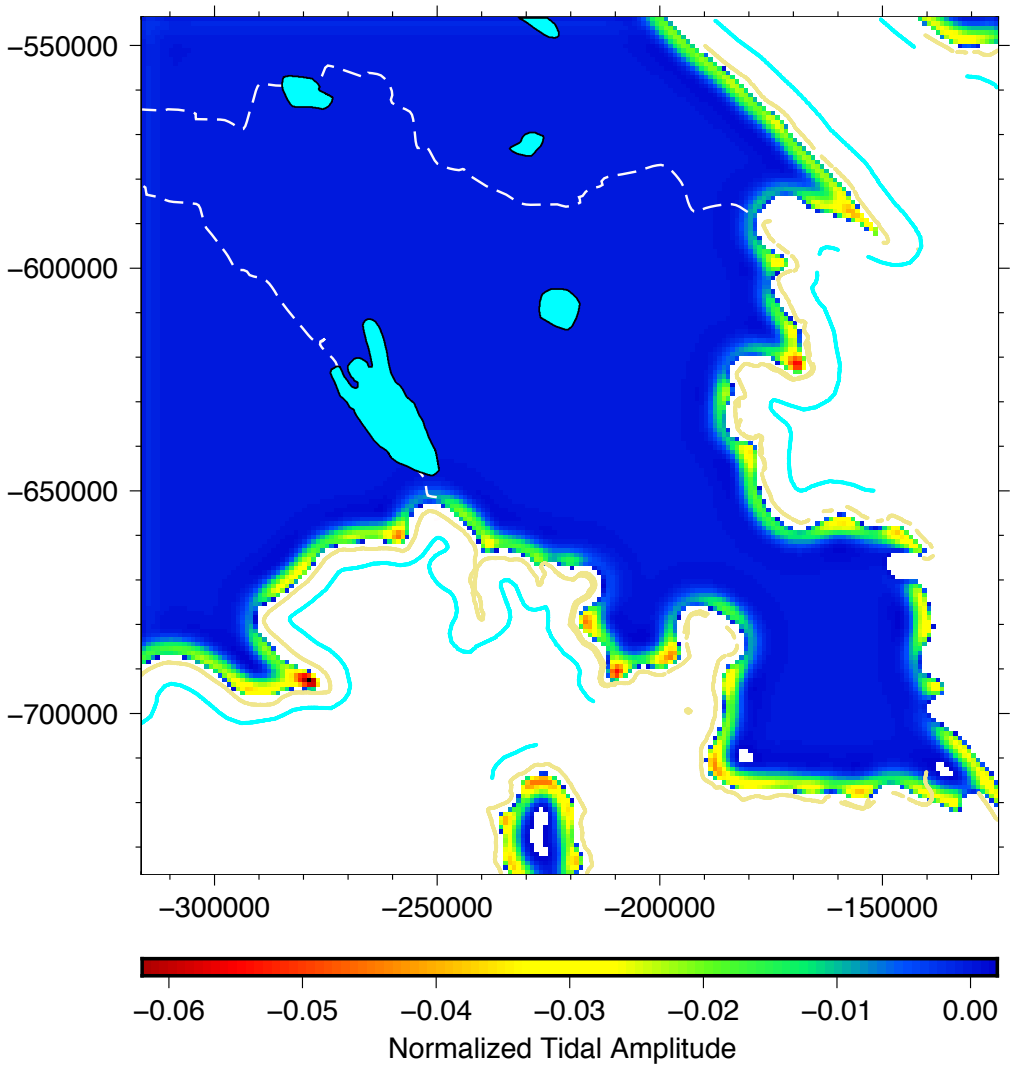

Figure 5.13: Magnitude of the flexural bulge upstream of the grounding line for Whillans Ice Stream, with InSAR-derived limits of flexure (*Rignot et al.*, 2011a, E. Rignot, *pers. comm.*, 2011) shown in yellow and cyan. Active subglacial lakes (*Fricker and Scambos*, 2009) shown in cyan; inferred subglacial water flow paths (*Carter and Fricker*, 2012) shown as dashed white lines. Areas where subglacial water is predicted to cross the grounding line have small magnitudes of upstream flexure, suggesting that enhanced interaction between fresh and saline water through tidal pumping of seawater upstream is not a significant process.

accuracy. This comparison would yield information on the variability of unknown bed parameters by highlighting where the model deviates from observations. This type of study using a model that dynamically determines the grounding line location using a realistic domain has not been comprehensively performed and would provide important constraints on basal properties that are otherwise difficult to estimate. Such studies will be the focus of future work using either a single-layered model with variable elasticity of the substrate or a multi-layered flexure model.

5.5.2 Tidal Phase Lags across the Flexure Zone

cGPS data acquired in both the peninsula and the embayment regions experienced a delayed response to changes in ocean tide. At the peninsula, cross-correlation between STR2 and the tide gauge (STR5) exhibited a delay of 1.5 minutes, which was not seen at other stations in this region of the flexure zone. An active seismic survey along this transect revealed significant "positive topography" (i.e., a bump or reigel) 2.1–2.4 km seaward of the grounding line (*Horgan et al.*, 2013b), which is ∼300–600 m downstream of STR2. This type of prominent bump in bathymetry reduces local water-column thickness. Since tides propagate as shallow-water waves (e.g., *Dronkers and Schönfeld*, 1959), the propagation velocity of the traveling wave, v, can be related to water column thickness, z, by:

$$v = \sqrt{gz}, \tag{5.3}$$

where g is acceleration due to gravity. Thus a local reduction in water column thickness slows propagation. Therefore, we suggest that the phase lag at STR2 is due to a lag in forcing compared to the stations around it, rather than a local (spatial scales of 1–2 km) viscous ice response.

At the embayment site, the relationship between phase lag and distance along the transect followed a regular pattern: the lag until peak correlation with ocean tide decreased with distance seaward. Heights at GZ15 and GZ16 fluctuated in phase with ocean tide. Heights at GZ14, 6.3 km upstream from GZ15, also fluctuated with ocean tide, but were delayed by 16.5 minutes. 6.1 km landward at GZ12, the phase lag was an additional 15.5 minutes (a total of 32 minutes delayed). Viscoelastic treatments of ice flexure have demonstrated that the viscous component can affect the timing of flexural response (*Walker et al.*, 2013). However, the lack of this effect only ∼35 km away at the peninsula site, where ice has a similar flow history and forcing timescales, implies that either the rheological parameters of ice vary significantly over short spatial-scales or another process was responsible for the observed timing of ice-surface deflections. The most obvious difference that could cause a different flexural response at the two grounding-line sites is geometric: at the peninsula, the ice is unconfined with a comparatively thick water cavity (*Horgan et al.*, 2013b); however, at the embayment site, the flexure zone is confined and oriented orthogonal to the predominant tidal circulation (*MacAyeal*, 1984; *Padman et al.*, 2002), and the water column is shallow, with low water-column-thickness slopes (20–30 m near its mouth, shallowing to 0 m at the grounding line ∼50 km upstream, see *Muto et al.*, 2013).

We can approximately assess whether the phase lag at the embayment site is due to the geometry by using Eq. 5.3 to estimate the velocity at which the traveling wave should propagate into the embayment. The observed propagation velocities between GZ15 and GZ14 (6.3 m s^{-1}) and GZ14 and GZ12 (6.4 m s^{-1}) correspond to a water column of ∼4 m. Seismic-sounding estimates show that the water column thins over the same distance from ∼12 m at GZ15 ($v = 10.8$ m s^{-1}) to ∼6 m at GZ12 ($v = 7.7$ m s^{-1}) (*Horgan et al.*, 2013b). While the estimated

propagation velocity based on geophysically-inferred water column thickness is 20%–70% greater than that observed with GPS-derived height measurements, the propagation of tides in shallow embayments and estuaries is a complex, non-linear process, especially in the sub-ice-shelf cavity, where there is an additional frictional interface. We do not expect an exact agreement between GPS observations and Eq. 5.3 and instead use this analysis to establish that our observed phase lags are generally consistent with propagation dynamics in shallow water.

Near the grounding line, phase lags exponentially increase landward, with peak lags occurring right at the landward limit of flexure (F) (Figure 5.11). In the 1.9 km between GZ12 and SIO1 (the most landward GPS station with heights containing a clear tidal component), the phase lag increases by 43 minutes. One mechanism for accommodating this slowing of tidal propagation is through significant frictional drag on the water-sediment and water-ice interfaces, implying significant dissipation of tidal energy. This hypothesis is consistent with previous work modeling tides beneath ice shelves (e.g., *MacAyeal*, 1984; *Makinson and Nicholls*, 1999; *Holland*, 2008). Moreover, these studies showed that increased frictional drag induces vertical shear and drives increased vertical mixing of the water column, disrupting stratification and freshwater plume development. Ice-shelf melt rates should therefore remain low as the well-mixed water insulates basal ice. Field observations using phase-sensitive radar across this embayment during the 2014–2015 austral summer confirmed low ($O(0.01)$ m yr^{-1}) basal melt-rates (O. Marsh, *pers. comm.*, 2015).

5.5.3 Tidal-Frequency Grounding Line Migration

We found no evidence of tidally-driven grounding-line migration at the mouth of Whillans Ice Stream in the cGPS observations. This effect would manifest

itself by "bottoming out" during falling tide (e.g., *Schmeltz et al.*, 2001; *Brunt et al.*, 2010). No station from either experiment straddling the grounding line at the embayment site exhibited such behavior. While this leads us to conclude that, within GPS precision, ice-bed decoupling likely does not have an impact in this embayment, we cannot realistically assess the impact this process would have elsewhere.

Seismic surveys by *Horgan et al.* (2013a) revealed a ∼1 km wide and ∼7 m deep channel carved into the ocean-bottom sediments (light blue line showing seismically imaged water beneath SC23 and SC24 in Figure 5.12). This channel was hypothesized to potentially act as a conduit to focus subglacial and/or ocean processes (*Horgan et al.*, 2013a). However, we saw no effect of this channel in the height data acquired by the array of cGPS stations. While this result may suggest that channelization of the ocean cavity does not impact cavity circulation near the grounding line, it is also possible that there is no measureable ice-surface change as a result of a change in ocean circulation since the channel is narrow compared to the flexural wavelength of ice ∼800 m thick. (i.e., the width of the perturbation is much less than the flexural wavelength).

We can use the GPS data to precisely map the grounding line location, taking advantage of the fact that the grounding line did not migrate over the duration of these GPS experiments. Using cross-correlations, we found SIO0, SIO1, and SIO9 to be positively correlated, though highly damped, to tidal height, suggesting they are within the flexure zone. Tidal signals at these sites were low (on the order of 0.06 m at SIO1 and 0.02 m at SIO0 and SIO9), which is lower than the typical precision of PPP-processed GPS data. Therefore, we also calculated the normalized tidal amplitudes at these sites; this method increases the signal-to-noise ratio at each station by averaging hundreds of data points. Using normalized

tidal amplitudes, we found that SIO0 and SIO1, which are both landward of the InSAR-mapped limit of flexure (*Rignot et al.*, 2011a), showed positive normalized amplitudes that are consistent with ice flexure (Figure 5.14). By looking at both the phase- and amplitude-domains of a dense GPS grid, we can conclude that locations with magnitudes of vertical movement typically considered below the measurements' noise floor are within the flexure zone. Assuming both methods were accurate, there are then two possibilities for the disagreement between the inland limit of flexure determined in this study and that determined by double-differenced InSAR, generally accepted to be the most precise method for mapping grounding lines in Antarctica: (1) there was grounding line retreat between the collection of InSAR data (Feb.–Apr. 2009) and the collection of GPS data (2013–2014); or (2) there was variability in grounding-line location on timescales >2 weeks (e.g., migration with semi-annual tides) and neither the GPS-derived nor InSAR-derived snapshot of the flexure limit represents the true grounding-line location. Future work will investigate which of these scenarios is more likely to have occurred.

5.6 Summary

We used data from GPS experiments across two different grounding-line geometries (a convex peninsula and a concave embayment) and a two-dimensional model in the flexure zone of Whillans Ice Stream to assess the impact of two processes on the fate of subglacial water as it reaches the ocean cavity: (1) flexurally-driven pumping of seawater upstream into the subglacial hydrology system, and (2) alteration of subglacial water-pressure gradients due to mechanical decoupling of the ice-bed interface. We found that when ice flexure is modeled over a realistic domain, the upstream flexural-bulge that could drive tidal pumping is dispersed in regions where subglacial water is predicted to discharge into the ocean cavity.

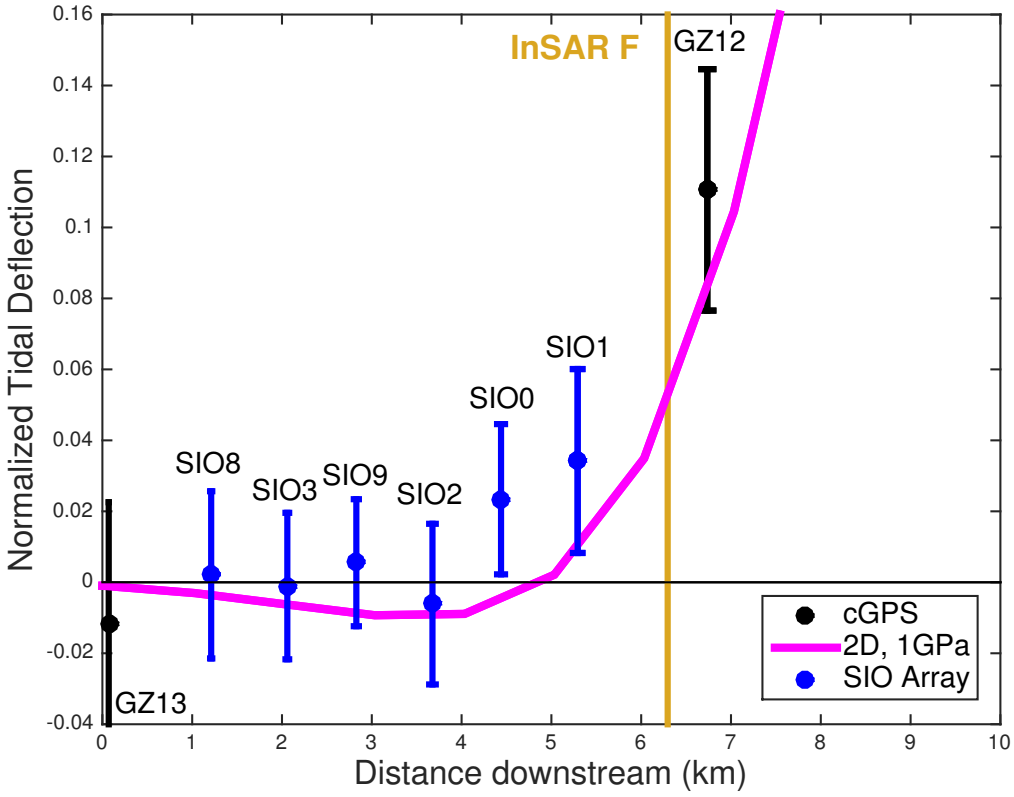

Figure 5.14: Normalized tidal amplitudes from our cGPS experiment across the grounding line at the site located at the landward tip of the embayment demonstrating the use of a dense cGPS grid to precisely locate a grounding line using seasonal data.

Therefore, we conclude that this process likely does not have a significant impact on the subglacial hydrologic system or ice-ocean dynamics. Over grounding-line peninsulas, the magnitude of the process was amplified, suggesting that it could be a mechanism for grounding-line stabilization. Unfortunately over the two 14+ day periods that we sampled, we did not observe any grounding line migration; therefore, we could not investigate the importance of this process on the the mixing of subglacial and ocean water. We did, however, use these GPS experiments to estimate the upstream limit of flexure, which was located ∼1.5 km upstream from the InSAR-derived estimate of F, suggesting either the presence of interannual grounding line variability or a small grounding line retreat in the area.

5.7 Acknowledgements

This work was carried out as part of the WISSARD project, supported by NASA grant NNX11AQ78H (Siegfried and Fricker) and NSF grant ANT-0838885 (Severinghaus and Fricker). We thank UNAVCO, Raytheon Polar Services, Antarctic Support Contract (ASC), Kenn Borek Air, and the New York Air National Guard for logistical support; and E. Garcia and D. Sandwell for model code and helpful discussion on elastic flexure.

Chapter 5, in full, is currently being prepared for submission for publication of the material. The dissertation author was the primary investigator and author of this material.

Chapter 6

Summary and Future Work

6.1 Summary of Dissertation

We used a data-driven approach to better understand processes that control the distribution and movement of subglacial water in Antarctica, applying a unique blend of ground-based GPS data, satellite altimetry, and two-dimensional modeling. The main objectives of this dissertation were to:

1. Extend the observational record of active subglacial lakes,
2. Assess the impact of subglacial lake drainage events on regional ice dynamics, and
3. Investigate processes that affect subglacial water transport as it nears the grounding line.

Below, we summarize our specific efforts to address each objective.

6.1.1 Objective 1

To address objective 1, we combined ground and spaceborne data to develop a new technique for observing active subglacial lake activity (**Chapter 2**) and applied this technique to 37 active subglacial lakes across Antarctica, extending the existing time series by up to six years (**Chapter 3**). We developed the new method for observing the surface expression of subglacial lake activity on the lower confluence of Whillans and Mercer ice streams, West Antarctica. We used ground-based GPS height observations to cross-calibrate the new record from CryoSat-2 radar altimetry, which started in mid-2010, with the existing record from ICESat laser altimetry, which ended in 2009. In addition to developing the method to extend subglacial lake activity records in time, we demonstrated in **Chapter 2** that data from the CryoSat-2 mission provides increased spatial information that was only previously accessible through optical-image differencing, a powerful method, but one that can only be employed on cloudless, summer days.

Chapter 3 applied the method developed in **Chapter 2** to 37 of the 124 active subglacial lakes in the continent-wide inventory. The existing inventory only contains observations covering 4.5 years (2003 to 2008), leaving many important details about the physical nature of subglacial lakes unknown. Our application of the new CryoSat-2-based method in **Chapter 3** revealed that multiple active lakes around Antarctica continued to fill and drain past the end of the ICESat mission in 2009. While we could only extend the activity record for a small subset of known subglacial lakes, this effort represents the first comprehensive attempt to continue monitoring these lakes after their initial discovery. We suggested that the full distribution of active subglacial lakes likely represents a continuum of hydrologic features, from small, transient pockets of water to large, permanent (at

least on decadal scales) features that impound water and prevent lubrication of the downstream ice-bed interface. Understanding the variability that exists within this continuum is critical to assessing to what extent active subglacial lakes impact ice flow of Antarctic ice streams and outlet glaciers.

6.1.2 Objective 2

To address objective 2, we investigated in detail the impact of one drainage event on ice dynamics (**Chapter 4**). We estimated continuous ice velocity at eight GPS locations to demonstrate that the interaction of an ice stream with an episodic, evolving subglacial hydrology system is complex and cannot be captured with basic models. We also analyzed changes to the stick-slip motion of Whillans Ice Plain to demonstrate that the modulation of ice flow by ocean tides is a more complex process than had previously been recognized. These changes in ice velocity and basal dynamics occurred on sub-annual timescales, at frequencies higher than has previously been associated with internally-driven Antarctic ice stream processes. While we cannot assess the consequences of these short-timescale events on large-scale ice-sheet dynamics, episodic, internally-driven transients can bias observations used to infer long-term ice-sheet changes.

6.1.3 Objective 3

To address objective 3, we explored two processes that have been hypothesized to alter subglacial water transport near the grounding line using the vertical component of GPS observations and a two-dimensional elastic flexure model (**Chapter 5**). Our modeling results suggested that flexurally-driven pumping of water upstream of the grounding line probably does not enhance mixing of fresh and saline water; rather, our results were consistent with previous work demon-

strating that the flexural bulge upstream of the grounding line could instead be a grounding-line stabilizing process through till compaction. Last, we evaluated whether GPS methods were precise enough to investigate the impact of ice-bed decoupling during high tide on subglacial hydrology near the grounding line. We could not identify any locations near the grounding line of Whillans Ice Stream where this process was occurring. Our results highlighted the need for precise, time-resolved measurements to understand the complex, time-varying processes that govern interactions between ice, ocean, and sediments near the grounding line.

6.2 Future Work

Our data-driven approach to understanding dynamic subglacial hydrology in Antarctica successfully provided new, detailed insights into the basal interface, yet there are still large gaps in our knowledge preventing the inclusion of an evolving basal water system into large-scale, predictive models of ice-sheet flow. In the following sections, we highlight three avenues for future work to shrink these data gaps.

6.2.1 Continued monitoring—the need for long time-series

More than anything else, the work presented in this dissertation demonstrated that, to understand the coevolution of Antarctic subglacial systems across the spectrum of physical settings, we need long records. These records must include high temporal-resolution data of both subglacial lake activity and coincident ice dynamics. There are three main directions for continuing precise monitoring of active subglacial lakes, a combination of which will be necessary for characterizing the full distribution of subglacial lakes in Antarctica:

1. Improve existing coverage by unwrapping CryoSat-2 SARIn-mode phase data to create "swaths" of heights in regions of steep terrain. *Hawley et al.* (2009) and *Gray et al.* (2013) demonstrated that phase-unwrapping of SARIn-mode data can increase data density by nearly two orders of magnitude in regions of sloped terrain. The effectiveness of this method in areas of rough terrain is still an open question. This method then should be rigorously validated before being implemented to improve the coverage for lakes in sloping and/or rugged areas, especially in East Antarctica.

2. Develop algorithms for detection of new subglacial lakes. The *Smith et al.* (2009) inventory of subglacial lakes we used to direct our research in **Chapter 3** only identified subglacial lakes that were active during a relatively limited 4.5-year window, likely only detecting a subset of the full distribution of lakes present beneath Antarctica. Although CryoSat-2 altimetry is generally less precise than ICESat altimetry, large surface-height changes can still be easily identified, especially in areas of small regional-scale surface changes. With now five full years of data coverage from the CryoSat-2 mission, a lake-detecting algorithm should be developed and implemented to identify potential locations of new subglacial lakes.

3. Prepare for the next generation of polar altimetry missions by planning cross-calibration experiments. **Chapter 2** demonstrated the importance of overlapping datasets for cross-calibrating time series from disparate observational techniques. The ICESat-2 laser altimetry mission, which has a data collection scheme unlike both its predecessor ICESat(-1) and CryoSat-2, is scheduled for launch in 2017. Cross-calibration between the CryoSat-2 and ICESat-2 missions will remain a challenge without precise, independent, and

coincident measurements of reference ice-surfaces. Subglacial lakes are an ideal location for such cross-calibration experiments because of their large and variable magnitude of height-change rates. A subset of active subglacial lakes with a history of cyclic behavior should be chosen and instrumented to ensure an independent surface-height reference to cross-calibrate altimetry missions.

6.2.2 Novel methods for imaging the subglacial environment

Classical glaciophysical techniques such as radio-echo sounding and active-seismic surveying have been used to investigate the physical character of active subglacial lakes in Antarctica. For example, ground-based observations of Subglacial Lake Whillans (*Christianson et al.*, 2012; *Horgan et al.*, 2012) inferred the presence of liquid water, but could not constrain the total lake-water volume, nor precisely quantify the amount of pore-water present in the underlying sediments. Airborne RES surveys of active subglacial lakes (e.g., *Wright et al.*, 2012, 2014; *Siegert et al.*, 2014) have had limited success in identifying the ice-bed interface beneath a surface-height anomaly identified by ICESat as a definite hydrological feature. This paradox highlights the larger point that the set of lakes identified from surface expressions and the set of lakes identified through RES have minimal overlap (see Figure 1.1; *Wright and Siegert*, 2012). Consequently, we need to develop novel, complementary techniques for imaging the ice-bed interface that are specifically sensitive to water in order to resolve the disconnect between our current methods.

One example of a technique that could potentially improve mapping the subglacial environment is the transient control-source electromagnetic (CSEM) method, which uses low-frequency EM induction to detect subsurface conductive features. This technique has been used to map liquid bodies in many different

environments, ranging from near surface groundwater (e.g., *Danielsen et al.*, 2003) to melt-rich conduits at the lithosphere-asthenosphere boundary (e.g., *Naif et al.*, 2013). More recently, a helicopter-based implementation of CSEM was used to image subsurface brines beneath Taylor Glacier, East Antarctica (*Mikucki et al.*, 2015), establishing CSEM as a viable technique in Antarctica. Future work implementing novel (to glaciology) techniques like CSEM will be critical to understanding the physical nature of subglacial hydrology and its dynamics.

6.2.3 Repeated geophysical surveying

One important finding of this dissertation is that Antarctic ice streams, like mountain glaciers and Greenland outlet glaciers, are capable of responding rapidly to changes in their basal boundary condition. We still do not know, however, whether these short-term changes are merely high-frequency noise of the ice sheet that we now have the technical capacity to observe or whether these changes are, at least in part, driving long-term evolution of the system. One way to begin to answer this question is to estimate not just velocity fluctuations due to a lake drainage event or height changes from tidally-driven flexure, but to perform detailed surveys before, during, and after such processes to evaluate if any significant, permanent changes took place. For example, repeat RES surveying (e.g., *Smith et al.*, 2012) could identify any redistribution of till across the ice-bed interface related to episodic basal water movement. Repeat seismic surveys across the flexure zone, especially in conjunction with phase-sensitive radar measurements to precisely determine ice thickness changes, could assess any near-shore changes to the ocean cavity related to basal melt or sedimentation. This type of study requires repeated surveying of the same location to assess how changes evolve through the whole rock-ice-ocean system, as well as the flexibility to collect data at opportune times

(e.g., immediately after a lake drainage). Our current knowledge of the temporal variability of glacial processes, especially related to subglacial lakes and grounding zones, is driven mainly by modeling studies constrained by limited geophysical observations. Only through repeated measurements of the surface, the ice column, and the basal environment, in conjunction with realistic modeling that includes coupling between the ice, water, sediment, and ocean systems, will we be able to understand the role of dynamic subglacial hydrology in Antarctica.

References

Alley, R. B. (1989). Water-pressure coupling of sliding and bed deformation: I. Water system. *Journal of Glaciology*, 35(119):108–118.

Alley, R. B., Anandakrishnan, S., Bentley, C. R., and Lord, N. (1994). A water-piracy hypothesis for the stagnation of Ice Stream C, Antarctica. *Annals of Glaciology*, 20(1):187–194.

Alley, R. B., Anandakrishnan, S., Dupont, T. K., Parizek, B. R., and Pollard, D. (2007). Effect of Sedimentation on Ice-Sheet Grounding-Line Stability. *Science*, 315(5820):1838–1841.

Alley, R. B., Blankenship, D. D., Bentley, C. R., and Rooney, S. T. (1986). Deformation of till beneath ice stream B, West Antarctica. *Nature*, 322(6074):57–59.

Anandakrishnan, S. and Alley, R. B. (1997). Stagnation of ice stream C, West Antarctica by water piracy. *Geophysical Research Letters*, 24(3):265–268.

Anandakrishnan, S., Catania, G. A., Alley, R. B., and Horgan, H. J. (2007). Discovery of Till Deposition at the Grounding Line of Whillans Ice Stream. *Science*, 315(5820):1835–1838.

Andrews, L. C., Catania, G. A., Hoffman, M. J., Gulley, J. D., Lüthi, M. P., Ryser, C., Hawley, R. L., and Neumann, T. A. (2014). Direct observations of evolving subglacial drainage beneath the Greenland Ice Sheet. *Nature*, 514(7520):80–83.

Bamber, J. L., Vaughan, D. G., and Joughin, I. (2000). Widespread Complex Flow in the Interior of the Antarctic Ice Sheet. *Science*, 287(5456):1248–1250.

Bartholomaus, T. C., Anderson, R. S., and Anderson, S. P. (2008). Response of glacier basal motion to transient water storage. *Nature Geoscience*, 1(1):33–37.

Beem, L. H., Tulaczyk, S. M., King, M. A., Bougamont, M., Fricker, H. A., and Christoffersen, P. (2014). Variable deceleration of Whillans Ice Stream, West Antarctica. *Journal of Geophysical Research: Earth Surface*, 119(2):212–224.

Bell, R. E. (2008). The role of subglacial water in ice-sheet mass balance. *Nature Geoscience*, 1(5):297–304.

Bell, R. E., Ferraccioli, F., Creyts, T. T., Braaten, D., Corr, H., Das, I., Damaske, D., Frearson, N., Jordan, T., Rose, K., Studinger, M., and Wolovick, M. (2011). Widespread Persistent Thickening of the East Antarctic Ice Sheet by Freezing from the Base. *Science*, 331(6024):1592–1595.

Bell, R. E., Studinger, M., Shuman, C. A., Fahnestock, M. A., and Joughin, I. (2007). Large subglacial lakes in East Antarctica at the onset of fast-flowing ice streams. *Nature*, 445(7130):904–907.

Bell, R. E., Studinger, M., Tikku, A. A., Clarke, G. K., Gutner, M. M., and Meertens, C. (2002). Origin and fate of Lake Vostok water frozen to the base of the East Antarctic ice sheet. *Nature*, 416(6878):307–310.

Bindschadler, R. A., King, M. A., Alley, R. B., Anandakrishnan, S., and Padman, L. (2003). Tidally Controlled Stick-Slip Discharge of a West Antarctic Ice Stream. *Science*, 301(5636):1087–1089.

Bindschadler, R. A., Scambos, T. A., Choi, H., and Haran, T. M. (2010). Ice sheet change detection by satellite image differencing. *Remote Sensing of Environment*, 114(7):1353–1362.

Bindschadler, R. A., Stephenson, S. N., MacAyeal, D. R., and Shabtaie, S. (1987). Ice Dynamics at the Mouth of Ice Stream B, Antarctica. *J. Geophys. Res.*, 92(B9):8885.

Blankenship, D. D., Bentley, C. R., Rooney, S. T., and Alley, R. B. (1986). Seismic measurements reveal a saturated porous layer beneath an active Antarctic ice stream. *Nature*, 322(6074):54–57.

Borsa, A. A., Moholdt, G., Fricker, H. A., and Brunt, K. M. (2014). A range correction for ICESat and its potential impact on ice-sheet mass balance studies. *The Cryosphere*, 8(2):345–357.

Brunt, K. M., Fricker, H. A., and Padman, L. (2011). Analysis of ice plains of the Filchner–Ronne Ice Shelf, Antarctica, using ICESat laser altimetry. *Journal of Glaciology*, 57(205):965–975.

Brunt, K. M., Fricker, H. A., Padman, L., Scambos, T. A., and O'Neel, S. (2010). Mapping the grounding zone of the Ross Ice Shelf, Antarctica, using ICESat laser altimetry. *Annals of Glaciology*, 51(55):71–79.

Budd, W. F., Jenssen, D., and Smith, I. N. (1984). A three-dimensional time-dependent model of the West Antarctic ice sheet. *Annals of Glaciology*, 5:29–36.

Budd, W. F., Keage, P. L., and Blundy, N. A. (1979). Empirical studies of ice sliding. *Journal of Glaciology*, 23:157–170.

Carter, S. P., Blankenship, D. D., Peters, M. E., Young, D. A., Holt, J. W., and Morse, D. L. (2007). Radar-based subglacial lake classification in Antarctica. *Geochemistry, Geophysics, Geosystems*, 8(3):Q03016.

Carter, S. P., Blankenship, D. D., Young, D. A., Peters, M. E., Holt, J. W., and Siegert, M. J. (2009). Dynamic distributed drainage implied by the flow evolution of the 1996-1998 Adventure Trench subglacial lake discharge. *Earth and Planetary Science Letters*, 283(1-4):24–37.

Carter, S. P. and Fricker, H. A. (2012). The supply of subglacial meltwater to the grounding line of the Siple Coast, West Antarctica. *Annals of Glaciology*, 53(60):267–280.

Carter, S. P., Fricker, H. A., and Siegfried, M. R. (2013). Evidence of rapid subglacial water piracy under Whillans Ice Stream, West Antarctica. *Journal of Glaciology*, 59(218):1147–1162.

Catania, G., Hulbe, C., Conway, H., Scambos, T. A., and Raymond, C. (2012). Variability in the mass flux of the Ross ice streams, West Antarctica, over the last millennium. *Journal of Glaciology*, 58(210):741–752.

Chen, G. (1998). *GPS Kinematic Position for the Airborne Laser Altimetry at Long Valley, California*. PhD thesis, Department of Earth, Atmospheric, and Planetary Sciences, Massachusetts Institute of Technology, Cambridge, MA.

Christianson, K., Jacobel, R. W., Horgan, H. J., Anandakrishnan, S., and Alley, R. B. (2012). Subglacial Lake Whillans — Ice-penetrating radar and GPS observations of a shallow active reservoir beneath a West Antarctic ice stream. *Earth and Planetary Science Letters*, 331-332:237–245.

Christianson, K., Parizek, B. R., Alley, R. B., Horgan, H. J., Jacobel, R. W., Anandakrishnan, S., Keisling, B. A., Craig, B. D., and Muto, A. (2013). Ice sheet grounding zone stabilization due to till compaction. *Geophys. Res. Lett.*, 40(20):5406–5411.

Christoffersen, P. and Tulaczyk, S. (2003). Response of subglacial sediments to basal freeze-on 1. Theory and comparison to observations from beneath the West Antarctic Ice Sheet. *Journal of Geophysical Research: Solid Earth*, 108(B4).

Church, J. A., Clark, P. U., Cazenave, A., Gregory, J. M., Jevrejeva, S., Levermann, A., Merrifield, M. A., Milne, G. A., Nerem, R. S., Payne, P. D. N. A. J., Pfeffer, W. T., Stammer, D., and Unnikrishnan, A. S. (2013). Sea Level Change. In Stocker, T. F., Qin, D., Plattner, G. K., Tignor, M., Allen, S. K., Boschung,

J., Nauels, A., Xia, Y., Bex, V., and Midgley, P. M., editors, *Climate Change 2013: The Physical Science Basis. Contribution of Working Group I to the Fifth Assessment Report of the Intergovernmental Panel on Climate Change*, pages 1137–1216, Cambridge, United Kingdom and New York, NY, USA. Cambridge University Press.

Clarke, G. (1987). A short history of scientific investigations on glaciers. *Journal of Glaciology*, 33b:4–24.

Creyts, T. T. and Schoof, C. G. (2009). Drainage through subglacial water sheets. *J. Geophys. Res.*, 114(F4).

Cuffey, K. M. and Paterson, W. S. B. (2010). *The Physics of Glaciers, Fourth Edition*. Academic Press.

Danielsen, J. E., Auken, E., Jørgensen, F., Søndergaard, V., and Sørensen, K. I. (2003). The application of the transient electromagnetic method in hydrogeophysical surveys. *Journal of Applied Geophysics*, 53(4):181–198.

Das, S. B., Joughin, I., Behn, M. D., Howat, I. M., King, M. A., Lizarralde, D., and Bhatia, M. P. (2008). Fracture Propagation to the Base of the Greenland Ice Sheet During Supraglacial Lake Drainage. *Science*, 320(5877):778–781.

Dasgupta, S., Laplante, B., Meisner, C., Wheeler, D., and Yan, J. (2008). The impact of sea level rise on developing countries: a comparative analysis. *Climatic Change*, 93(3-4):379–388.

Davis, C. H. and Moore, R. K. (1993). A combined surface- and volume-scattering model for ice-sheet radar altimetry. *Journal of Glaciology*, 39:675–686.

Davis, C. H. and Zwally, H. J. (1993). Geographic and seasonal variations in the surface properties of the ice sheets by satellite-radar altimetry. *Journal of Glaciology*, 39:687–697.

Depoorter, M. A., Bamber, J. L., Griggs, J. A., Lenaerts, J. T. M., Ligtenberg, S. R. M., van den Broeke, M. R., and Moholdt, G. (2013). Calving fluxes and basal melt rates of Antarctic ice shelves. *Nature*, 502(7469):89–92.

Dowdeswell, J. A., Ottesen, D., Evans, J., Ó Cofaigh, C., and Anderson, J. B. (2008). Submarine glacial landforms and rates of ice-stream collapse. *Geology*, 36(10):819–822.

Dronkers, J. J. and Schönfeld, J. C. (1959). *Tidal computations in shallow water*. Rijkswaterstaat Communications.

Engelhardt, H. and Kamb, B. (1997). Basal hydraulic system of a West Antarctic ice stream: Constraints from borehole observations. *Journal of Glaciology*, 43(144):207–230.

Flament, T., Berthier, E., and Rémy, F. (2014). Cascading water underneath Wilkes Land, East Antarctic ice sheet, observed using altimetry and digital elevation models. *The Cryosphere*, 8(2):673–687.

Flowers, G. E. (2015). Modelling water flow under glaciers and ice sheets. *Proceedings of the Royal Society of London A: Mathematical, Physical and Engineering Sciences*, 471(2176):20140907.

Fretwell, P., Pritchard, H. D., Vaughan, D. G., Bamber, J. L., Barrand, N. E., Bell, R., Bianchi, C., Bingham, R. G., Blankenship, D. D., Casassa, G., Catania, G., Callens, D., Conway, H., Cook, A. J., Corr, H. F. J., Damaske, D., Damm, V., Ferraccioli, F., Forsberg, R., Fujita, S., Gim, Y., Gogineni, P., Griggs, J. A., Hindmarsh, R. C. A., Holmlund, P., Holt, J. W., Jacobel, R. W., Jenkins, A., Jokat, W., Jordan, T., King, E. C., Kohler, J., Krabill, W., Riger-Kusk, M., Langley, K. A., Leitchenkov, G., Leuschen, C., Luyendyk, B. P., Matsuoka, K., Mouginot, J., Nitsche, F. O., Nogi, Y., Nost, O. A., Popov, S. V., Rignot, E., Rippin, D. M., Rivera, A., Roberts, J., Ross, N., Siegert, M. J., Smith, A. M., Steinhage, D., Studinger, M., Sun, B., Tinto, B. K., Welch, B. C., Wilson, D., Young, D. A., Xiangbin, C., and Zirizzotti, A. (2013). Bedmap2: improved ice bed, surface and thickness datasets for Antarctica. *The Cryosphere*, 7:375–393.

Fricker, H. A., Carter, S. P., Bell, R. E., and Scambos, T. (2014). Active lakes of Recovery Ice Stream, East Antarctica: a bedrock-controlled subglacial hydrological system. *Journal of Glaciology*, 60(223):1015–1030.

Fricker, H. A. and Padman, L. (2002). Tides on Filchner-Ronne Ice Shelf from ERS radar altimetry. *Geophysical Research Letters*, 29(12):1622.

Fricker, H. A. and Padman, L. (2012). Thirty years of elevation change on Antarctic Peninsula ice shelves from multimission satellite radar altimetry. *Journal of Geophysical Research: Oceans*, 117(C2).

Fricker, H. A., Powell, R., Priscu, J., Tulaczyk, S., Anandakrishnan, S., Christner, B., Holland, D., Horgan, H., Jacobel, R., Mikucki, J., Mitchell, A., Scherer, R., and Severinghaus, J. (2011). Siple Coast Subglacial Aquatic Environments: The Whillans Ice Stream Subglacial Access Research Drilling (WISSARD) project. In Siegert, M., Kennicutt, C., and Bindschadler, B., editors, *Subglacial Antarctic Aquatic Environments*. AGU Monograph Series, Washington DC.

Fricker, H. A. and Scambos, T. (2009). Connected subglacial lake activity on lower Mercer and Whillans Ice Streams, West Antarctica, 2003–2008. *Journal of Glaciology*, 55(190):303–315.

Fricker, H. A., Scambos, T., Bindschadler, R., and Padman, L. (2007). An Active Subglacial Water System in West Antarctica Mapped from Space. *Science*, 315(5818):1544.

Fricker, H. A., Scambos, T., Carter, S., Davis, C., Haran, T., and Joughin, I. (2010). Synthesizing multiple remote-sensing techniques for subglacial hydrologic mapping: application to a lake system beneath MacAyeal Ice Stream, West Antarctica. *Journal of Glaciology*, 56(196):187–199.

Fricker, H. A., Siegfried, M. R., and Carter, S. P. (2015). A decade of progress in observing and modeling Antarctic subglacial water systems. *Philos. Trans. Roy. Soc. A*, *[Accepted]*.

Garcia, E. S., Sandwell, D. T., and Luttrell, K. M. (2014). An iterative spectral solution method for thin elastic plate flexure with variable rigidity. *Geophysical Journal International*, 200(2):1012–1028.

Goldberg, D. N., Schoof, C., and Sergienko, O. V. (2014). Stick-slip motion of an Antarctic Ice Stream: The effects of viscoelasticity. *Journal of Geophysical Research: Earth Surface*, 119(7):1564–1580.

Goodwin, I. D. (1988). The nature and origin of a jökulhlaup near Casey Station, Antarctica. *J. Glaciol*, 34(116):95–101.

Gray, L., Burgess, D., Copland, L., Cullen, R., Galin, N., Hawley, R. L., and Helm, V. (2013). Interferometric swath processing of Cryosat data for glacial ice topography. *The Cryosphere*, 7(6):1857–1867.

Gray, L., Joughin, I., Tulaczyk, S., Spikes, V. B., Bindschadler, R., and Jezek, K. (2005). Evidence for subglacial water transport in the West Antarctic Ice Sheet through three-dimensional satellite radar interferometry. *Geophysical Research Letters*, 32(3):L03501.

Haran, T. M., Fahnestock, M. A., and Scambos, T. A. (2002). De-striping of modis optical bands for ice sheet mapping and topography. In *AGU Fall Meeting Abstracts*, volume 1, page 1003.

Hawley, R. L., Shepherd, A., Cullen, R., Helm, V., and Wingham, D. J. (2009). Ice-sheet elevations from across-track processing of airborne interferometric radar altimetry. *Geophys. Res. Lett.*, 36(22).

Heinert, M. and Riedel, B. (2007). Parametric modelling of the geometrical ice-ocean interaction in the Ekstroemisen grounding zone based on short time-series. *Geophysical Journal International*, 169(2):407–420.

Holdsworth, G. (1969). Flexure of a floating ice tongue. *Journal of Glaciology*, 8:385–397.

Holland, P. R. (2008). A model of tidally dominated ocean processes near ice shelf grounding lines. *Journal of Geophysical Research: Oceans*, 113(C11).

Horgan, H. J., Alley, R. B., Christianson, K., Jacobel, R. W., Anandakrishnan, S., Muto, A., Beem, L. H., and Siegfried, M. R. (2013a). Estuaries beneath ice sheets. *Geology*, 41(11):1159–1162.

Horgan, H. J., Anandakrishnan, S., Jacobel, R. W., Christianson, K., Alley, R. B., Heeszel, D. S., Picotti, S., and Walter, J. I. (2012). Subglacial Lake Whillans — Seismic observations of a shallow active reservoir beneath a West Antarctic ice stream. *Earth and Planetary Science Letters*, 331:201–209.

Horgan, H. J., Christianson, K., Jacobel, R. W., Anandakrishnan, S., and Alley, R. B. (2013b). Sediment deposition at the modern grounding zone of Whillans Ice Stream, West Antarctica. *Geophys. Res. Lett.*, 40(15):3934–3939.

Hulbe, C. L. and MacAyeal, D. R. (1999). A new thermodynamical numerical model of coupled ice sheet, ice stream, and ice shelf flow. *Journal of Geophysical Research*, 104(25):349–366.

Iken, A. and Bindschadler, R. A. (1986). Combined measurements of subglacial water pressure and surface velocity of Findelengletscher, Switzerland: conclusions about drainage system and sliding mechanism. *Journal of Glaciology*, 32(110):101–119.

Jacobel, R. W., Robinson, A., and Bindschadler, R. A. (1994). Studies of the grounding-line location on Ice Streams D and E, Antarctica. *Annals of Glaciology*, 20(1):39–42.

Jenkins, A. (1991). A one-dimensional model of ice shelf-ocean interaction. *Journal of Geophysical Research*, 96(C11):20671–20.

Jenkins, A. (2011). Convection-driven melting near the grounding lines of ice shelves and tidewater glaciers. *J. Phys. Oceanogr.*, 41(12):2279–2294.

Joughin, I., Abdalati, W., and Fahnestock, M. (2004a). Large fluctuations in speed on Greenland's Jakobshavn Isbrae glacier. *Nature*, 432(7017):608–610.

Joughin, I., Bamber, J. L., Scambos, T., Tulaczyk, S., Fahnestock, M., and MacAyeal, D. R. (2006). Integrating satellite observations with modelling: basal shear stress of the Filcher-Ronne ice streams, Antarctica. *Philosophical Transactions of the Royal Society of London A: Mathematical, Physical and Engineering Sciences*, 364(1844):1795–1814.

Joughin, I., Bindschadler, R. A., King, M. A., Voigt, D., Alley, R. B., Anandakrishnan, S., Horgan, H., Peters, L., Winberry, P., Das, S. B., and Catania, G. (2005). Continued deceleration of Whillans Ice Stream, West Antarctica. *Geophys. Res. Lett.*, 32(22).

Joughin, I., Gray, L., Bindschadler, R., Price, S., Morse, D., Hulbe, C., Mattar, K., and Werner, C. (1999). Tributaries of West Antarctic Ice Streams Revealed by RADARSAT Interferometry. *Science*, 286(5438):283–286.

Joughin, I., Smith, B. E., and Medley, B. (2014). Marine Ice Sheet Collapse Potentially Under Way for the Thwaites Glacier Basin, West Antarctica. *Science*, 344(6185):735–738.

Joughin, I., Tulaczyk, S., Bindschadler, R., and Price, S. F. (2002). Changes in west Antarctic ice stream velocities: Observation and analysis. *J. Geophys. Res.*, 107(B11).

Joughin, I., Tulaczyk, S., MacAyeal, D. R., and Engelhardt, H. (2004b). Melting and freezing beneath the Ross ice streams, Antarctica. *Journal of Glaciology*, 50(168):96–108.

Kamb, B. (1987). Glacier surge mechanism based on linked cavity configuration of the basal water conduit system. *Journal of Geophysical Research*, 92(B9):9083–9100.

Kamb, B. (2001). The West Antarctic Ice Sheet: Behavior and Environment. In Alley, R. B. and Bindschadler, R. A., editors, *Basal zone of the West Antarctic ice streams and its role in lubrication of their rapid motion*, volume 77 of *Antarctic Research Series*, pages 157–199. American Geophysical Union.

Kamb, B. and LaChapelle, E. (1964). Direct observation of the mechanism of glacier sliding over bedrock. *Journal of Glaciology*, 5:159–172.

Kapitsa, A. P., Ridley, J. K., Robin, G. Q., Siegert, M. J., and Zotikov, I. A. (1996). A large deep freshwater lake beneath the ice of central East Antarctica. *Nature*, 381:684–686.

King, M. (2004). Rigorous GPS data-processing strategies for glaciological applications. *Journal of Glaciology*, 50(171):601–607.

Langbein, J. (2008). Noise in GPS displacement measurements from Southern California and Southern Nevada. *Journal of Geophysical Research: Solid Earth*, 113(B5).

Le Brocq, A. M., Payne, A. J., Siegert, M. J., and Alley, R. B. (2009). A subglacial water-flow model for West Antarctica. *Journal of Glaciology*, 55(193):879–888.

Le Brocq, A. M., Ross, N., Griggs, J. A., Bingham, R. G., Corr, H. F. J., Ferraccioli, F., Jenkins, A., Jordan, T. A., Payne, A. J., Rippin, D. M., and Siegert, M. J. (2013). Evidence from ice shelves for channelized meltwater flow beneath the Antarctic Ice Sheet. *Nature Geoscience*, 6(11):945–948.

Li, X., Rowley, R. J., Kostelnick, J. C., Braaten, D., Meisel, J., and Hulbutta, K. (2009). GIS analysis of global impacts from sea level rise. *Photogrammetric Engineering & Remote Sensing*, 75(7):807–818.

Lingle, C. S. (1984). A numerical model of interactions between a polar ice stream and the ocean: Application to ice stream E, West Antarctica. *J. Geophys. Res.*, 89(C3):3523.

MacAyeal, D. R. (1984). Numerical simulations of the Ross Sea tides. *J. Geophys. Res.*, 89(C1):607.

Magnússon, E., Rott, H., Björnsson, H., and Pálsson, F. (2007). The impact of jökulhlaups on basal sliding observed by SAR interferometry on Vatnajökull, Iceland. *Journal of Glaciology*, 53(181):232–240.

Makinson, K. and Nicholls, K. W. (1999). Modeling tidal currents beneath Filchner-Ronne Ice Shelf and on the adjacent continental shelf: Their effect on mixing and transport. *J. Geophys. Res.*, 104(C6):13449.

Marsh, O. J., Rack, W., Golledge, N. R., Lawson, W., and Floricioiu, D. (2014). Grounding-zone ice thickness from InSAR: inverse modelling of tidal elastic bending. *Journal of Glaciology*, 60(221):526–536.

McMillan, M., Corr, H., Shepherd, A., Ridout, A., Laxon, S., and Cullen, R. (2013). Three-dimensional mapping by CryoSat-2 of subglacial lake volume changes. *Geophysical Research Letters*, 40(16):4321–4327.

Mengel, M. and Levermann, A. (2014). Ice plug prevents irreversible discharge from East Antarctica. *Nature Climate Change*, 4(6):451–455.

Mikucki, J. A., Auken, E., Tulaczyk, S., Virginia, R. A., Schamper, C., Sørensen, K. I., Doran, P. T., Dugan, H., and Foley, N. (2015). Deep groundwater and potential subsurface habitats beneath an Antarctic dry valley. *Nature Communications*, 6:6831.

Moon, T., Joughin, I., Smith, B., van den Broeke, M. R., van de Berg, W. J., Noël, B., and Usher, M. (2014). Distinct patterns of seasonal Greenland glacier velocity. *Geophysical Research Letters*, 41(20):7209–7216.

Morgan, V. I., Jacka, T. H., Akerman, G. J., and Clarke, A. L. (1982). Outlet glacier and mass-budget studies in Enderby, Kemp and Mac. Robertson lands, Antarctica. *Annals of Glaciology*, 3:204–210.

Muto, A., Christianson, K., Horgan, H. J., Anandakrishnan, S., and Alley, R. B. (2013). Bathymetry and geological structures beneath the Ross Ice Shelf at

the mouth of Whillans Ice Stream, West Antarctica, modeled from ground-based gravity measurements. *Journal of Geophysical Research: Solid Earth*, 118(8):4535–4546.

Naif, S., Key, K., Constable, S., and Evans, R. L. (2013). Melt-rich channel observed at the lithosphere–asthenosphere boundary. *Nature*, 495(7441):356–359.

National Academies of Sciences, Engineering, and Medicine (2015). *A Strategic Vision for NSF Investments in Antarctic and Southern Ocean Research*. The National Academies Press, Washington, DC.

Oswald, G. and Robin, G. Q. (1973). Lakes beneath the Antarctic ice sheet. *Nature*, 245:251–254.

Padman, L., Fricker, H. A., Coleman, R., Howard, S., and Erofeeva, L. (2002). A new tide model for the Antarctic ice shelves and seas. *Annals of Glaciology*, 34(1):247–254.

Parizek, B. R., Alley, R. B., Anandakrishnan, S., and Conway, H. (2002). Subcatchment melt and long-term stability of ice stream D, West Antarctica. *Geophysical Research Letters*, 29(8):55–1.

Parizek, R., Alley, R. B., and Hulbe, C. L. (2003). Subglacial thermal balance permits ongoing grounding-line retreat along the Siple Coast of West Antarctica. *Annals of Glaciology*, 36(1):251–256.

Pattyn, F. (2010). Antarctic subglacial conditions inferred from a hybrid ice sheet/ice stream model. *Earth and Planetary Science Letters*, 295(3-4):451–461.

Payne, A. J., Holland, P. R., Shepherd, A. P., Rutt, I. C., Jenkins, A., and Joughin, I. (2007). Numerical modeling of ocean-ice interactions under Pine Island Bay's ice shelf. *Journal of Geophysical Research*, 112(C10):C10019.

Pratt, M. J., Winberry, J. P., Wiens, D. A., Anandakrishnan, S., and Alley, R. B. (2014). Seismic and geodetic evidence for grounding-line control of Whillans Ice Stream stick-slip events. *Journal of Geophysical Research: Earth Surface*, 119(2):333–348.

Pritchard, H. D., Arthern, R. J., Vaughan, D. G., and Edwards, L. A. (2009). Extensive dynamic thinning on the margins of the Greenland and Antarctic ice sheets. *Nature*, 461(7266):971–975.

Reeh, N., Christensen, E. L., Mayer, C., and Olesen, O. B. (2003). Tidal bending of glaciers: a linear viscoelastic approach. *Annals of Glaciology*, 37(1):83–89.

Reeh, N., Mayer, C., Olesen, O. B., Christensen, E. L., and Thomsen, H. H. (2000). Tidal movement of Nioghalvfjerdsfjorden glacier, northeast Greenland: Observations and modelling. *Annals of Glaciology*, 31(1):111–117.

Rignot, E., Mouginot, J., Morlighem, M., Seroussi, H., and Scheuchl, B. (2014). Widespread, rapid grounding line retreat of Pine Island, Thwaites, Smith, and Kohler glaciers, West Antarctica, from 1992 to 2011. *Geophys. Res. Lett.*, 41(10):3502–3509.

Rignot, E., Mouginot, J., and Scheuchl, B. (2011a). Antarctic grounding line mapping from differential satellite radar interferometry. *Geophysical Research Letters*, 38(10):L10504.

Rignot, E., Mouginot, J., and Scheuchl, B. (2011b). Ice Flow of the Antarctic Ice Sheet. *Science*, 333(6048):1427–1430.

Robin, G. Q., Swithinbank, C. W. M., and Smith, B. M. E. (1970). Radio echo exploration of the Antarctic ice sheet. In *IASH Publication 86: International Symposium on Antarctic Glaciological Exploration (ISAGE), Hanover, New Hampshire, USA, 1968*, pages 97–115.

Rose, K. E. (1979). Characteristics of ice flow in Marie Byrd land, Antarctica. *Journal of Glaciology*, 24:63–75.

Rosier, S. H. R., Gudmundsson, G. H., and Green, J. A. M. (2014). Insights into ice stream dynamics through modeling their response to tidal forcing. *The Cryosphere*, 8(5):1763–1775.

Röthlisberger, H. (1972). Water pressure in intra- and subglacial channels. *Journal of Glaciology*, 11:177–203.

Sandwell, D. T. (1984). Thermomechanical evolution of oceanic fracture zones. *Journal of Geophysical Research*, 89:11401–11413.

Sandwell, D. T. (1987). Biharmonic spline interpolation of GEOS-3 and SEASAT altimeter data. *Geophysical Research Letters*, 14(2):139–142.

Sayag, R. and Worster, M. G. (2011). Elastic response of a grounded ice sheet coupled to a floating ice shelf. *Physical Review E*, 84(3).

Sayag, R. and Worster, M. G. (2013). Elastic dynamics and tidal migration of grounding lines modify subglacial lubrication and melting. *Geophys. Res. Lett.*, 40(22):5877–5881.

Scambos, T. A., Berthier, E., and Shuman, C. A. (2011). The triggering of subglacial lake drainage during rapid glacier drawdown: Crane Glacier, Antarctic Peninsula. *Annals of Glaciology*, 52(59):74–82.

Scambos, T. A., Haran, T. M., Fahnestock, M. A., Painter, T. H., and Bohlander, J. (2007). MODIS-based Mosaic of Antarctica (MOA) data sets: Continent-wide surface morphology and snow grain size. *Remote Sensing of Environment*, 111(2):242–257.

Schmeltz, M., Rignot, E., and Macayeal, D. R. (2001). Ephemeral grounding as a signal of ice-shelf change. *Journal of Glaciology*, 47(156):71–77.

Schroeder, D. M., Blankenship, D. D., and Young, D. A. (2013). Evidence for a water system transition beneath Thwaites Glacier, West Antarctica. *Proceedings of the National Academy of Sciences*, 110(30):12225–12228.

Sergienko, O. V., MacAyeal, D. R., and Bindschadler, R. A. (2007). Causes of sudden, short-term changes in ice-stream surface elevation. *Geophysical Research Letters*, 34(22):L22503.

Shepherd, A., Wingham, D., Payne, T., and Skvarca, P. (2003). Larsen Ice Shelf Has Progressively Thinned. *Science*, 302(5646):856–859.

Shuman, C. A., Zwally, H. J., Schutz, B. E., Brenner, A. C., DiMarzio, J. P., Suchdeo, V. P., and Fricker, H. A. (2006). ICESat Antarctic elevation data: Preliminary precision and accuracy assessment. *Geophysical Research Letters*, 33(7):L07501.

Siegert, M. J. (2005). Lakes beneath the ice sheet: The occurrence, analysis, and future exploration of Lake Vostok and other Antarctic subglacial lakes. *Annual Review of Earth and Planetary Sciences*, 33(1):215–245.

Siegert, M. J., Carter, S., Tabacco, I., Popov, S., and Blankenship, D. D. (2005). A revised inventory of Antarctic subglacial lakes. *Antarctic Science*, 17(03):453–460.

Siegert, M. J., Ross, N., Corr, H., Smith, B., Jordan, T., Bingham, R., Ferraccioli, F., Rippin, D., and Le Brocq, A. (2014). Boundary conditions of an active West Antarctic subglacial lake: implications for storage of water beneath the ice sheet. *The Cryosphere*, 8:15–24.

Siegfried, M. R., Fricker, H. A., Roberts, M., Scambos, T. A., and Tulaczyk, S. (2014). A decade of West Antarctic subglacial lake interactions from combined ICESat and CryoSat-2 altimetry. *Geophysical Research Letters*, 41(3):891–898.

Siegfried, M. R., Hawley, R. L., and Burkhart, J. F. (2011). High-Resolution Ground-Based GPS Measurements Show Intercampaign Bias in ICESat Elevation Data Near Summit, Greenland. *IEEE Transactions on Geosciences and Remote Sensing*, 49(10):3393–3400.

Smith, A. M. (1991). The use of tiltmeters to study the dynamics of Antarctic ice-shelf grounding lines. *Journal of Glaciology*, 37(125):51–58.

Smith, A. M., Bentley, C. R., Bingham, R. G., and Jordan, T. A. (2012). Rapid subglacial erosion beneath Pine Island Glacier, West Antarctica. *Geophys. Res. Lett.*, 39(12):L12501.

Smith, B. E., Fricker, H. A., Joughin, I. R., and Tulaczyk, S. (2009). An inventory of active subglacial lakes in Antarctica detected by ICESat (2003–2008). *Journal of Glaciology*, 55(192):573–595.

Stearns, L. A., Smith, B. E., and Hamilton, G. S. (2008). Increased flow speed on a large East Antarctic outlet glacier caused by subglacial floods. *Nature Geoscience*, 1(12):827–831.

Studinger, M., Bell, R. E., Karner, G. D., Tikku, A. A., Holt, J. W., Morse, D. L., Richter, T. G., Kempf, S. D., Peters, M. E., Blankenship, D. D., Sweeney, R. E., and Rystrom, V. L. (2003). Ice cover, landscape setting, and geological framework of Lake Vostok, East Antarctica. *Earth and Planetary Science Letters*, 205(3-4):195–210.

Thomas, R. H., MacAyeal, D. R., Eilers, D. H., and Gaylord, D. R. (1984). Glaciological Studies on the Ross Ice Shelf, Antarctica, 1973–1978. In Bentley, C. R. and Hayes, D. E., editors, *The Ross Ice Shelf: Glaciology and Geophysics*, volume 77 of *Antarctic Research Series*, pages 21–53. Wiley-Blackwell.

Thompson, J., Simons, M., and Tsai, V. C. (2014). Modeling the elastic transmission of tidal stresses to great distances inland in channelized ice streams. *The Cryosphere*, 8(6):2007–2029.

Truffer, M., Echelmeyer, K. A., and Harrison, W. D. (2001). Implications of till deformation on glacier dynamics. *Journal of Glaciology*, 47(156):123–134.

Tulaczyk, S., Kamb, W. B., and Engelhardt, H. F. (2000). Basal mechanics of Ice Stream B, West Antarctica: 1. Till mechanics. *Journal of Geophysical Research*, 105(B1):463–482.

Tulaczyk, S., Kamb, W. B., and Engelhardt, H. F. (2000). Basal mechanics of Ice Stream B, West Antarctica: 2. Undrained plastic bed model. *Journal of Geophysical Research*, 105(B1):483–494.

Tulaczyk, S., Mikucki, J. A., Siegfried, M. R., Priscu, J. C., Barcheck, C. G., Beem, L. H., Behar, A., Burnett, J., Christner, B. C., Fisher, A. T., A., F. H., Mankoff, K. D., Powell, R. D., Rack, F., Sampson, D., Scherer, R. P., Schwartz, S. Y., and the WISSARD Science Team (2014). WISSARD at Subglacial Lake Whillans, West Antarctica: scientific operations and initial observations. *Annals of Glaciology*, 55(65):51–58.

Vaughan, D. G. (1995). Tidal flexure at ice shelf margins. *Journal of Geophysical Research*, 100:6213–6213.

Vaughan, D. G., Corr, H. F., Smith, A. M., Pritchard, H. D., and Shepherd, A. (2008). Flow-switching and water piracy between Rutford Ice Stream and Carlson Inlet, West Antarctica. *Journal of Glaciology*, 54(184):41–48.

Vaughan, D. G., Rivera, A., Woodward, J., Corr, H. F., Wendt, J., and Zamora, R. (2007). Topographic and hydrological controls on subglacial Lake Ellsworth, West Antarctica. *Geophysical Research Letters*, 34(18).

Walker, R. T., Parizek, B. R., Alley, R. B., Anandakrishnan, S., Riverman, K. L., and Christianson, K. (2013). Ice-shelf tidal flexure and subglacial pressure variations. *Earth and Planetary Science Letters*, 361:422–428.

Walter, J. I., Brodsky, E. E., Tulaczyk, S., Schwartz, S. Y., and Pettersson, R. (2011). Transient slip events from near-field seismic and geodetic data on a glacier fault, Whillans Ice Plain, West Antarctica. *Journal of Geophysical Research: Earth Surface*, 116(F1).

Weertman, J. (1964). The theory of glacier sliding. *Journal of Glaciology*, 5(39):287–303.

Whillans, I. M., Bolzan, J., and Shabtaie, S. (1987). Velocity of ice streams B and C, Antarctica. *J. Geophys. Res.*, 92(B9):8895.

Winberry, J. P., Anandakrishnan, S., and Alley, R. B. (2009). Seismic observations of transient subglacial water-flow beneath MacAyeal Ice Stream, West Antarctica. *Geophys. Res. Lett.*, 36(11).

Winberry, J. P., Anandakrishnan, S., Alley, R. B., Wiens, D. A., and Pratt, M. J. (2014). Tidal pacing, skipped slips and the slowdown of Whillans Ice Stream, Antarctica. *Journal of Glaciology*, 60(222):795–807.

Wingham, D. J., Francis, C. R., Baker, S., Bouzinac, C., Cullen, R., de Chateau-Thierry, P., Laxton, S. W., Mallow, U., Mavrocordatos, C., Phalippou, L., Ratier, G., Rey, L., Rostan, F., Viau, P., and Wallis, D. (2006a). CryoSat: a mission to determine the fluctuations in Earth's land and marine ice fields. *Advances in Space Research*, 37:841–871.

Wingham, D. J., Siegert, M. J., Shepherd, A., and Muir, A. S. (2006b). Rapid discharge connects Antarctic subglacial lakes. *Nature*, 440(7087):1033–1036.

Wright, A. and Siegert, M. (2012). A fourth inventory of antarctic subglacial lakes. *Antarctic Science*, 24(06):659–664.

Wright, A., Young, D., Roberts, J., Schroeder, D., Bamber, J., Dowdeswell, J., Young, N., Le Brocq, A., Warner, R., Payne, A., et al. (2012). Evidence of a hydrological connection between the ice divide and ice sheet margin in the Aurora Subglacial Basin, East Antarctica. *Journal of Geophysical Research: Earth Surface*, 117(F1).

Wright, A. P., Young, D. A., Bamber, J. L., Dowdeswell, J. A., Payne, A. J., Blankenship, D. D., and Siegert, M. J. (2014). Subglacial hydrological connectivity within the Byrd Glacier catchment, East Antarctica. *Journal of Glaciology*, 60(220):345–352.

Zwally, H. J., Abdalati, W., Herring, T., Larson, K., Saba, J., and Steffen, K. (2002). Surface Melt-Induced Acceleration of Greenland Ice-Sheet Flow. *Science*, 297(5579):218–222.

Zwally, H. J., Giovinetto, M. B., Beckley, M. A., and Saba, J. L. (2012). Antarctic and Greenland Drainage Systems, GSFC Cryospheric Sciences Laboratory, at http://icesat4.gsfc.nasa.gov/cryo_data/ant_grn_drainage_systems.php.

Zwally, H. J., Giovinetto, M. B., Li, J., Cornejo, H. G., Beckley, M. A., Brenner, A. C., Saba, J. L., and Yi, D. (2005). Mass changes of the Greenland and Antarctic ice sheets and shelves and contributions to sea-level rise: 1992–2002. *Journal of Glaciology*, 51(175):509–527.